DIFFERENTIAL INHIBITION OF CARBOLYTIC ENZYMES AND SUPPRESSION OF LPS-INDUCED INFLAMMATION BY ISOLATED COMPOUNDS FROM BITTER MELON (*MOMORDICA CHARANTIA*)

A Thesis

by

SIDDANAGOUDA SHIVANAGOUDRA

Submitted to the Office of Graduate and Professional Studies of
Texas A&M University
in partial fulfillment of the requirements for the degree of

MASTER OF SCIENCE

Chair of Committee,	Bhimanagouda S. Patil
Committee Members,	G.K. Jayaprakasha
	Giridhar Athrey
Head of Department,	Dan Lineberger

May 2019

Major Subject: Horticulture

ABSTRACT

Several plants have been used extensively for the treatment of diabetes and its related conditions throughout the world. Most plants contain a diverse range of phytochemicals and can often have anti-diabetic effects. Among the multitude of plants, *Momordica charantia* L. is a well-known plant, and it is cultivated as a medicinal vegetable for the management of diabetes in tropical and subtropical areas such as East Africa, Asia, South America, and the Caribbean. Various extracts and isolated compounds have been reported to have significant anticancer and antitumor activity, glucose reducing the effect and AMP-activated protein kinase activities. To further understand the role of compounds from this plant, the current thesis work describes the isolation, structure elucidation, and bioactivities of compounds from the bitter melon.

In the first study, three cucurbitane-type triterpene aglycones such as four compounds were isolated from the EtOAc extract of bitter melon fruit. Charantoside XI is a novel cucurbitane-type triterpene containing a carboxylic acid from *Momordica charantia*. The isolated compounds were assessed for their anti-diabetic and anti-inflammatory activities.

In the second study, six triterpene glycosides such as momordicoside I, F_1, K, F_2, G, and Karaviloside XI, a new phenolic derivative 2-hydroxy-5-*O*-β-D-xylopyranosyl benzoic acid, benzoic acid, phenylalanine, and quercetin-7-O-β-glucopyranoside were isolated from the polar extracts of bitter melon and evaluated for in vitro and in silico anti diabetic and anti-inflammatory activities.

DEDICATION

To my father (Ramanagouda Shivanagoudra), mother (Annapurna) and friends for their unconditional love and support.

ACKNOWLEDGEMENTS

I would like to thank my committee chair, Dr. Bhimanagouda S. Patil for taking me on this Master's program at VFIC, for being a great advisor and teacher and for guiding me through my thesis. Dr. Patil has always been a good supportive source of encouragement and has motivated me during the hard times in research. I would like to offer my sincerest thanks to Dr. G.K Jayaprakasha for his constant support and encouragement throughout my research. I add a special thanks to him, for the amount of time and effort spent teaching and correcting me in conducting all the experiments. I would like to thank Dr. Giridhar Athrey for being my committee member and his guidance and support throughout this research.

I am grateful to Dr. Wilmer H. Perera for his exceptional analytical chemistry skills and the invaluable research integrity that he taught me and the help he provided through all my research. I would like to thank Dr. Jashbir Singh and Dr. Deepak M. Kasote for their tons of encouragement and motivation while doing this research. I would like to extend my heartfelt gratitude to Dr. Basavaraj Girennavar and Mrs. Zabin K. Bagewadi for their encouragement and support to pursue this degree by supporting the projects that I worked on during my master's program.

I would like to thank my parents, brother, and sister for their love and never-ending support. Moreover, thanks to my all friends at the VFIC, Karen Corleto, Ripan Goswami, Pratibha Acharya, Luna Wang, Rita Metrani, Marisa Gomez, and Priyanka Chaudhary,

for their help, support and contribution in times of need; research and thesis writing in particular.

CONTRIBUTORS AND FUNDING SOURCES

Contributors

This work was supervised by a thesis committee consisting of Professor Bhimanagouda S. Patil the committee chair of the Department of Horticultural Sciences, Professor G.K. Jayaprakasha of Department of Horticultural Sciences and Dr. Giridhar Athrey of the Department of Poultry Science.

All work for the thesis was completed independently by the student.

Funding Sources

This study was supported by the United States Department of Agriculture-NIFA-SCRI- 2017-51181-26834 through the National Center of Excellence for Melon at the Vegetable and Fruit Improvement Center of Texas A&M University

NOMENCLATURE

HPLC	High performance liquid chromatography
NMR	Nuclear magnetic resonance spectroscopy
UPLC-HRESIMS	Ultra Performance Liquid Chromatography- high-resolution mass spectral analysis
COSY	Correlation spectroscopy
HMQC	Heteronuclear single quantum coherence spectroscopy
HMBC	Heteronuclear multiple bond correlation
PPA	Porcine pancreatic α-amylase
TCD	3β,7β,25-trihydroxycucurbita-5,23(E)-dien-19-al
IDG	25ξ-isopropenylchole-5, 6-ene-3-O-D-glucopyranoside

TABLE OF CONTENTS

Page

LIST OF FIGURES

FIGURE Page

LIST OF TABLES

TABLES Page

CHAPTER 1

INTRODUCTION

The numerous plants have been explored from ancient times by man for the treatment of diseases. In the last few decades, there is a multitude of research carried out on plants mentioned in ancient literature for the treatment of diabetes, and related conditions. [1] Many of the presently available drugs for the treatment of various metabolic diseases have been derived directly or indirectly from the plants. [2] Most plants contain a diverse range of phytochemicals and can often have anti-diabetic effects. Among the multitude of plants, *Momordica charantia* is a well-known plant belongs to family *Cucurbitaceae*, and it is cultivated as a medicinal vegetable for the management of diabetes in tropical and subtropical areas of the world including East Africa, Asia, South America, and the Caribbean. [3] The origin of this plant is in Asia, and the precise place is unclear in-between China and India. [4]

Diabetes mellitus is the most common chronic disease and considered as major leading causes of death in the world. According to the American Diabetes Association, around 30.3 million Americans found to have diabetes in 2015. [5] It is estimated that this figure will reach 330 million by 2030. The progression of Type II diabetes is typically characterized by insulin resistance, loss of normal β-cell activity and followed by the progressive decline of pancreatic β-cell function that results in insufficient insulin secretion.[6] *Momordica charantia L.* is commonly used traditional medicinal plant by the indigenous populations of Asia and Africa, seems to be beneficial for reducing risk from

Type II diabetes. Data from *in vitro, in vivo* and preclinical studies, suggest that bitter melon extracts have a moderate hypoglycemic effect. Also, numerous pharmacological studies also proved its antidiabetic and hypoglycaemic effects through various postulated mechanisms.[7]

Among various health benefits, the anti-diabetic activity of bitter melon has been related to various triterpenoids. To date, more than 240 bitter melon cucurbitane triterpenoids have been reported from different plant parts including leaves, stems, roots, fruits, and vines. [8] Isolated cucurbitane triterpenoids and their glycosides have been reported to have significant anticancer, [9] and antitumor activity, [10] glucose reducing effect [11], and AMP-activated protein kinase activities. [12] Among these momordicosides, K and L, and momordicines I and II were believed to be responsible for the bitter taste of the fruit. Charantin is one of the major glycoside isolated from the fruits of *M. charantia* that may have insulin-like properties.[13] Aglycones of charantin were isolated and identified as sitosterol and stigmastadienol. However, the concentration or bioefficacy of charantin on diabetes have not been well characterized. [14] In response to accumulating data correlating bitter melon and successful diabetes management, several preclinical and clinical trials have been conducted. Over 20 clinical studies have hypothesized that extracts and bioactive compounds present in the bitter melon may be responsible for the hypoglycemic activity. [15] [16]

In conclusion, in case of *in vivo* and *in vitro,* several pre-clinical and clinical studies validate the hypoglycaemic potential of bitter melon extracts from the fruit, seeds, and leaves. [17,18,19] However, the available data is not sufficient to understand the exact

anti-diabetic mechanism of action of *M. charantia* extracts on type 2 diabetes due to intermittent results. Due to lack of proper controls, and poor methodologies, these preliminary studies are not interpretable. So, reliable *in vitro* and *in vivo* studies are required to prove the potential anti-diabetic activity of *M. charantia*. Hence, the present study focused on *in vitro* screening for α-amylase and α-glucosidase.

Overall, accumulative evidence demonstrated that health-promoting properties of bitter gourd are due the specific natural compounds. [20,21] Existing literature suggests that *M. charantia* consists of an array of natural compounds, which makes it a functional food, especially in the reducing risk from diabetes. However, the exact mechanism of each of these compounds in the observed antidiabetic potential of *M. charantia* is still obscure. Published reports include mostly isolation of compounds using plants or fruit material and extracting with toxic solvents with unreproducible methods. Therefore, it is imperative that pre-clinical and clinical evaluation studies should employ standardized preparation of *M. charantia* and provide comprehensive details of extraction procedure used to isolate either the active ingredient or list the details of the extraction solvent used (e.g., water, ethanol, methanol, etc.). Therefore, our study focussed on precise methods to isolate bioactive compounds from *M. charantia* using different methods of extraction, the solvent used for extraction and reproducible chromatography techniques.

Therefore, in the present study, we isolated and characterized active components from *M. charantia*, and confirmed their *in vitro* antidiabetic activity. Furthermore, the *In silico* studies helped to understand the antidiabetic mechanism of actions of isolated

compounds. Taken together, the present study will contribute to establishing *M. charantia* as a "functional food for diabetes."

The hypothesis for this thesis is that the bitter compounds purified from *M. charantia* are associated with potential antidiabetic and anti-inflammatory activities

The hypothesis has been divided into three objectives:

1. To isolate and structure elucidation of natural compounds from *M. charantia*.
2. To assess *in vitro* antidiabetic and anti-inflammatory potential of purified compounds.
3. To conduct *in silico* molecular docking studies of purified compounds to confirm their antidiabetic mechanism of action.

CHAPTER 2

REVIEW OF LITERATURE

2.1 Characteristics of *Momordica charantia*

M. charantia is a vegetable with high nutrition value, and it has a remarkably long history of use, both as a food and medicine. *M. charantia* perennial slender, climber annual vine, grows 2-3 m long. The fruit is 2-10 cm long (up to 20 cm in cultivated varieties), and covered with longitudinal ridges and warts. The plant and fruit have a characteristic bitter taste. Hence it is commonly known as bitter melon or bitter gourd.[22] Bitter melon also gained many familiar names, indicating its diversified usage in numerous cultures. The plant thrives in tropical areas of Asia, Amazon, East Africa, and the Caribbean.

2.2 Nutritional value of *M. charantia*

Bitter gourd (Momordica charantia L.) is one of the important cucurbitaceous vegetables, and it is considered as a prized vegetable among the other cucurbits because of its high nutritious value especially ascorbic acid and iron. [23] The fruit has a high calorific value of 241.66 Kcal/100 g compared to leaves 213.26 Kcal/100 g and seeds 176.61 Kcal/100 g. Leaves of *Momordica charantia* is the rich source of calcium (20510 ppm) compared with potassium (413 ppm), sodium (2200 ppm) as well as zinc (120 ppm). Additionally, fruits of *M. charantia* is also rich in vitamins such as Vitamin A (β-carotene)

(0.03 ppm), vitamin E (α-tocopherol) (800 ppm), folic acid (20600 ppm), cyanocobalamin (5355 ppm) and ascorbic acid (66000 ppm). [24, 25]

2.3 Medicinal uses of *M. charantia*

Traditionally *M. charantia* has been used as a medicine in many developing countries. Indigenous populations of Asia and Africa have been using different extracts of *M.charantia* as a tonic, stomachic, stimulant, emetic, antibilious, laxative, and alternative. [26] The traditional Indian medicines indicate the usage of *M. charantia* typically for treatment of wounds, treatment of worms and parasites (internally and externally). In Turkish folk medicine, bitter gourd is used for the treatment of gastric ailments including peptic ulcers.[27] The various plant's parts have been used traditionally for the treatment of hyperlipidemia, digestive disorders, microbial infections, and menstrual problems. [28]

Also, the plant is well-known for its medicinal properties, including antidiabetic, anticancer, anti-inflammation, antivirus, and cholesterol-lowering effects. Several phenolic constituents in *M. charantia* may have the potential as an antioxidant, antimutagen, antitumor, anti-inflammatory, and anticarcinogenic properties. [25, 29] *M. charantia* extract can also be used as a potential antibacterial agent to treat infections caused by *Escherichia coli, Salmonella, Staphylococcus aureus, Staphylococcus, Pseudomonas,* and *Streptobacillus.* [30] Protein isolated from *M. charantia* has been shown to possess broad antiviral activity against different subtypes of influenza A (A/New Caledonia/20/99 H1N1, A/Fujian/411/01 H3N2, and A/Thailand/1 (KAN-1)/2004 H5N1).

[31] Regarding its anti-inflammatory activity, *M. charantia* decreases prostaglandin E2 (PGE2), interleukin (IL)-7 and tumor necrosis factor-α and increases transforming growth factor- and IL-10 secretion in RAW 264.7 macrophages, Caco-2 cells, and THP1 cells. [32, 33, 34] Several studies also showed the *M. charantia* fruit extract exhibits hypocholesterolemia, hypotriglyceridemic effects in the STZ-induced diabetic rat. [35] Many *in vitro* and *in vivo* preliminary studies of *M. charantia* crude extract have shown anti-cancer activity against choriocarcinoma, lymphoid leukemia, lymphoma, melanoma, breast cancer, skin, tumor, and prostatic cancer. [36, 37]

2.4 Phytochemical profile of *M. charantia*

M.charantia contains an array of novel and biologically active phytochemicals. Based on the varieties, origin and harvesting times including maturity stages (immature, mature and ripe fruits) the chemical composition varies in bitter melon. Despite its characteristic bitter taste, bitter melon is consumed in many cultures due to its reported potential health benefits attributed to the presence of health-promoting compounds, such as polyphenols, cucurbitane type triterpenoids, and their glycosides, saponins, carotenoids, flavonoids, sterols, alkaloids, reducing sugars, resins, oils, and free acids. [7, 38] Some of the important simple phenols, benzoic acid derivatives compounds such as gallic acid, protocatechuic acid, gentisic acid, vanillic acid, chlorogenic acid, tannic acid, caffeic acid, *p*-coumaric acid, *p*-hydroxybenzoic acid, chlorogenic, syringic acid, ferulic and sinapic acid were identified in the pericarp, pulp, and seeds of *M. charantia.* [39, 40] The

fruit is emerald green color during the young stage and turns to orange-yellow when ripe. As the fruit ripens, the fruit becomes less bitter, and it contains a high content of carotenoids. The fruit is divided into three irregular valves during full maturity and fruit curl backward and releases numerous reddish-brown or white seeds encased in scarlet arils. [41] Bitter melon has recently received much attention due to cucurbitane-type triterpenoids and their various biological activities. The natural cucurbitacins constitute a group of various triterpenoid substances which are known for their bitterness and toxicity. Cucurbitacins were initially isolated from the Cucurbitaceae, and were later identified, either non-glycosylated or glycosylated, in plants of the families Brassicaceae, Scrophulariaceae, Begoniaceae, Elaeocarpaceae, Datiscaceae, Desfontainiaceae, Polemoniaceae, Primulaceae, Rubiaceae, Sterculiaceae, Rosaceae, and Thymelaeaceae.[42] The basic skelton of cucurbitane tritepenoid is shown in **Figure 1** and **Table 1** summarizes various natural compounds isolated from *M. charantia* and their biological activities. Some proteins in bitter melon including MAP-30, MRK29, ribosome inactivating protein gelonin, α-momocharin, β-momocharin, and momordicin and they can treat tumors and HIV. [43, 44] In the last four decades, using various parts of the plant and extraction techniques, more than 240 cucurbitane-type triterpenoids and their glycosides have been isolated and purified. [45]

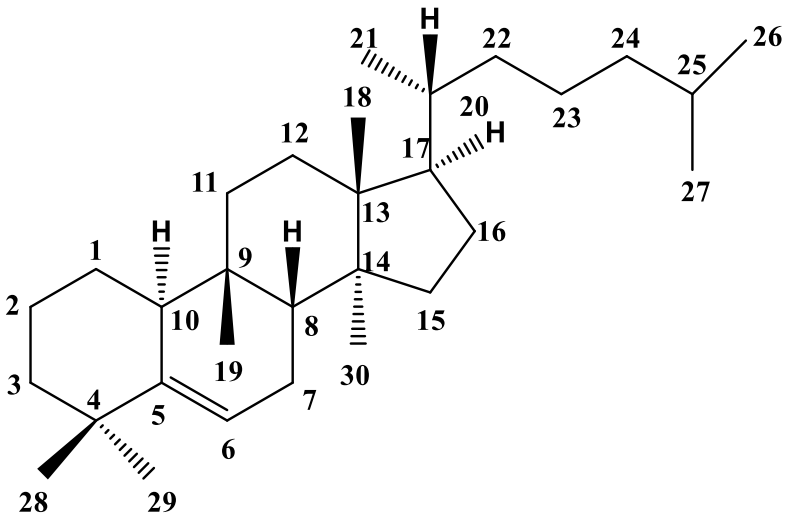

Figure 1 The basic structure of cucurbitacins reported from *M. charantia*

Table 1 Reported natural compounds and their biological activities isolated from *M. charantia*.

S. No	Parts	Natural compounds	Bioactivity	Reference
1	freeze-dried powder		reduction in the hepatic total cholesterol and triglyceride levels	[8]
2	Fruit MeOH extract	**Cucurbitane triterpenoids** *(19*R*,23*E*)-5β,19-epoxy-19-methoxycucurbita-6,23,25-trien-3*β*-ol *(23*E*)-3β -hydroxy-7β-methoxycucurbita-5,23,25-trien-19-al * (23*E*)-3 β -hydroxy-7 β,25-dimethoxycucurbita-5,23-dien-19-al		[46]
3	MeOH extract of the stems	**Cucurbitane triterpenoids** *(23*E*)-25-methoxycucurbit-23-ene-3 β,7 β-diol * (23*E*)-cucurbita-5,23,25-triene-3 β,7 β -diol * (23*E*)-25-hydroxycucurbita-5,23-diene-3,7-dione * 23*E*)-cucurbita-5,23,25-triene-3,7-dione		[47]
4	Bio-guided fractionation of the methanol extract whole fruit	**Cucurbitane triterpenoids** ***** 3 β ,25-dihydroxy-7 β -methoxy-cucurbita-5,23(*E*)-diene * 3β -hydroxy-7β ,25-dimethoxycucurbita-5,23(*E*)-diene * 3-*O*- β -D-allopyranose, 7 β ,25-dihydroxycucurbita-5,23(*E*)-dien-19-al.	*in vivo* hypoglycemic activity	[48]
5	Dried fruit	**Cucurbitane-Type Triterpenes** ***** karavilagenins A, B, and C **cucurbitane-type triterpene glycosides** ***** karavilosides I, II, III, IV, and V		[49]
6	Dried fruits	**cucurbitane-type triterpene glycosides** ***** charantosides I, II, III, IV, V, VI, VII and VIII	Cancer Chemo preventive Effects	[50]

Table 1 continued

S. No	Parts	Natural compounds	Bioactivity	Reference
7	fresh fruits	**cucurbitane-type triterpenoid saponins** ***** momordicoside M, N, and O		[51]
8	Stems	**Cucurbitane-Type Triterpenoids** ***** cucurbita-5,23(E)-diene-3β,7 β,25-triol ***** 3 β -acetoxy- 7β-methoxycucurbita-5,23(E)-dien-25-ol * cucurbita-5(10),6,23(*E*)-triene-3 β,25-diol * cucurbita-5,24-diene-3,7,23-trione		[52]
9	Roots	**Cucurbitane Glycosides** ***** kuguaglycosides A– H * karaviloside III, *karavilosideV *karaviloside XI, and *momordicoside K		[53]
10	Roots	**Trinorcucurbitane triterpenoids** ***** kuguacins A–E		[54]
11	Fruits	**cucurbitane-type triterpene glycosides** ***** (7β,25-dimethoxycucurbita-5(6),23(*E*)-dien-19-al 3-*O*-β-D-allopyranoside * 25-methoxycucurbita-5(6),23(*E*)-dien-19-ol 3-*O*-β-D-allopyranoside * momordicosides A, F1, F2, G, K, and L *goyaglycoside-c,d		[55]
12	Fresh fruits	**Cucurbitane triterpenoids** *momordicosides Q, R, S, and T	Activation of the AMPK Pathway	[56]
13	vines and leaves	**cucurbitane triterpenoids** *** Kuguacins F–S**		[57]
14	Fresh fruits	**Cucurbitane triterpene glycosides** ***** momordicoside U, V, and W		[58]

Table 1 continued

S. No	Parts	Natural compounds	Bioactivity	Reference
15		**pentanorcucurbitane Triterpenoids** ***** 22-hydroxy-23,24,25,26,27-pentanorcucurbit-5-en-3-one * 3,7-dioxo-23,24,25,26,27-pentanorcucurbit-5-en-22-oic acid **trinorcucurbitane triterpene** *** 25,26,27-trinorcucurbit-5-ene-3,7,23-trione**	cytoprotective activity	[59]
16	Stems	**cucurbitane triterpenes** ***** (23E)-7β-methoxycucurbita-5,23,25-trien-3 β-ol * 23,25-dihydroxy-5 β,19-epoxycucurbit-6-ene-3,24-dione		[60]
17	Stems	**multiflorane triterpenoid** ***** 3β-hydroxymultiflora-8-en-17-oic acid * cucurbita-1(10),5,22, 24-tetraen-3α-ol * 5 β,19 β -epoxycucurbita-6,22,24-trien-3a-ol	Antioxidant activity	[61]
18	Stems	**Octanorcucurbitane Triterpenoids** *** octanorcucurbitacins A—D**	Hydroperoxide-Induced Hepatotoxicity activity	[59]
19	Dried fruits	**Saponins** ***** 3β,7 β,25-trihydroxycucurbita-5,23(E)-dien-19-al * momordicine I * momordicine II * 3-hydroxycucurbita-5,24-dien-19-al-7,23-di-O-β-glucopyranoside (4), and kuguaglycoside	*In-vitro* insulin secretion activity	[62]
20	Fruit	**cucurbitane triterpenoids** ***** (23E)-5β,19-epoxycucurbita-6,23,25-triene-3b-ol * (19R, 23E)-5 β,19-epoxy-19-ethoxycucurbita-6,23-diene-3b,25-diol		[63]
21	lyophilized powder of wild bitter gourd	**Cucurbitane-Type Triterpenoids** * cucurbita-6,22(E),24-trien-3β-ol-19,5β-olide * 5β,19-epoxycucurbita-6,22(E),24-triene-3β,19-diol * 3β-hydroxycucurbita-5(10),6,22(E),24-tetraen-19-al	estrogenic activity	[64]

Table 1 continued

S. No	Parts	Natural compounds	Bioactivity	Reference
22	Stems	**Sterols** ***** 5α,6α -epoxy-3 β -hydroxy-(22*E*,24*R*)-ergosta-8,22-dien-7-one * 5α,6 α -epoxy-(22*E*,24*R*)-ergosta-8,22-diene-3β,7 α-diol		[65]
23	Fresh fruit	**C30 sterol glycoside** ***** 25ξ-isopropenylchole-5, (6)-ene-3-O-*β*-D-glucopyranoside		[66]
24	Fresh fruit	**cucurbitane-type triterpeneglycosides** ***** charantagenins D and E, **Sterol** * 7-oxo-stigmasta-5, 25-diene-3-O-β-D-glucopyranoside	Cytotoxicity Activities	[67]
25	Fruit	* (23E)-3 β,25-dihydroxy-7β-methoxycucurbita-5,23-dien-19-al * (23S*)-3β-hydroxy-7β,23-dimethoxycucurbita-5,24-dien-19-al * (23R*)-23-O-methylmomordicine IV * (25)-26-hydroxymomordicoside L	Cancer Chemopreventive Effects	[68]
26	Fruit	**cucurbitane-type triterpene glycosides** ***** 3*β*, 7*β*-dihydroxy-25-methoxycucurbita-5, 23-diene-19-al	antitumor activity	[21]
27	Seeds	**Bidesmoside Triterpenoid Saponins** ***** 28-*O*-*β*-Dxylopyranosyl(1→3)-*β*-D-xylopyranosyl(1→4)-*α*-L-rhamnopyranosyl (1→2)-[*α*-L-rhamnopyranosyl(1→3)]-*β*-D-fucopyranosyl gypsogenin 3-*O*-*β*-D-glucopyranosyl (1→2)-*β*-Dglucopyranosiduronic Acid * 28-*O*-*β*-D-xylopyranosyl(1→4)-*α*-L-rhamnopyranosyl (1→2)-[*α*-L-rhamnopyranosyl(1→3)]-*β*-D-fucopyranosyl gypsogenin 3-*O*-*β*-D-glucopyranosyl(1→2)-*β*-D-glucopyranosiduronic acid	Potential Antidiabetic activity	[20]

Table 1 continued

S. No	Parts	Natural compounds	Bioactivity	Reference
28	fruits	**cucurbitane-type triterpene glycosides** *charantosides D-G		[69]
29	Immature fruit	**Cucurbitane Triterpenoids** ***** kuguacin X * kuguaglycoside I		[70]
30	aerial parts	***C**ucurbita-6,24-dien-3b,23-diol-19,5b-olide * (19R)-5β,19-epoxy-19-methoxycucurbita-6,24-dien- 3 β,23-diol * (19S)-5 β,19-epoxy-19-methoxycucurbita-6,24-dien-3 β,23-diol * (19R)-5 β,19-epoxy- 19-isopropoxycucurbita-6,24-dien-3 β,23-diol * 3β,23-dihydroxy-5-methoxycucurbita-6,24-dien-19- al * (19R)-7β,19-epoxy-19-methoxycucurbita-5,24-dien-3β,23-diol		[71]

2.5 Anti-diabetic effect of *M. charantia*

Numerous traditional herbal remedies have been used to treat diabetes in Asia and other developing countries.[72, 73] Among them *M. charantia* is one of the plants that has been investigated thoroughly for the treatment of diabetes and related conditions. The wide range of biological activities has been proven by the support of many scientific investigations for the beneficial effects of *M. charantia*. Among many scientific investigations, plant stands out for its promising antidiabetic activity. [7] Previous *in vitro* and *in vivo* pharmacological investigations on *M. charantia* have demonstrated that the

extracts and bioactive compounds help in regulating glucose uptake, [74, 75] stimulate insulin secretion from pancreatic cells, [62, 76] protect pancreatic β-cells from inflammatory conditions, [77] display insulin mimetic activities and reduce lipid accumulation in adipose cells. [78] Other evidence indicates that bitter melon extracts may decrease hepatic gluconeogenesis, increase hepatic glycogen synthesis, and increase peripheral glucose oxidation in erythrocytes and adipocytes. [3] Some of the purified cucurbitane type triterpene glycosides have showed AMP-activated protein kinase activity which is a plausible hypoglycemic mechanism of *M. charantia.*[6, 79] The anti-diabetic activity, due to saponins present in *M. charantia, is* attributed in reversing atrophy of pancreatic islets of β cells, which in turn helps in insulin secretion and an increase in hepatic glycogen level. In addition, many *in vitro* studies have been conducted on investigating effects of crude extracts, isolated compounds on inhibition of α-glucosidase and α-amylase and PTP 1B inhibition. [80,81] Several *in vivo* studies demonstrate that *M. charantia* extract causes hypoglycemia, (stimulation of peripheral skeletal muscle glucose utilization), inhibits intestinal glucose uptake, inhibits adipocyte differentiation, suppresses key gluconeogenic enzymes (glucose-6-phosphatase and fructose-1,6-bisphosphatase), preserves pancreatic β cells and insulin secretory function, and reduces serum lipid levels.

2.6 Clinical trials

Few clinical trials on *M. charantia* have been observed to reduce serum glucose levels in many animal studies and human clinical studies.[82-85] There are more than 20

clinical trials have been conducted using plant parts or formulated products. **Table 2** lists some of the previously conducted clinical trials across the world. In many clinical studies the results seem promising. However, some previous experiments had serious methodologic errors including small sample size, and poorer statistical analyses and most did not even have a control group and some studies are randomized trials. For these reasons, firm conclusions on effectiveness could not be drawn. Also in all these studies, the toxicity, dosage, and adverse effects have not been systematically assessed.[3, 17]

Table 2 Reported clinical trials on M. charantia.

Study design	**Subjects (duration)**	**Source**	**Outcome measures**	**Statistical significance**	**Reference**
Open-label Uncontrolled supplementation trial	42 individuals (3 months)	4.8 g lyophilized wild type bitter gourd powder in capsules	The metabolomic syndrome was decreased incidence rate was highest at the end of the three-month supplementation period, and it was significantly different from that at baseline ($p = 0.021$).	Yes	[86]
Random design	26 subjects (4 weeks)	Tablets		Yes	[87]
Multicenter, randomized, double-blind, active control trial	4 groups (4 weeks)	The capsule contained 500 mg of dried powder of the fruit pulp, containing 0.04-0.05%	bitter melon 2000 mg/day has shown a significant decline in fructosamine at week 4 in tested patients.	Yes	[88]

Table 2 continued

Study design	Subjects (duration)	Source	Outcome measures	Statistical significance	Reference
A double-blind, randomized controlled trial	40 with T2D (twenty trials and twenty control subjects) (3 months)	Commercial herbal supplement capsules	There was no significant effect on mean fasting blood sugar	No	[17]
Controlled trial	15 with T2D in 3 groups (1 week)	The methanol extract of ground whole fruit	Augmented hypoglycemic activity in NIDDM patients	Yes	[89]
Randomized controlled trial	50 with T2D (26 trial and 24 control subjects) (4 weeks)	Tablets from whole dried fruit	(1) Fasting postprandial blood Glucose (2) Fructose amine	No	[90]
Case series	100 with T2D (Single treatment)	Fresh fruit	a significant reduction ($p < 0.001$) of both fasting and post-prandial serum glucose levels	Yes	
Case series	12 with impaired OGTT (3-7 weeks)	Arm 1: dried fruit Arm 2: aqueous extract	Aqueous extract showed significant Hypoglycemic effects in diabetic patients were found to be highly significant $P<0.01$)	Arm 1: No Arm 2: Yes	[84]
Case series	8 with DM (1 week)	Powdered dried fruit	significantly lowered blood glucose level in tested patients	Yes	[91]

Table 2 continued

Study design	Subjects (duration)	Source	Outcome measures	Statistical significance	Reference
Case series	9 T2D (Single treatment, then 7-11 weeks)	Fresh fruit juice + fried fruit	improves glucose tolerance in diabetes	(1) Yes (with juice) No (with fried fruit) (2) Yes (with fried fruit)	[83]
Case series	19 with DM (Single treatment)	'Polypeptide-p' isolated from M. charantia	Effective hypoglycemic agent	Yes	[92]
Controlled trial	Trial subjects: 9 DM Control subjects: 5 DM + 5 normal (Single treatment)	Aqueous extract refined to subcutaneous injection (insulin)	showed a consistent hypoglycemic effect in patients with diabetes mellitus	Yes	[82]
Case series	15 with DM (6-14 weeks)	Fresh fruit juice and dried powder	no significant improvement in glucose tolerance	No	[93]

2.7 Simple and quick tools for dereplication of antidiabetic principles using *In-silico* molecular docking

Substantial data are available in the category of secondary metabolites of *M. charantia* like isolation, identification, and characterization. Moreover, in the past two decades, many additional bioactive secondary metabolites were isolated from bitter gourd due to considerable progress in techniques for dereplication, isolation, and analysis. Interestingly, newly isolated compounds were only in minute concentration. Therefore,

commercially available natural compounds are too expensive which represents a bottleneck for in-depth biological characterization. To overcome these issues and moreover as a way to close the knowledge gap of this vast pool of pharmacologically almost untapped pure constituents, the application of *in silico*-based methods might be a promising strategy for prioritizing bio-assays. Again, in this study, *in silico* experiments helps to explore the possible mechanism of action of these metabolites through the inhibition of α-amylase and α-glucosidase. The results obtained from this *in silico* approach will be compared to experimental bioactivity data to distinguish between true and false positives or negatives.

Some of the programs used for virtual screening and docking studies are AutoDock, CLC drug discovery workbench, DOCK, FlexX, FRED, Glide, GOLD, and MOE. These programs help to understand valuable information of ligand crystal structure, conformation and the orientation of the lead molecule, which provides the binding energy of the target receptor and finally the best-docked ligand structure. Thus, docking studies play a significant role in rational designing of drugs and aids the drug discovery process.

The anti-diabetic potential of *M. charantia* using structure-based screening of glycoalkaloids and related compounds against enzyme; aldose reductase was previously established. By taking ligands from 10 different medicinally important plants, the experiment was designed to understand the binding mechanisms of these ligands with aldose reductase protein (receptor) using XP docking program of Maestro, version 9.4, Schrödinger software. Synthetic drug metformin was used as a standard for comparison. Vicine, a natural compound present in *M. charantia,* was found to possess strong anti-

diabetic activity compared to that of standard metformin. Isomers of vicine were also generated and docked with the receptor aldose reductase and found to have similar GLIDE score as that of vicine. [94]

CHAPTER 3

CUCURBITANE-TYPE COMPOUNDS FROM *MOMORDICA CHARANTIA*: ISOLATION, *IN VITRO* ANTIDIABETIC AND ANTI-INFLAMMATORY ACTIVITIES, AND *IN SILICO* MODELING APPROACHES [1]

3.1 Synopsis

Momordica charantia L., commonly known as bitter gourd or bitter melon, belongs to the Cucurbitaceae family. Various *in vitro* and *in vivo* studies have indicated that bitter melon extracts have anti-diabetic properties. However, relativity little is known about the specific bioactive compounds responsible for their antidiabetic properties. In the present study, three cucurbitane-type triterpene aglycones 3β,7β,25-trihydroxycucurbita-5,23(E)-dien-19-al, charantal, and charantoside XI, and one sterol glucoside 25ξ-isopropenylchole-5, 6-ene-3-O-D-glucopyranoside, were isolated from bitter melon fruit. The structure of each compound was elucidated by one and two-dimensional nuclear magnetic resonance, and HR-ESI-MS. The isolated compounds were evaluated for their anti-diabetic properties (inhibition of amylase and glucosidase enzymes) and anti-inflammatory activities. All compounds exhibited significant *in vitro* inhibition of α-

[1] Reprinted with permission from "Cucurbitane-type compounds from *Momordica charantia: Isolation, in vitro* antidiabetic, anti-inflammatory activities and in silico modeling approaches" by Siddanagouda. R.S, Wilmer. H. Perera, Jose. L. Perez, Giridhar. Athrey, Yuxiang Sun, G.K. Jayaprakasha, B.S. Patil, 2019. Bioorganic Chemistry (2019), 87, 31-42. Copyright [2019] by Elsevier.

amylase and α-glucosidase, comparable to acarbose. Furthermore, computational molecular docking of all compounds showed molecular interactions with key amino acid residues in the catalytic sites of both enzymes, revealing their potential binding modes at the molecular level. Additionally, the purified compounds showed significant anti-inflammatory activity, differentially downregulating the expression of *NF-κB, INOS, IL-6, IL-1β, TNF-α,* and *Cox-2* in murine macrophage RAW264.7 cells activated by lipopolysaccharide. Our findings suggest that these compounds purified from bitter melon have potential anti-diabetic and anti-inflammatory activities and therefore hold promise for the development of a plant-based management strategy for diabetic complications and inflammation-mediated conditions.

3.2 Introduction

Diabetes is a chronic metabolic disease, and its frequency has been rapidly increasing worldwide in recent years. [95] The incidence of type II diabetes is predicted to grow by 6% annually. Recent estimates report that by 2025, India, China, and the United States of America will have the most significant number of people with diabetes, compared with other countries. [96] Diabetes is a preventable, chronic disease that has a complex etiology and several strategies can be used for understanding and managing the disease. Once diabetes has developed, the next option is the management of hyperglycemia. Several synthetic drugs, including sulfonylureas (promote insulin secretion), biguanides and thiazolidinediones (insulin utilization), acarbose and voglibose

(α-amylase and α-glucosidase inhibitors) can be used to manage post-prandial hyperglycemia. [95] For example, α-amylase, and α-glucosidase inhibitors reduce the levels of glucose in the bloodstream by reducing the rate of polysaccharide degradation. Despite significant developments over the last decade in treating Type II diabetes, numerous diabetic patients have been unable to reach their recommended therapeutic targets. Therefore, it is necessary to develop safe and bioactive natural anti-diabetic compounds that have fewer adverse effects than existing synthetic medications. [97] Bitter melon (*Momordica charantia*) extracts have been reported to inhibit the activities of α-amylase and α-glucosidase enzymes, but the bioactive component remains elusive.

Bitter melon (*Momordica charantia*) is cultivated as a medicinal vegetable for the management of diabetes in tropical and subtropical areas including East Africa, Asia, South America, and the Caribbean. [98] Among various health benefits, the anti-diabetic activity of bitter melon has been related to various triterpenoids. In response to accumulating data correlating bitter melon and successful diabetes management, several preclinical and clinical trials have been conducted.

Diabetes mellitus leads to hyperglycemic conditions, and like many other chronic diseases, inflammation is widely known to be a contributing factor. [99, 100] Subclinical chronic inflammation is a common feature in diabetes and associated with changes in levels of inflammatory biomarkers [101]. The release of pro-inflammatory cytokines, such as interleukin-1β, IL-6, TNF-α, other inflammatory mediators like nitric oxide (NO), prostaglandins (PGE_2), and the resulting activation of macrophages have a significant role in the development of a diabetic complication. [102, 103] The increased expression of

inflammatory cytokines can amplify the inflammatory responses, leading to aggravation of diabetes and its long term complications including insulin resistance, age-related neurodegenerative disorders, and Alzheimer's disease. [104] Recently, a few studies have explored the effect of bitter melon on inflammation, but the identification of the bioactive compounds responsible for this activity is still an active research topic. [105-107]

In this chapter, we present the isolation and structural elucidation of four compounds from an ethyl acetate extract of Chinese bitter melon. We evaluated the α-amylase and α-glucosidase inhibitory activities of these purified compounds. Moreover, molecular docking allowed us to model the potential interactions of these compounds with the enzymes, to unveil the possible mechanism of inhibition. Additionally, purified bitter melon compounds were screened for their potential anti-inflammatory properties using lipopolysaccharide (LPS)-activated RAW264.7 macrophage cells.

3.3 Experimental

3.3.1 Chemicals

Silica-gel 60Å particle size (40–63 µm), glacial AcOH, phosphate-buffered saline (PBS), and RPMI-1640 were purchased from VWR International (Radnor, PA). The RAW 264.7 mouse monocyte-macrophage cell line was procured from the American Type Culture Collection (ATCC, USA). Fetal bovine serum (FBS), penicillin, streptomycin, *n*-hexane, $CHCl_3$, MeOH, ACN, $(CH_3)_2CO$, EtOAc, ACN drum grade, and MeOH (HPLC

grade), D-(+)glucose, dinitrosalicylic acid (DNSA), dextrose, sodium chloride, acarbose, and Porcine Pancreatic α-amylase (PPA) were purchased from Sigma-Aldrich (St. Louis, MO). Genes including *GAPDH*, *Cox-2*, *TNF-α*, *IL-6*, *IL-1β*, iNOS, NF-κB and the Aurum Total RNA Mini Kit, iScript cDNA synthesis kit, and SsoAdvanced Universal SYBR Green Supermix were purchased from Bio-Rad Laboratories (Hercules, CA). Silica gel 60 F_{254} thin-layer chromatography plates, HCl, and H_3PO_4 were purchased from EMD Millipore, Burlington, MA). RP-C18 cosmosil 140 was purchased from Nacalai Tesque, Inc, (Kyoto, Japan). Flash silica gel cartridges (Redi*Sef* ®R_f) were procured from Teledyne ISCO, Lincoln, NE. Perdeuterated MeOH, $CHCl_3$, and pyridine were purchased from Cambridge Isotope Laboratories, Inc. (Tewksbury, MA, USA). Nano-pure water (18.2 MΩ-cm) was obtained from a NANO pure purification system (Barnstead/ Thermolyne, Dubuque, IA).

3.3.2 General experimental procedure

Flash chromatography system Teledyne ISCO CombiFlash Rf 4x system equipped with a fiber optic spectrometer, a UV-vis (λ 200–700 nm) detector, was used for the purification. Individual fractions were collected and analyzed using an Agilent 1200 Series HPLC (Agilent, Foster City, CA) system consisting of a degasser, quaternary pump, autosampler, column oven, and a diode array detector. The separation was carried out using an RP C-18 Gemini series column (250 ×4.6 mm; 5 µm) (Phenomenex, Torrence, CA), with a flow rate of 0.8 ml/min. The oven temperature was set at 40°C and

chromatograms were recorded at 210, 280, and 320 nm. The elution was carried out using gradient mode elution with 3 mM phosphoric acid (A) and acetonitrile (B). Initially, elution was carried out in isocratic 20% B for 2 min, followed by 20–50% B (2–6 min), 50–90% B (7–10 min), and 90–95% B (11–18 min) followed by isocratic 95% B up to 23 min and returned to 20% B (24–26 min). The column was equilibrated for 2 min before the next injection. UPLC-HRESIMS were acquired using a maXis impact mass spectrometer (Bruker Daltonics, Billerica, MA) coupled to a 1290 Agilent LC (Agilent, Santa Clara, CA) using a quadrupole time of flight mass detector equipped with an electrospray ionization interface controlled by Bruker software (Bruker Compass Data Analysis Version 4.2). Data acquisition and processing were done using the Bruker software (Bruker Compass Data Analysis Version 4.2). The NMR spectra 1D (^{1}H; ^{13}C and DEPT 135) and 2D NMR spectra were recorded with a JEOL spectrometer (USA, Inc., Peabody, MA) at 25°C, operating at 400 MHz (^{1}H) and 100 MHz (^{13}C) using standard JEOL pulse programs. The chemical shifts are given in δ (ppm) and were referenced to residual solvent signals. Samples were dissolved based on their solubility in methanol-d_4, pyridine-d_5, and $CHCl_3$-d. Optical rotations were measured on a ATAGO SAC -i polarimeter in MeOH at 21.8°C.

3.3.3 Extraction

Fresh fruits of Chinese bitter melon (136 kg) were purchased from a local market (BCS Food Market, College Station, TX) in October 2015. Fruits were chopped into small

pieces, then the seed and fruit parts were separated and air dried. Dried samples of Chinese bitter melon were blended using a Vita-prep™ blender to 40–60 mesh size powder (Vita-Mix Corporation, Cleveland, OH). Total fruit powder (5.6 kg) was defatted using *n*-hexane and extracted using ethyl acetate using a Soxhlet apparatus at 60–70°C for 32 h. Extracts were concentrated under reduced pressure using rotary evaporator (Buchi, New Castle, DE), freeze-dried and stored at -80°C for further use. The EtOAc extract of 33.8g (dry weight) was used for further experiments.

3.3.4 Fractionation of the crude ethyl acetate extract

The ethyl acetate crude (EtOAc) extract (103.7 g) was impregnated with 40 g of silica gel and chromatographed over silica gel (2.5 kg silica-gel 60 Å 40–63 µm) column chromatography. Initially, the column was eluted with *n*-hexane, *n*-hexane/EtOAc (95:5, 90:10, 85:15, 80:20, 60:40, 50:50, 40:60, 25:75, and 0:100 v/v) and a similar step gradient with EtOAc/acetone, acetone/MeOH and finally with MeOH to give 40 fractions of 300 ml each. Fractions were concentrated under reduced pressure using a rotary evaporator and pooled based on TLC chromatographic profile.

3.3.5 Purification

Fraction 20 (600 mg) was impregnated with 200 mg silica gel and air-dried in a hood. The air-dried sample was homogenized using a pestle and mortar. Next, the sample

was subjected to flash chromatography in a 120 g silica gel cartridge, at 60 ml/min over 60 min, eluted using a gradient program with *n*-hexane and EtOAc from 100–0% with increasing polarity of eluents. In total, 210 fractions, 3.15 l (210×15 ml each) were collected, and fractions were pooled based on silica gel TLC profiles to give subfractions 1–17. Fractions 13 and 16 were crystallized in a test tube to yield compound **1** (15 mg), and fraction 16 yielded compound **2** (9 mg). Similarly, pools 25–30 of 1738 mg from chromatography 1 were subjected to flash chromatography using RP-Cosmosil 140 C18 column of 43 g using H_2O: MeOH (100–0%, 60 ml/min flow rate) linear gradient to afford 82 fractions, 1230 ml (82×15 ml each). Collected fractions were pooled based on HPLC Retention Time. Fractions 16–23, RT 14.2 min, H_2O: MeOH (15:85) were pooled to yield compound **3** (24.4 mg). Similarly, fractions 35–40 (1263 mg) from chromatography 1 were subjected to flash chromatography in a 120 g silica gel cartridge with a 90-min gradient program, flow rate of 85 ml/min of solvent A1 (ethyl acetate): B1(acetone) gradient elution of 100–0% to give 113 fractions of 15 mL each. Fractions (84–92) (EtOAc: acetone 7:3) yielded compound **4** (24.9 mg).

3.3.6 Inhibition of α-amylase assay

α-Amylase inhibitory activity was determined using a published protocol with minor modifications. [108] All four compounds were prepared to 10 mM in 500 µl DMSO and used for the inhibition of α-amylase assay. Two concentrations of 10 and 20 µl (equivalent to 0.43 and 0.86 mM) of all purified compounds were used for the assay, which

was conducted in triplicate. The acarbose (10 and 20 µl equivalent to 0.067 and 0.13 mM) was used as a positive control. The absorbance was measured at 540 nm in a KC-4 microplate reader (BioTek Instruments, Inc., Winooski, VT) and % inhibition was calculated according to the published method.

3.3.7 Inhibition of α-glucosidase assay

The α-Glucosidase activity of purified compounds was determined according to the method with slight modifications, using α-glucosidase from *S. cerevisiae*. [109] Acarbose was used as a standard in this experiment. The α-glucosidase activity was determined by measuring the yellow-colored para-nitrophenol released from pNPG at 405 nm. The absorbance was measured at 405 nm in a KC-4 microplate reader (BioTek Instruments, Inc., Winooski, VT, USA). Percentage inhibition was calculated as %Inhibition = ($Abs_{control} - Abs_{test}$) X100/ $Abs_{control}$.

3.3.8 In silico molecular docking of purified compounds against α-amylase and α-glucosidase

Mode of inhibition of compounds **1**–**4** on the Porcine Pancreatic α-amylase (PPA) and isomaltase enzymes was further assessed by molecular docking analysis.

3.3.8.1 Preparation of protein and ligand structure

The 3-D coordinates of the crystal structures of proteins were downloaded from the RCSB protein data bank (PDB, http://www.rcsb.org/pdb) in PDB format. Porcine Pancreatic α-amylase complexed with acarbose (PDB ID: 1OSE) was downloaded from the PDB. The complexed acarbose was removed using Biovia Discovery studio 4.5 (DS 4.5, Dassault Systems BIOVIA, Discovery Studio Modeling Environment, Release 4.5, San Diego. 2015). Similarly, for α-glucosidase, the crystal structure (PDB ID:3A4A) of isomaltase from *S. cerevisiae* was downloaded from the PDB. Later, both proteins were prepared by removing all water molecules, and a CHARMm force field was applied using the Receptor-Ligand interactions tool in DS. Further, binding of acarbose to 1OSE and active residues of the crystal structure of isomaltase were identified using the Computer Atlas of Topography of Proteins (CASTp), a program for identifying and characterizing active protein sites, binding sites, and functional residues located on the protein surface. The discovery studio tool was used to convert this file into the PDB format. Two-dimensional structures of purified compounds were drawn using ChemDraw tool (PerkinElmer Informatics, 2016) and saved as a molecular format file (MDL MOL format). The “Prepare ligand” protocol of DS 4.5 was used to prepare the ligands which remove duplicate structures, standardizes the charges of common groups, calculates the ions and ionization of the ligand's functional groups, 2D-3D conversion, verifying and optimizing the structures, and other tasks established by user-defined parameters. All the ligands were typed with the CHARMM36 force field using DS4.5.

3.3.8.2 Molecular docking using Autodock 4.2

The four ligands were docked with α-amylase and α-glucosidase using the Lamarckian genetic algorithm (LGA) provided by the AutoDock Program (ADT, version: 1.5.6) version 4.2. Polar hydrogens were added to the receptor, Kollman charges were assigned, and solvation parameters were added with the "Addsol" option in AutoDock. For the inhibitors, charges of the Gasteiger type were assigned. The internal degree of freedom and torsion were defined using the "Ligand Torsions" menu option of AutoDock. The grid maps representing the protein were calculated using the "AutoGrid" option. The protein was centered on the geometric center before docking, and the dimensions of the cubic grid box were set to 126 Å of x, y, and z with a spacing of 0.375 Å for both proteins. Blind Docking was carried over the whole receptors (i.e., 1OSE and 3A4A) using Genetic Algorithm. The best ligand-receptor structure from the docked structures was chosen based on the lowest energy and minimal solvent accessibility of the ligand. The 2D visualization of ligand interactions with the protein domain was analyzed using DS4.5, and PyMOL molecular graphics system (PyMOL Molecular Graphics System, San Carlos, CA, USA) was used to visualize the 3D interactions between ligands and receptors better.

3.3.9 Cell culture and maintenance

The RAW 264.7 mouse monocyte-macrophage cell line was procured from American Type Culture Collection (ATCC, USA) and cultured in RPMI 1640 medium

supplemented with 10% (*v/v*) fetal bovine serum and antibiotics (100 U/ml penicillin and 100 µg/ml streptomycin). Cells were incubated at 37°C in a humidified incubator with 5% CO_2. The media was changed every 48 h and cells that reached 80% confluence were used for further experiments.

3.3.9.1 RNA isolation and quantitative real-time polymerase chain reaction (qRT-PCR)

RAW 264.7 cells were seeded into 6-well plates at a density of 5.0×10^5 cells/well. Cells were incubated at 37°C and 5% CO_2 for 24 h. Following incubation, the cells were treated with 25 µM of purified compounds (**1**–**4**) for 1 h. After 1 h, LPS (1 µg/ml) was added to specified wells, and the cells were incubated for an additional 18 h. Following the incubation period, total RNA was extracted using the Aurum Total RNA Mini Kit. RNA concentrations were determined using a Nanodrop Spectrophotometer (Thermo Scientific NanoDrop Products). Purified RNA from cell lysate was used to synthesize cDNA according to the manufacturer's manual (iScript cDNA Synthesis Kit, Bio-Rad). Real-time PCR was performed on a Bio-Rad using the SYBR Green PCR Master Mix, according to the protocol provided by the manufacturer and relative expression was compared and normalized to the expression of GAPDH in the same sample.

3.3.10 Statistical analysis

Statistical analysis was performed using JMP Pro14 (SAS, NC, U.S.A.) statistical software. All data were expressed as mean ± SD. All statistical comparison compared through one-way analysis of variance (ANOVA), using Tukey's HSD post hoc test ($p < 0.01$, n=3).

3.4 Results and discussion

3.4.1 Structural elucidation of compounds

An ethyl acetate extract from Chinese bitter melon fruit was subjected to silica gel and reverse-phase flash chromatography to separate one new cucurbitane-type triterpene (compound **3**) together with two known triterpene aglycones (compounds **1** and **2**), and one sterol glucoside (compound **4**). Compounds **1, 2,** and **4** were characterized by 1-D and 2-D NMR and high-resolution mass spectroscopy data (**Table 3** and **Figure A1–A8**). Compounds **1** and **2** were identified as 3β, 7β, 25-trihydroxycucurbita-5, 23(E)-dien-19-al (TCD) and charantal, respectively. The chemical shifts of these compounds were matched to reported data. [110, 111] Previously, TCD and charantal were isolated from leaf extracts of *M. charantia*, and this is the first report of their isolation from fruit. Compound 4 was previously isolated from the fresh fruit of *M. chrantia* and was identified as 25ξ-isopropenylchole-5,(6)-ene-3-*O*-*β*-D-glucopyranoside (IDG). [112]

Compound **3** was purified as a white amorphous powder, $[\alpha]^{25}_{D}$ -24.16 (*c* 0.1, MeOH). HR-ESIMS of compound **3** showed a molecular ion at *m/z* 523.34233 $[M+Na]^+$ (calculated *m/z* 523.3399 $[M+Na]^+$) suggesting a molecular formula of $C_{31}H_{48}O_5Na$. The molecular weight of compound **3** was compared with our in-house database of all triterpenes and sterols isolated from *M. charantia* until 2018.

The ^{13}C Attached proton test (APT) NMR data of compound **3** (**Figure 2**) showed 31 carbons with six methines (including one oxymethine group), seven methylenes, seven methyl groups, five quaternary carbons, one aldehyde, one carboxylic acid, and four olefinic carbons, one tri-substituted and three di-substituted. The complete assignment of Heteronuclear Multiple Quantum Coherence (HMQC) correlations is shown in Supplementary **Figure A9 and Table A1**. The lack of olefinic carbons in kuguacin C, the presence of two tri-substituted olefinic carbons, and the absence of methoxy groups in the purified compound **3** suggested its structural novelty. Six tertiary groups appeared at $\delta_H(\delta_c)$ 0.9 (15.5), 1.25 (30.3), 1.25 (30.2), 1.17 (27.5), 1.21 (25.6), and 0.82 (18.8) ppm corresponding to methyl groups at positions 18, 26, 27, 28, 29, and 30, respectively, and one secondary at 0.95 (19.3) ppm (d, *J*= 5.8 Hz) corresponding to a methyl group at position 21. Positions of the methyl groups were assigned through Heteronuclear Multiple Bond Correlation HMBC (**Figure 2**) and COSY correlations.

Table 3 ^{1}H and ^{13}C NMR data for purified compounds **1**, **2**, and **4** from the EtOAc extract of *Momordica charantia*

	Compound 1 ($CDCl_3$)		**Compound 2 (CD_3OD)**		**Compound 4 (pyridine-d5)**	
Position	δH (ppm)	δC (ppm)	δH (ppm)	δC (ppm)	δH (ppm)	δC (ppm)
1	1.76; 1.54	21.4	1.31, m; 1.21, m	35.8	1.00, m; 1.77, m	37.66
2	1.95; 1.90	28.6	1.82, m; 1.31, m	28.7	2.12, m; 2.18, m	30.27
3	3.55 (1H, m)	76.3	3.46 br, s	77.2	3.99, m	78.84
4	-	41.6	-	42.4	2.49, m; 2.77, m	39.46
5	-	145.7	-	147.5	-	140.84
6	5.88 (1H, br d, *J*=3.9 Hz	124.2	5.81 (1H, dd, *J*=1.7, 5.3 Hz)	124	5.37 (br s)	122.2
7	3.95 (1H, br d, *J*=4.7 Hz)	66.5	3.92 (d, *J*=5.2 Hz)	67	1.90, m; 1.95, m	32.36
8	2.07 m	47.8	2.45 (1H, m)	37.8	1.4, m	32.23
9	-	50.1	1.83	51	0.92, m	50.36
10	2.51 (1H, br dd *J*=12.0; 4.0 Hz)	36.8	-	46.7	-	37.1
11	2.21; 1.57 m	23.8	1.53, m; 1.40, m	22.3	1.38, m; 1.48, m	21.47
12	1.93; 1.39 m	27.6	1.79, m; 1.66, m	29.7	1.12, m; 2.02, m	39.98
13	-	45.5	-	45.3	-	42.5
14	-	47.8	-	51.4	1.01, m	56.86
15	1.37; 1.37 m	34.9	1.36, m; 1.32, m	23.4	1.55, m; 1.55, m	24.67
16	1.68; 1.68 m	29.2	1.66, m; 1.56, m	29.96	1.30, m; 1.84, m	28.65
17	1.49 m	50.1	1.45 (1H, m)	51.2	1.06, m	56.28
18	0.87 (3H, s)	15.1	0.81 (3H, s)	15.5	0.69 (3H, s)	12.15
19	9.71 (1H, s)	208.5	0.71 (3H, s)	18.9	0.95 (3H, s)	19.61
20	1.49	36.4	1.45 (1H, m)	37.7	1.44, m	35.94
21	0.89 (3H, s)	18.9	0.84 (3H, d, *J*=5.8 Hz	19.3	0.88 (3H, d, *J*=6.3 Hz	19.1
22	2.12; 1.71	39.3	2.05; 1.71 (2H, m,m)	40.4	1.07, m; 1.41, m	34.15
23	5.57 (1H, m)	125.3	5.48 (1H, m)	126		30.45
24	5.55 (1H, d, *J*=14.4 Hz	139.9	5.48 (1H, d, *J*=6.34 Hz)	141	1.27, m; 1.83, m	29.83
25	-	70.9	-	71.4	1.94, m	49.85
26	1.29 (3H, s)	30.2	1.16 (3H, s)	29.98	1.39, m; 1.39, m	26.95
27	1.29 (3H, s)	30.1	1.16 (3H, s)	29.87	0.87 (3H, t, *J*=7.8 Hz	12.51
28	1.04 (3H, s)	27.4	0.98 (3H, s)	27.9	-	147.81
29	1.23 (3H, s)	25.6	1.15 (3H, s)	26.3	4.83, m; 4.90, m	112.21
30	0.73 (3H, s)	18.1	9.78 (1H, s)	210.1	1.64 (3H, s)	18.01
Glu-1'					5.06 (d, J=7.3 Hz)	102.69
Glu-2'					3.99, m	75.47
Glu-3'					4.3 (dd, *J*=6.7, 7.9 Hz)	78.75
Glu-4'					4.31, m	71.4
Glu-5'					-	78.26
Glu-6'					4.32 (dd, *J*=2.2, 11.7 Hz); 4.48 (dd, *J*=4.7, 11.5 Hz)	63.1

The side chain of compound 3 was identified through HMBC correlations of 71.3 ppm (C-25) with the methyl groups at position 26 and 27 (1.25 ppm, s, 6H), and with olefinic protons at 5.58 ppm. Additionally, COSY correlations between 5.58 ppm with 2.16 and 1.78 ppm (CH_2 at C-22) were also observed. The side chain -$CH(CH_3)$ CH_2CH=CH-$C(CH_3)_2$ of compound **3** was similar to those previously reported for kuguacin A and S, and momordicine VII. [113] [54] The ^{3}J HMBC correlation of the oxymethine proton at 4.82 ppm with the tri-substituted olefinic carbon at 146.5 ppm suggested a C-5 and C-6 double bond. ^{3}J HMBC correlation of the methine proton at 2.65 ppm (J = 13.2 and 4.3 Hz) characteristic of H-10 with 124.2 ppm together with the COSY and HMBC correlations of the olefinic proton at 5.93 ppm with the oxymethine proton at 4.03 ppm and with the methine carbon at 51.3 ppm at C-8, respectively, corroborated the double bond position and the oxymethine group at C-7. The aldehyde group was found to be in position C-19 attached at C-9 (51.2 ppm), and the carboxylic acid at C-3 evidenced through ^{3}J HMBC correlations of the aldehyde carbon with protons H-8 and H-10 and carboxylic acid group with 4.82 ppm at C-3. This is the first report of a cucurbitane-type triterpene containing a carboxylic acid; hence compound **3** was identified and named charantoside XI. The complete 2D NMR of compound 3 are shown in **Figure A10-A13**. The structures of all the identified compounds are shown in **Figure 3**.

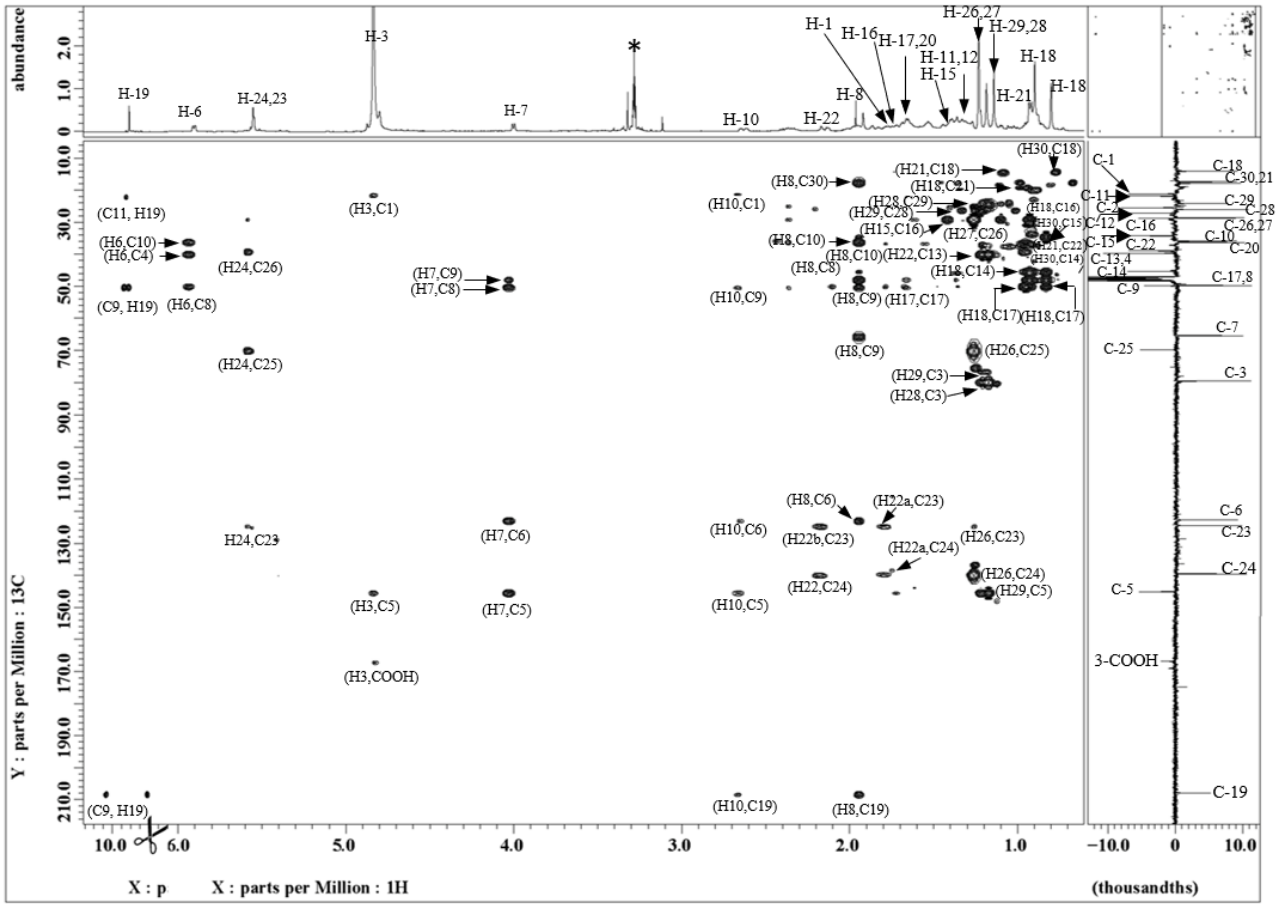

Figure 2 Complete assignments of HMBC spectra of compound 3 (charantoside XI). Spectra were recorded in MeOH-d4.1HNMR on X-axis and 13C attached proton test (APT) is on the Y-axis of the spectrum. The solvent signal is marked with an asterisk (*).

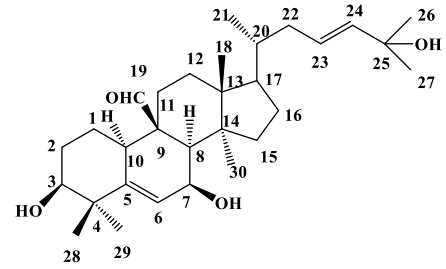

3β,7β,25-trihydroxycucurbita-5,23(E)-dien-19-al (1)

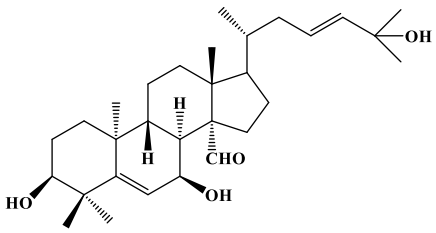

Charantal (2)

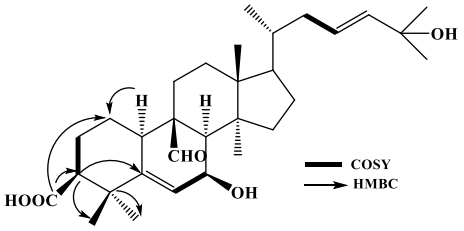

Charantoside XI (3)

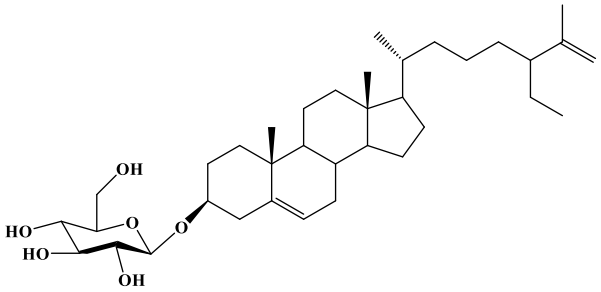

25ξ–isopropenylchole-5,(6)-ene-3-*O*-*β*–D-glucopyranoside (4)

Figure 3 Structures of identified compounds (1–4) from the EtOAc extract of Momordica charantia and important COSY and HMBC correlations in compound 3.

3.4.2 Inhibition of α-amylase and α-glucosidase activity

The inhibitory effect of purified compounds on α-amylase and α-glucosidase at two concentrations were tested and results were compared with acarbose (**Figure 4A**). Compounds **1-4** showed inhibition of 44-61% and 63-79% of α-amylase at 0.43 mM and 0.87 mM concentrations respectively. Acarbose exhibited significantly higher inhibitory activity (88%) at 0.13 mM. Among the isolated compounds, IDG showed the highest inhibitory activity (79%) followed by charantal (70%) and TCD (69%) against α-amylase at 0.87 mM concentration. The novel compound, charantoside XI, showed moderate inhibition of 62% against α-amylase.

Similarly, inhibition of α-glucosidase was evaluated at 0.67 mM, and 1.33 mM concentrations and results were compared with positive control acarbose at 0.06 and 0.13 mM (**Figure 4B**). Maximum of 81.9% inhibition was observed for acarbose at 0.13 mM, followed by IDG (71%), TCD (65%), charantal (60%) and charantoside XI (5%) at 1.33 mM. The inhibitory activity of compounds **1**–**4** may be due to their differences in structural configuration. Nevertheless, TCD has been demonstrated for reducing the blood glucose level in diabetes-induced male ddY mice and showed moderate anti-HIV activity with EC_{50} value of 25.62 μg/mL. [54, 114] In the present study, TCD showed good inhibitory activity against the two enzymes. Also, IDG showed significantly higher inhibition compared to the other compounds and comparable activity to that of acarbose. The suppression of salivary, pancreatic α-amylase and α-glucosidase in the brush border membrane of small intestine regulates the digestion of complex carbohydrates, which in

turn controls the blood glucose [115]. The inhibitory mechanism of these compounds may be due to conformational changes derived from the presence of a sugar moiety in IDG, possibly allowing the binding of IDG to these enzymes. A higher number of attachments of sugar moieties would be needed to further evaluate the influence of cucurbitane glycosides on the inhibition of these enzymes.

3.4.3 Molecular docking

3.4.3.1 Virtual molecular docking study for inhibition of α-amylase by the purified compounds

In order to predict the mode of interactions of compounds **1**–**4** with α-amylase, molecular docking was carried out using Autodock 4.2. The enzyme α-amylase is composed of A, B, and C domains. Domain A is the largest with residues 1–99 and 169–404. Domain A forms a central eight-stranded parallel β-barrel with active site residues Asp197, Glu233, and Asp300. Domain B is the smallest (residues 100–168) and forms a calcium binding site against the wall of the β-barrel of domain A. Protein groups making ligand interactions with this calcium include Asn100, Arg158, Asp167, and His201. Domain C (residues 405–496) is made up of an antiparallel β-structure and is loosely associated with domains A and B. [116] The refined α-amylase structure is well characterized and has a network of water molecules occupying the cleft of the active site and hydrogen-bonding with polar side chains of Asp300, Glu233, and Aspl97, with the chloride ligand

Asn298, and with the main chain through Ala307 N and Trp59. Also, the binding cleft is characterized by aromatic residues such as Trp58, Trp59, Tyr62, His101, Pro163, Ile235, Tyr258, His305, and Ala307. [117] The three main residues Aspl97, Glu233, and

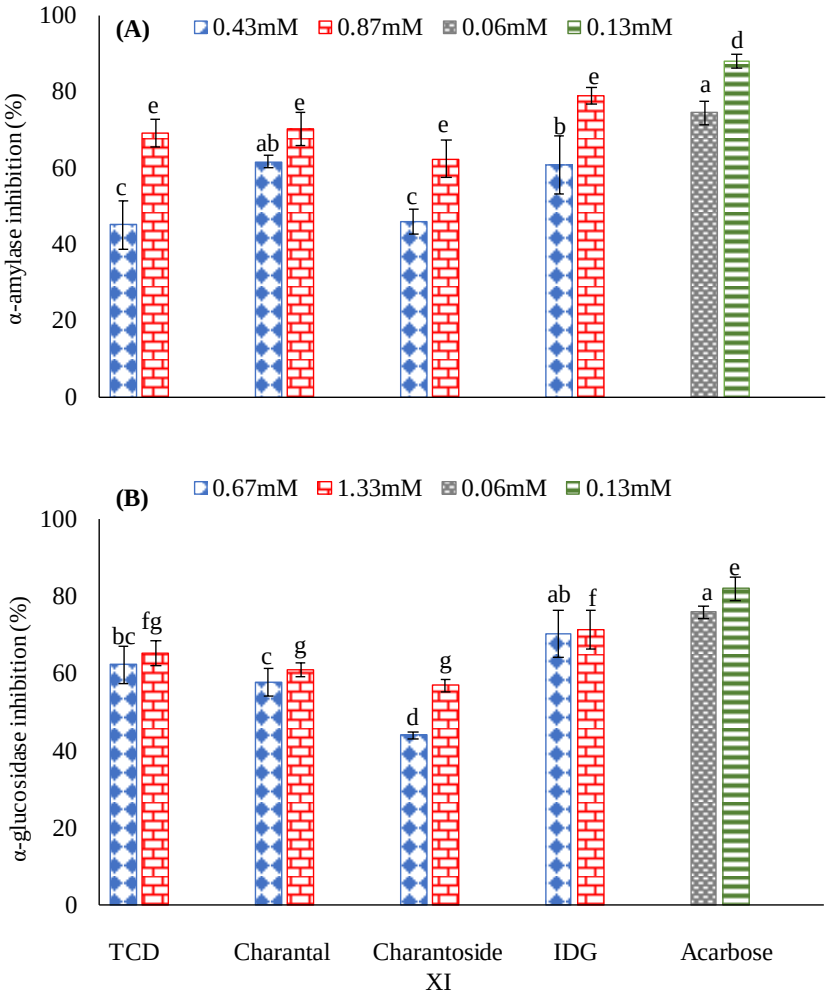

Figure 4 Effect of purified compounds on the inhibition of (A). α-amylase and (B). α-glucosidase, acarbose was used as a positive control and all the experiments were conducted in triplicate with two biological replications. The results are represented as means ± SD for (n=6). Identical letters at each concentration are not significantly different at $p \leq 0.001$. Abbreviations, TCD: (3β,7β,25-trihydroxycucurbita-5,23(E)-dien-19-al) and IDG: 25ξ-isopropenylchole-5, (6)-ene-3-O-β-D-glucopyranoside.

Asp300 are close together in the active site of α-amylase and are known as the binding cleft, which lies in a deep depression at the center of α-amylase. [118]

The results of the 2D and 3D molecular docking images of compounds **1**–**4** are shown in **Figure 5A–5D**. The 2D schematic ligand-protein complex images are shown in Fig. S9. All compounds were anchored to the catalytic site of α-amylase through various bonds. **Table 4** summarizes the binding affinity and binding interactions of purified compounds **1**–**4** with porcine pancreatic α-amylase (PDB ID: 1OSE). As shown in **Figure 5A**, the refined docking of TCD generated the best pose with a minimum binding energy of -10.55 kcal/mol. The 2D schematic **Figure A14A** and 3D diagram (**Figure 5A**) illustrate TCD inserted into the cavity of α-amylase. TCD interacted with amino acid residues Glu233, Ile235, Lys200, Tyr151, Gly306, His305, Trp59, Trp58, Val163, and Leu162 in domain A of α-amylase. Five conventional hydrogen bonds were found between TCD and amino acid residues (Glu233, Ile235, Tyr151, Gly306, and His305) with bond lengths of 4.02, 3.45, 6.84, 3.85, and 4.06 Å, respectively. These hydrogen bonds strengthened the interactions between TCD and α-amylase. The interactions of TCD include alkyl and pi-alkyl interactions between Trp59, Trp58, Val163, and Leu162.

Similarly, charantal bound to the active site of α-amylase with a binding energy -8.76 kcal/mol. As shown in **Figure 5B and Figure A14B**, charantal interacted with crucial amino acid residues including Trp58, His305, Trp59, Val163, Leu162, Lys200, His201, Ile235, and Glu240 in domain A of α-amylase. Hydroxyl groups at position C-3 and C-25 of charantal formed strong conventional hydrogen bonds with amino acid residues Trp59

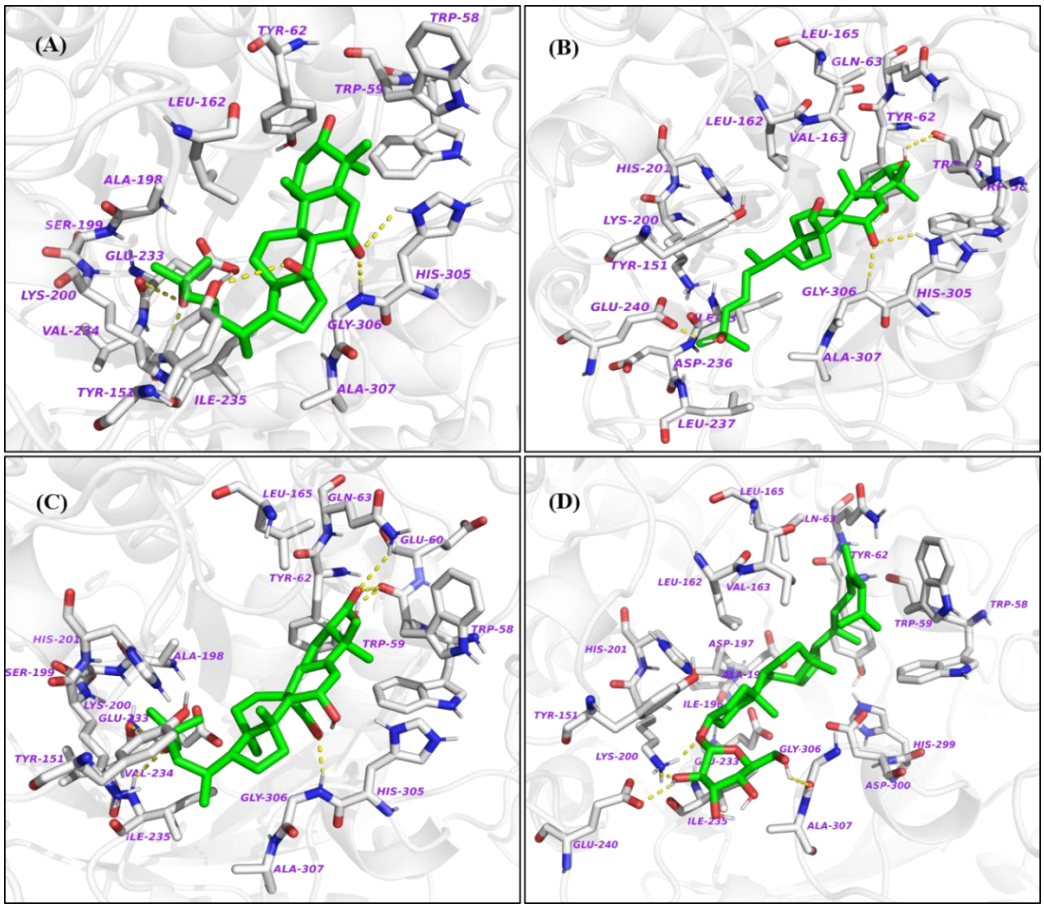

Figure 5 The 3D ligand-protein interactions for (A). 3β,7β,25-trihydroxycucurbita-5,23(E)-dien-19-al, (B). charantal, (C). charantoside XI, and (D). 25ξ-isopropenylchole-5, (6)-ene-3-O-β-D-glucopyranoside, in the binding pocket of α-amylase. The ligands in the 3D structure are shown in green and hydrogen bonds are shown in yellow.

and Glu240 with a bond length of 4.47 and 4.81 Å, respectively. We also observed pi-alkyl and alkyl interactions of charantal with several amino acid residues including Trp58, His305, Val163, Leu162, Lys200, His201, and Ile235 with bond lengths of 5.30, 5.25, 5.14, 4.69, 4.35, 5.85, and 4.08 Å respectively.

The refined docking of charantoside XI with α-amylase generated the best pose with a minimum binding energy of -9.79 kcal/mol. The 3D schematic in **Figure 5C** shows that charantoside XI established several hydrogen bonds within the α-amylase enzymatic pocket and interacted with several amino acid residues, including Glu233, Gly306, Trp59, Gln63, Trp58, His305, Val163, Leu162, and Ile235 (**Figure A14C**). Four conventional hydrogen bonds were established between charantoside XI and the active pocket of α-amylase, in which the carboxylic acid at position 3 formed H-bonds with Trp59 and Gly63 with a bond length of 4.23 and 4.29 Å, respectively. Similarly, hydroxyl groups at C-25 and the CHO group at C-19 position established hydrogen bonding with Glu233 and Gly306 with a bond length 3.26 and 3.75 Å, respectively. Charantoside XI also established pi-alkyl and alkyl interactions with Ile235, Leu162, Val163, His 305, Trp 58 with bond lengths of 4.69, 5.25, 5.76, and 5.78 Å, respectively.

Figure 5D displays a 2-D schematic interaction of IDG with α-amylase. IDG generated the best docking pose with a minimum binding energy of -11.98 kcal/mol, which indicates that IDG showed the strongest binding affinity with the α-amylase protein. The strong binding affinity may be related to IDG's high α-amylase inhibitory activity observed in our study (78.9%). IDG was found to anchor at the catalytic site of α-

amylase by making conventional hydrogen bonds to residues Gly306, Glu240, and Gly306 resulting in a potent inhibition of α-amylase.

3.4.2.2 Virtual molecular docking study for inhibition of α-glucosidase by the purified compounds

Similarly, to elucidate how the purified compounds interact with α-glucosidase, molecular docking analysis was carried out to investigate the binding mode of compounds within the binding pocket of α-glucosidase. To date, the crystal structure of α-glucosidase from *Saccharomyces cerevisiae* (the enzyme used for the biological assay) has not been resolved. Therefore, the compounds were docked to isomaltase crystal structure 3A4A downloaded from the Protein Data Bank. Isomaltase from *S. cerevisiae* co-crystallized with maltose has 85% similarity to yeast α-glucosidase (MAL12) through homology modeling [101]. Asp69, His112, Arg213, Asp215, Glu276, His351, Asp352, and Arg442 are key residues in the active catalytic site of α-glucosidase. [119] **Table 2** summarizes the binding affinity and binding interactions of purified compounds **1**–**4** with the crystal structure of isomaltase from *S. cerevisiae*.

Table 2 lists the binding energy of TCD, charantal, charantoside XI, and IDG with interacting residues, including H-bond interacting residues and Van der Waals interacting residues, along with the number of H-bonds. The 2D schematic and 3D interactions of TCD are shown in **Figure 6A** and **Figure A15A**. TCD interacted with crucial amino acid residues, namely Lys156, Ser241, Ser240, Asp307, Arg315, Phe303, Arg442, His280,

Asp242, and Tyr158. According to the Autodock 4.2 simulation results, the α-glucosidase–TCD inhibitor complex showed -10.87 kcal/mol binding energy. TCD made five hydrogen bonds with interacting residues Lys156, Ser241, and Asp305, and two hydrogen bonds with His 208. The hydroxyl group at position 25 established two hydrogen bonds with Lys156 and Ser241 with bond lengths of 4.34 and 3.97 Å, respectively. Similarly, the hydroxyl group at position 7 of TCD established two hydrogen bonds with His280 with bond lengths of 4.26, 5.38 Å. The aldehyde group at position 19 was able to establish a hydrogen bond with Asp 307 with a bond length of 5.74 Å. Moreover, the hydroxyl group at position 3 formed Van der Waals interaction with Arg442 with a bond length of 3.98 Å, which is critical interaction to inhibit enzyme to a greater extent. Charantal had binding energy of -10.78 kcal/mol and occupied the active region of isomaltase by interacting with amino acid residues Lys156, Phe303, Gly353, Glu411, Arg315, Tyr158, and Ser240. The 2D schematic (**Figure A15B**) and 3D interactions of charantal are shown in **Figure 6B**. In the conformation of isomaltase–charantal complex, the three hydroxyl groups at position 3, 7, and 25 of the ligands formed hydrogen bonds with the amino acid residues Lys156, Gln353, and Glu411 with bond lengths of 4.14, 4.53, and 4.61 Å, respectively. These hydrogen bonds overtly strengthened the interaction between charantal and isomaltase. Methyl and aldehyde groups at position 18 and 19 established strong Van der Waals bonding with amino acid residues Arg315 and Ser240 with bond lengths of 4.32 and 3.40 Å, respectively. The above interactions resulted in an inhibition constant of 12.91 nM.

Table 4 Binding affinity and binding interactions of purified compound (**1**–**4**) with porcine pancreatic α-amylase (PDB ID: 1OSE) and α-glucosidase (PDB ID: 3A4A)

Receptor	Compound	Binding energy (kcal/mol)	Hydrogen bonds	Interactions	Hydrogen bonds	Inhibition constant (nM)
α-Amylase (PDB ID:1OSE)	TCD	-10.55	5	Glu 233, Ile 235, Tyr 151, Gly 306, His 305, Trp 59, Trp 58, Val 163, Leu 162	Ile 235 (3.45 Å), Glu 233 (3.45 Å), Tyr 151 (6.84 Å), Gly 306 (3.85 Å), His 305 (4.06 Å)	18.53
	Charantal	-8.76	2	Trp 59, His 305, Trp 58, Ile 235, Lys 200, His 201, Leu 162, Val 163, Tyr 62	Glu 240(4.81 Å), Trp 59 (4.47 Å)	377.84
	Charantoside XI	-9.79	4	Glu 233, Gly 306, Gly 63, Trp 59, Gly 306, His 305, Val 163, Leu 162, Ile 235	Glu 233 (3.26 Å), Gly 306(3.75 Å), Trp 59 (4.29 Å), Gly 63 (4.23 Å)	66.39
	IDG	-11.98	4	Trp 59, Trp 58, His 305, Tyr 62, Leu 162, Ala 198, Gly 306, Glu 240 Lys 200, Ile 235, His 201, Leu 165, Val 163	Glu 240(4.81 Å), Trp 59 (4.47 Å), Lys 200 (5.82, 4.67 Å),	1.65
α-Glucosidase (PDB ID:3A4A)	TCD	-10.87	5	Lys 156, Ser 241, Asp 307, Arg 315, Phe 303, Arg 442, His 280, Asp 242, Tyr 158	Lys 156 (4.34 Å), Ser 241 (3.97 Å), Asp (4.26 Å), His 280 (5.38 and 5.74 Å)	10.68
	Charantal	-10.78	3	Ser 240, Lys 156, Phe 303, Gly 353, Glu 411, Arg 315, Tyr 158, Ser 240	Lys 156 (4.14 Å), Glu 411 (4.61 Å), Gly 353(4.53 Å)	12.48
	Charantoside XI	-10.4	4	Phe 314, Leu 313, Arg 315, Phe 159, Asp 69, Arg 442, Tyr 158, Phe 303, Phe 314	Leu 313 (5.10 Å), Asp 307 (5.00 Å), Asp 69 (4.60 Å), Arg 442(6.42 Å)	23.86
	IDG	-10.58	3	Leu 313, Asp 242, Pro 312, Val 308, Val 319, and His 280	Leu 313 (4.98 and 3.94 Å), Asp 242 (5.16 Å)	12.23

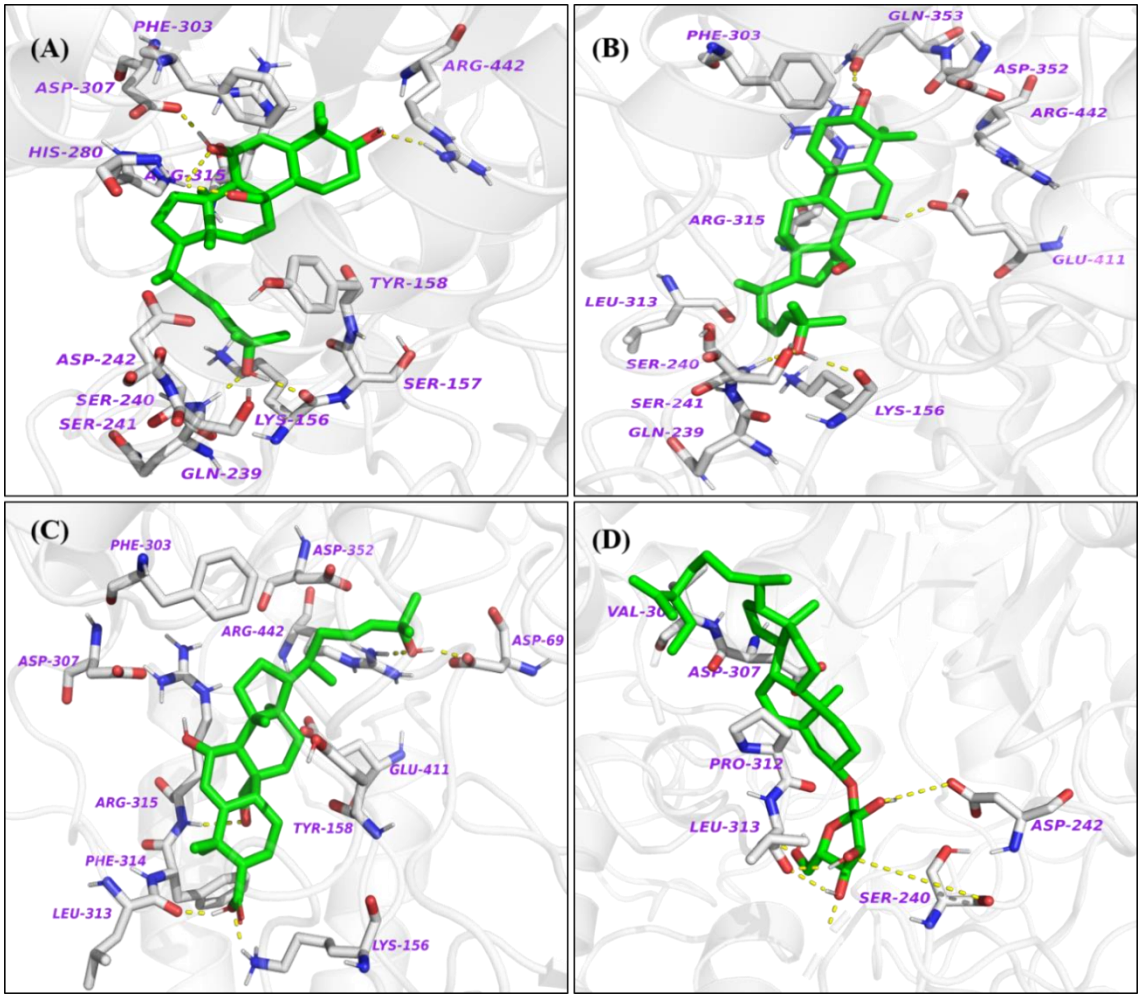

Figure 6 The 3D ligand-protein interactions for (A). 3β,7β,25-trihydroxycucurbita-5,23(E)-dien-19-al, (B). charantal, (C). charantoside XI and (D). 25ξ-isopropenylchole-5, (6)-ene-3-O-β-D-glucopyranoside, in the binding pocket of α-glucosidase. The ligands in the 3D structure are shown in green and hydrogen bonds are shown in yellow.

Figure 6C and Figure A15C shows the binding mode of charantoside XI in the active site of isomaltase. The ligand was stabilized in the active site of an enzyme by interacting with amino acid residues Phe314, Leu313, Arg315, Phe159, Asp 69, Arg442, Tyr158, Phe303, and Phe314. The carboxylic acid group at position 3, hydroxyl groups at positions 7 and 25, and the aldehyde group at position 19 formed five conventional hydrogen bonds with Asp307, Leu313, Arg315, Asp69, and Arg442 with bond lengths of 5.10, 5.00, 5.48, 4.60, and 6.42 Å, respectively. The interaction between the ligand and the catalytic residue Arg 442 was essential for the inhibition of isomaltase. The methyl groups at positions 18, 29, and 21 formed pi-alkyl interactions with amino acid residues Tyr58, Phe59, and Phe314. Finally, the binding energy was -10.4 kcal/mol and the inhibition constant was 23.86 nM.

IDG bound to residues Leu313, Asp242, Pro312, Val308, Val319, and His280 at the catalytic site of isomaltase. The 2D schematic and 3D interactions of IDG are shown in Fig. 5D. IDG generated the best docking pose with a minimum binding energy of -10.58 kcal/mol. The ligand was surrounded by catalytic residue Asp242, and the interaction was likely crucial for inhibition of the isomaltase. Three conventional hydrogen bonds were formed in which C-2’ and C-3’ on the sugar moiety formed H-bonds with Leu313 (3.94 and 4.98 Å) and Asp242 (5.16 Å). These hydrogen bonds strengthened the interactions between IDG and α-glucosidase. IDG formed pi-alkyl and alkyl interactions between Val308, Val319, and His280 with bond lengths of 4.63, 4.46, and 5.31 Å, respectively.

3.4.4 Gene expression

Four purified compounds from bitter melon were tested for anti-inflammatory activity in LPS-activated RAW 264.7 macrophages. All of the compounds tested differentially affect the expression of *NF-κB, iNOS, IL-6*, *IL-1β,* and *Cox-2* except *TNF-α*, which was not significantly different from the LPS control group regardless of the treatment (**Figure 7**). A significant decrease in expression of *NF-κB, iNOS, IL-1β,* and *Cox-2* was observed in the TCD treatment group when compared to the LPS control group. Similar results were observed in the cells treated with charantoside XI and IDG, except *NF-κB* displaying levels similar to the LPS control group. The expression of *iNOS, IL-1β,* and *Cox-2* was significantly lower compared to the LPS group, while the expression of *NF-κB* was not affected in the charantal treatment group. Surprisingly, the level of *IL-6* dramatically increased in response to treatment of cells with charantal. TCD, charantal, and charantoside XI are structurally similar; however, they differ in the position of the aldehyde and carboxylic acid groups, which may be responsible for their anti-inflammatory activity. TCD and charantoside XI have an aldehyde group at position 19 and both significantly down-regulated the expression of *NF-κB, iNOS, IL-1β, COX-2* compared to the LPS-treated control at 25 μM concentration. Charantal has an aldehyde group at position 30, and it was not observed to be significantly different from the LPS-activated cells for *NF-κB* and *TNF-α*. In charantoside XI, the presence of a carboxylic acid group at position 3 showed significant suppression of pro-inflammatory cytokines *iNOS, IL-1β,* and *Cox-2*. The IDG phytosterol glucoside did not induce significant suppression

of pro-inflammatory cytokines NF-κB, IL-6, and TNF-α. However, IDG treatment did downregulate *iNOS, IL-1β* and *Cox-2* compared to the LPS control group. IDG has a glucose moiety in position 3, while the other tested compounds have a hydroxyl or carboxylic acid group in that position. It is widely accepted that slight variation in the chemical structures of bioactive compounds can influence its activity. Our results show that regardless of the similarities of the triterpenoid nucleus, slight structural differences influence the expression of gene correlated to the regulation of the inflammatory response in RAW 264.7 macrophages.

Several triterpenoids have been isolated from various plants and evaluated for their bioactive potential. [120, 121] The structure-function activities of this class of compounds fluctuate in response to modifications to the 3 position. [122] In this study we observed that the glucose molecule attached to position 3 did not counteract the effect of LPS in inducing the expression of *NF-κB, IL-6,* and *TNF-α* and for the most part the effect of gene expression was not as pronounced at the other treatment compounds. Previous reports evaluating the bioactivity of triterpenoids have concluded that an increase in a number of glucose molecules or differences in its attached position may alter the compound's bioactivity by steric hindrance. Additionally, the change the number and position of hydroxyl groups may alter its polarity and in turn its interaction with membrane phospholipids, resulting in altered bioactivities. [123] Therefore, it is crucial to elucidate the composition of bitter melon metabolites further to understand better how these compounds may be used as beneficial treatments for the management of diabetes and other inflammation-mediated diseases. While more in-depth studies are required for a definitive

assessment of the anti-inflammatory properties of these compounds, this screening procedure is useful possibly narrowing down potential targets for further studies. For example, *NF-κB* is a significant component of the signaling cascade that lead to an inflammatory response resulting in the production of inflammatory cytokinins such as *iNOS, TNF-α,* and *IL-lβ*.

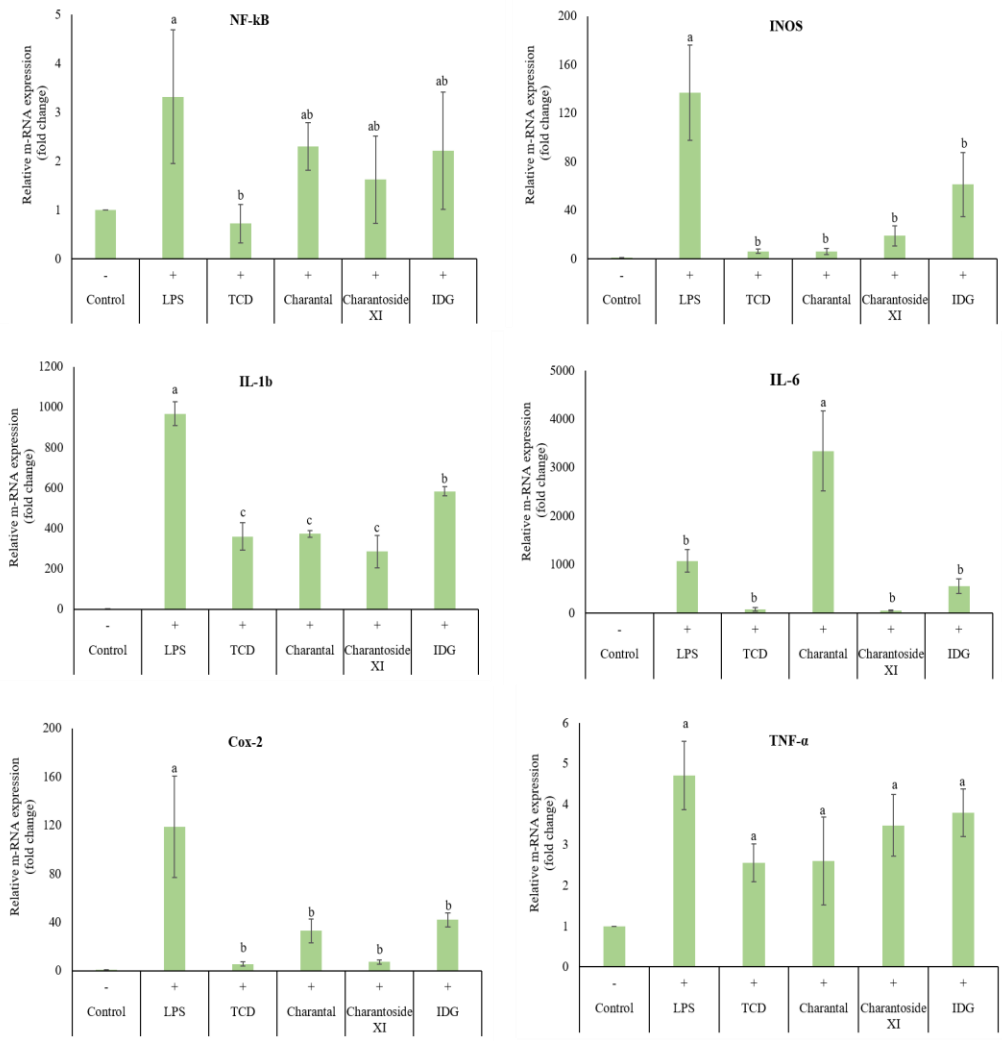

Figure 7 Effect of purified compounds on m-RNA expression of NF-κB, INOS, IL-1β, IL-6, Cox-2 and TNF-α in LPS induced murine macrophage RAW 264.7 cells. Data are expressed as mean ± SD for (n=9) and analyzed by one-way ANOVA. Identical letters within the same panel are not significantly different at $p \leq 0.001$ compared to LPS treatment group. Abbreviations TCD and IDG denotes 3β,7β,25-trihydroxycucurbita-5,23(E)-dien-19-al and 25ξ-isopropenylchole-5, (6)-ene-3-O-β-D-glucopyranoside, respectively.

3.5 Conclusions

In this study, a new cucurbitane-type triterpene aglycone and a known phytosterol, together with two previously identified compounds, were isolated from the fruit of *M. charantia*. These compounds showed variable α-amylase and α-glucosidase inhibitory activities, ranging from 56–79%. Our molecular docking studies for these enzymes revealed that all these compounds predominantly occupied the active site of the enzymes and formed H-bonds between the enzyme and hydroxyl groups in the cucurbitane skeleton. In the α-amylase molecular docking study, compounds **1**–**4** showed interactions with crucial amino acid residues including Glu233, Trp59 and showed binding energies between -8.76 and -11.98 kcal/mol with inhibition constants of 1.65–377 nM. Similarly, in the α-glucosidase molecular docking studies, compounds **1**–**3** showed interactions with crucial amino acid residue Arg442 and binding energies of -10.57 to -10.88 kcal/mol. Furthermore, the isolated compounds were screened for anti-inflammatory activities using RAW 264.7 macrophages. The results indicated that the compounds isolated from bitter melon have the potential to act as anti-inflammatory agents by lowering the expression of inflammation-related markers. Much more information is required to identify bitter melon as an antidiabetic agent positively, but the results of this study indicate that bitter melon, and compounds isolated from it, might have potential therapeutic uses.

CHAPTER 4

IN VITRO AND IN SILICO ANTIDIABETIC AND ANTI-INFLAMMATORY ACTIVITIES OF BIOACTIVE COMPOUNDS FROM MOMORDICA CHARANTIA

4.1 Synopsis

Bitter melon (*Momordica charantia*) is a tropical vegetable has been used to manage diabetes and related conditions. In the present study, ten compounds were isolated from acetone and methanol extracts of bitter melon. The chemical structures of compounds were unambiguously elucidated by 1D, 2D NMR, and high-resolution electrospray ionization mass spectrometry. All compounds exhibited significant inhibition of α-amylase activity and moderate inhibition of α-glucosidase activities. Momordicoside G (**5**) showed the highest α-amylase inhibition of 70.46% and 2-hydroxy-5-*O*-β-D-xylopyranosyl benzoic acid (**7**) showed the highest α-glucosidase inhibition of 56.37%. Furthermore, molecular docking studies of isolated compounds substantiated *in vitro* findings in which compounds **1–7** were able to bind to the active sites of both enzymes. Additionally, the isolated compounds significantly attenuated lipopolysaccharide (LPS)-induced inflammation, downregulating the expression of pro-inflammatory markers *NF-κB, INOS, IL-6, IL-1β, TNF-α*, and *Cox-2* in murine macrophage RAW264.7 cells activated by LPS. Moreover, 2-hydroxy-5-*O*-β-D-xylopyranosyl benzoic acid (**7**) was isolated for the first time, and it significantly suppressed the expression of *Cox-2* and *IL-6* compared to the LPS-treated group. Since α-amylase and α-glucosidase are targets of

anti-diabetes drugs, our findings suggest that compounds purified from bitter melon may have potential to use as functional food ingredients for the prevention and treatment of type 2 diabetes and related inflammatory conditions.

4.2 Introduction

Bitter melon *(Momordica charantia* L.,) is a popular vegetable that has good nutritional value and is typically used as a food in different parts of the world. [124] Moreover, bitter melon is commonly used for the treatment of diabeties and related conditions by indegenous populations of tropical and subtropical areas commonly used by indigenous populations of tropical and subtropical areas such as East Africa, Asia, South America, and the Caribbean. [21, 38] Previous *in vitro* and *in vivo* pharmacological investigations on *M. charantia* have demonstrated that the extracts and bioactive compounds help in regulating glucose uptake, [74, 75] stimulate insulin secretion from pancreatic cells, [62, 76] protect pancreatic β-cells from inflammatory conditions, [77] display insulin mimetic activities and reduce lipid accumulation in adipocytes. [78]

Bitter melon has recently received much attention due to its cucurbitane-type triterpenoids contents and their various biological activities. At latest count, more than 240 cucurbitane-type triterpenoids and their glycosides have been isolated and purified from various plant parts of bitter melons. [45, 125] These compounds exhibit several biological activities including anti-diabetic, [126, 127] antioxidant, [128] anti-inflammatory, [105] anti-cancer, [129, 130] anti-obesity, [131] and hypoglycemia activity. [132] However, very little is

known about the specific bioactive compounds responsible for these antidiabetics and the anti-inflammatory properties due to minute quantity of compounds available in bitter melons.

Despite significant developments over the last several years in treating type 2 diabetes, no curative agents responsible for reducing the risk of type 2 diabetes have been uncovered. The increase in diabetes rate has been primarily attributed to increased weight gain, leading to obesity. [133] Several synthetic drugs have been used to manage the disease including sulfonylureas, biguanides, thiazolidinediones, acarbose, and voglibose. [95] Some of these drugs may prevent, delay or mask the occurrence of type 2 diabetes in case of a patient with impaired glucose tolerance. However, current therapeutic approaches have not appreciably altered the high incidence of diabetic complications. [134] Several synthetic drugs are also associated with side effects such as hypoglycemia, weight gain, and other severe complications. These conditions demand the development of safe and biologically active natural antidiabetic drugs that have less adverse effects than existing synthetic medications.

Acute inflammation is a necessary part of the body's defense processes to eliminate injurious stimuli to initiate healing. In contrast, chronic inflammation (CI) has been correlated with various diseases and disorders. [135] Inflammation and its acute responses are well understood, whereas very little is known on the development and progression of chronic inflammation. During this process, an increase in macrophage cells plays an essential role in defense at the inflammatory sites. However, these macrophages also produce several toxins including reactive oxygen or nitrogen species. [136]

Macrophages at the inflammatory site further stimulate chronic inflammation, activating the expression of genes encoding cycloxygenase-2 (*COX-2*), inflammatory cytokines (*TNF-α* and *NF-κB*). [137] Chronic inflammtion is a common feature in the natural course of diabetes, and the inflammatory mediators correlate with diabetic incidence and prevalence. Inflammatory responses contribute to type 2 diabetes incidence by triggering insulin resistance, and in turn, they are intensified in the presence of hyperglycemia and promote long-term diabetic complications. [138]

The present paper reports the extraction, purification and structure elucidation of 10 compounds from the polar extracts of bitter melon. The purified compounds were evaluated for α-amylase and α-glucosidase inhibition assay for the first time and tested for molecular docking studies. Furthermore, purified compounds were evaluated for anti-inflammatory properties using lipopolysaccharide (LPS)-activated RAW264.7 macrophage cells. This is the first report on isolation and identification of 2-hydroxy-5-*O*-β-D-xylopyranosyl benzoic acid.

4.3 Materials and methods

4.3.1 General experimental procedures

The purification of compounds was carried out on a flash chromatography system (Combiflash Rf, Teledyne ISCO, Lincoln, NE, USA). An Agilent 1200 Series HPLC (Agilent, Foster City, CA) and using an RP C-18 Gemini series column (250 ×4.6 mm; 5

μm) (Phenomenex, Torrence, CA), with a flow rate of 0.8 mL/min was used for the analysis of individual fractions. Optical rotations for compound **7** was taken on a ATAGO SAC -i polarimeter in MeOH at 25 °C. UPLC-HRESIMS were recorded on a maXis impact mass spectrometer (Brucker Daltonics, Billerica, MA) coupled to a 1290 Agilent LC (Agilent, Santa Clara, CA) controlled by Bruker software (Bruker Compass DataAnalysis Version 4.2). The NMR spectra 1D (^{1}H; ^{13}C and DEPT 135) and 2D NMR spectra were recorded on a JEOL spectrometer (USA, Inc., Peabody, MA) at 25°C, operating at 400 MHz (^{1}H) and 100 MHz (^{13}C) using standard JEOL pulse programs. Chemical shifts are given in δ (ppm) and were referenced to CD_3OD (δ_H 3.31 and δ_C 49.15), and coupling constants are reported in *Hz*.

4.3.2 Plant material and extraction using Soxhlet apparatus

The unripened fruits of *M. charantia* (120 kg) were purchased from a local marketplace (BCS Food Market, College Station, TX). Seeds were separated, and fruits were cut into small pieces. Fruits were air dried and powdered (40–60 mesh size) using a Vita-prep™ blender (Vita-Mix Corporation, Cleveland, OH). Total fruit powder (5.6 kg) was extracted with acetone and methanol using a Soxhlet like an apparatus at 60–70°C for 32 h. Extracts were concentrated using rotary evaporator (Buchi, New Castle, DE), to obtain acetone and methanol extract of 33.8 g and 47 g respectively.

4.3.3 Fractionation of acetone extract

The acetone crude extract (33.8 g) was chromatographed over silica gel (2.5 Kg silica-gel 60 Å 40-63 µm) and was eluted with *n*-hexane, *n*-hexane/EtOAc (95:5, 90:10, 85:15, 80:20, 60:40, 50:50, 40:60, 25:75 and 0:100 v/v) and similar step gradient with EtOAc/acetone, acetone/MeOH to afford 54 fractions of 250 mL each. On the basis of TLC analysis, fractions were pooled and concentrated under vacuum to afford eight subfractions (A1-A8). The schematic procedure for fractionation of acetone crude extract of *M. charantia* is shown in **Figure. A11.**

4.3.4 Purification of cucurbitane triterpenes by flash chromatography

Subfraction A3 (7.24 g) was impregnated with 3g of silica gel and subjected to flash chromatography in a 240 g silica gel cartridge at 60 mL/min using a gradient program with *n*-hexane:EtOAc from 100–0% to 0-100 % and similar gradient was followed with EtOAc/acetone to afford 150 fractions of 1.5 l (150×15 mL each) and were pooled based on silica gel TLC profiles to give subfractions B1–B15. Fraction B8 (859 mg) was further subjected to cross column using reversed-phase C18 flash chromatography (RP-Cosmosil 140 C18 column of 43 g) using H_2O: MeOH (100–0%, 60 mL/min) linear gradient to afford 80 fractions, 1200 mL (80×15 mL each). Fractions were analyzed using HPLC and pooled based on HPLC retention times. Fractions 65-70, RT 14.2 min, H_2O: MeOH

(15:85) were pooled to yield compound **1** (12.3 mg), and similarly, fractions 71-77, RT 14.9 min, H2O: MeOH (05:95) were pooled to yield compound **2** (14 mg).

Similarly, subfraction A5 (7.48 g) was impregnated with 2.5 g of silica gel and subjected to flash chromatography in a 240 g silica gel cartridge, at 60 mL/min using a gradient with *n*-hexane/EtOAc from 100–0% to 0-100%. In total, 180 fractions, 2.7 l (180×15 mL each) were collected and pooled based on silica gel TLC profiles to give subfractions C1–C10. Fraction C7 was subjected to cross column using C18 reversed-phase flash chromatography using H_2O: MeOH (100–0% to 0-100%, 35 mL/min) to afford 120 fractions, 1.8 l (120×15 mL each) which were analyzed using HPLC. Fractions (104-107) yielded compound **3** (13 mg).

Similarly, subfraction A8 (11.32 g) was subjected to 320 g silica gel flash chromatography using *n*-hexane/EtOAc gradient elution from 100-0% to 0-100% at 200 mL/min followed with EtOAc/acetone (100-0% to 0-100%) to afford 240 fractions, 3.6 l (240x15 mL each). Based on silica TLC profile fractions were pooled into 13 subfractions (D1-D13). Fractions D9 (1.33 g) from this chromatography were subjected to repeated silica gel flash chromatography and C18 reversed-phase flash chromatography to afford compound **4** (22.7 mg) and compound **5** (46 mg). Fraction D11(921.3 mg) was further subjected to repeated flash chromatography over C18 reversed-phase silica gel flash chromatography using H_2O: MeOH; 0-100% to yield compound **6** (19 mg).

4.3.5 Fractionation methanol extract

MeOH extract of (47 g) was loaded to the activated dowex-50 (H^+) column. The eluate from the dowex column was connected to the SP-70 column. The dowex column was washed with excess water, and the eluate was then absorbed on the SP-70 column. Later SP-70 column was eluted with linear gradient mobile phases consisting of acetonitrile (ACN) in water. The eluants obtained using 100 % water were collected analyzed using HPLC and concentrated under vacuum to afford subfractions A1-A3. Fraction A1 of (2.3 g) was subjected to cross column using C18 reversed-phase silica gel flash chromatography (RP-Cosmosil 140 C18 column of 43 g) using H_2O: MeOH (100–0%, 35 mL/min flow rate) to afford compound **7** (33 mg). Furthermore, fraction A3 of (5.7 g) was subjected to cross column using reversed-phase C18 flash chromatography (RP-Cosmosil 140 C18 column of 43 g) using H_2O: MeOH (100–0%, 60 mL/min) to isolate and identify compounds **8**, **9** and **10**.

4.3.6 Determination of absolute configuration of the sugar

The compound **7** (1 mg) was hydrolyzed by heating in 1M HCl (0.1 mL) and neutralized with Amberlite IRA400. After sample mixture was dried *in vacuo*, the residue was dissolved in pyridine (0.1 mL) containing L-cysteine methyl ester hydrochloride (0.5 mg) and heated at 60 °C for 1 h. A 0.1 mL solution of *o*-torylisothiocyanate (0.5 mg) in pyridine was added to the mixture, which was heated at 60 °C for 1 h. Finally, the reaction

mixture was analyzed by reversed-phase HPLC. Xylose was identified by comparison of the HPLC retention times of thiocarbamoyl thiazolidine derivatives prepared from sugar standards.

4.3.7 α-amylase inhibition assay

To understand the hyperglycemic activities of isolated compounds α-amylase was carried out using a published protocol with minor modifications. [139] Purified compounds 10 and 20 µL (equivalent to 0.43 and 0.86 mM) was used in the assay and results were compared with acarbose (10 and 20 µl equivalent to 0.067 and 0.13 mM). All experiments were conducted in triplicates with three biological replications.

4.3.8 α-glucosidase inhibition assay

Similarly, α-glucosidase inhibitory activity was evaluated using a published protocol with slight modifications [109]. All experiments were conducted in triplicates with three biological replications. Compounds 10 and 20 µL (equivalent to 0.67 and 1.13 mM) were used and results were compared with positive control.

4.3.9 *In silico* molecular docking studies

To explore the potential molecular interactions between purified compounds with

α-amylase and α-glucosidase, a molecular modeling study was performed for both**.**

4.3.9.1 *Protein structure preparation*

The X-ray crystal structures of Porcine Pancreatic α-amylase complexed with acarbose (PDB ID: 1OSE) and for α-glucosidase, the crystal structure (PDB ID:3A4A) of isomaltase from *S. cerevisiae* proteins were downloaded from the RCSB protein data bank (http://www.rcsb.org/pdb) in PDB format. Later, both proteins were prepared by removing all water molecules, and a CHARMm force field was applied using the Receptor-Ligand interactions tool in DS (Biovia Discover4y studio 4.5 (DS 4.5, Dassault Systems BIOVIA, Discovery Studio Modeling Environment, Release 4.5, San Diego. 2015). Further, active residues of the crystal structure of 1OSE and 3A4A were identified using the Computer Atlas of Topography of Proteins (CASTp), a program for identifying and characterizing active protein sites, binding sites, and functional residues located on the protein surface.

4.3.9.2 *Preparation of ligands*

Two-dimensional structures of purified compounds were drawn using ChemDraw tool (PerkinElmer Informatics, 2016) and saved as a molecular format file (MDL MOL format). The “Prepare ligand” protocol of DS 4.5 was used to prepare the ligands which remove duplicate structures, standardizes the charges of common groups, calculates the

ions and ionization of the ligand's functional groups, 2D-3D conversion, verifying and optimizing the structures, and other tasks established by user-defined parameters. All the ligands were typed with the CHARMM36 force field using DS4.5 and saved as PDB format.

4.3.9.3 *Molecular docking*

The seven ligands were docked with α-amylase and α-glucosidase using the Lamarckian genetic algorithm (LGA) provided by the AutoDock 4.2 Program (ADT, version: 1.5.6). Polar hydrogens were added to the receptor, Kollman charges were assigned, and solvation parameters were added with the "Addsol" option in AutoDock. For the inhibitors, charges of the Gasteiger type were assigned. The internal degree of freedom and torsion were defined using the "Ligand Torsions" menu option of AutoDock. The grid maps representing the protein were calculated using the "AutoGrid" option. The protein was centered on the geometric center before docking, and the dimensions of the cubic grid box were set to 126 Å of x, y, and z with a spacing of 0.375 Å for both proteins. Blind Docking was carried over the whole receptors (i.e., 1OSE and 3A4A) using Genetic Algorithm. The best ligand-receptor structure from the docked structures was chosen based on the lowest energy and minimal solvent accessibility of the ligand. The 2D visualization of ligand interactions with the protein domain was analyzed using DS4.5, and PyMOL molecular graphics system (PyMOL Molecular

Graphics System, San Carlos, CA, USA) was used to visualize the 3D interactions between ligands and receptors better.

4.3.10 Cell culture

The RAW 264.7 mouse monocyte-macrophage cell line is cultured in RPMI 1640 medium (VWR International (Radnor, PA)) supplemented with 10% (*v/v*) fetal bovine serum and antibiotics (100 U/mL penicillin and 100 μg/mL streptomycin). Cells were maintained in a humified atmosphere with 5% CO_2 at 37 °C.

4.3.10.1 Quantitative real-time polymerase chain reaction (qRT-PCR)

RAW 264.7 cells were plated at 5.0×10^5 cells/well into 6-well plates and incubated at 37°C and 5% CO_2 for 24 h. Following incubation, the cells were treated with 25 μM of purified compounds (**1**–**7**) dissolved in DMSO for 1 h. After 1 h, LPS (1 μg/mL) was added to specified wells, and the cells were incubated for an additional 18 h. LPS was freshly prepared as stock solution in saline at 1μg/mL, and freshly diluted in complete media and added to the specified wells. Following the incubation period, media was aspirated, cells washed with PBS, and detached and collected. Total RNA was extracted using the Aurum Total RNA Mini Kit (Bio-Rad). RNA concentrations were determined using a Nanodrop Spectrophotometer (Thermo Scientific NanoDrop Products). Purified RNA (500 ng) from cell lysate was used to synthesize cDNA according to the

manufacturer's manual (iScript cDNA Synthesis Kit, Bio-Rad). Real-time PCR was performed on a Bio-Rad using the SYBR Green PCR Master Mix, according to the protocol provided by the manufacturer and relative expression was compared and normalized to the expression of GAPDH in the same sample. Primers sequences are available upon request.

4.3.11 Statistical analysis

Statistical analysis was performed using JMP Pro14 (SAS, NC, U.S.A.) statistical software. Results were analyzed for normality with Shapiro–Wilk test and the variance with the Brown-Forsythe test. Based on the results of the Brown-Forsythe test one-way analysis of variance (ANOVA) was run. To evaluate significance differences between means Tukey's HSD test was run. A p-value of $p< 0.001$ was accepted as statistically significant, results are expressed as mean ± SD.

4.4 Results and discussion

4.4.1 Isolation and Structural elucidation of compounds

Ten compounds were isolated from methanol and acetone extracts of bitter melon. A schematic diagram of the isolation of compounds **1-10** is shown in **Figure A16**. The acetone extract of bitter melon fruits was fractionated by large normal-phase silica gel

chromatography. HPLC was used analyze fractions, and fractions containing same peaks containing fractions were pooled, lyophilized further, and subjected to flash chromatography to obtain six mono glycoside cucurbitane-type triterpenes. Compounds **1-6**. Compounds **1-6** were characterized by 1D and 2D NMR and high-resolution mass spectroscopic data. The complete assigned ^{1}H and ^{13}C NMR spectra are presented in **Figure A17-A28** and the respective spectral data has been depicted in **Tables 5** and **6**. The high-resolution mass spectra of the compounds **1-10** were presented in **Figure A29**. On the basis of spectral data, compounds **1-6** were identified as momordicoside I, F_1, K, F_2, G and karaviloside XI, respectively. The chemical shifts were compared with reported values. [140, 141] The MeOH extract was subjected to flash chromatography to obtain compounds **7-10**. Compound **7** was isolated as an amorphous white powder with optical rotation $[\alpha]^{25}_{D}$ +46.9 (*c* 0.1, MeOH). High-resolution electrospray ionization mass spectrometry (HR-ESIMS) and HR-ESIMS/MS data of compound **7** in negative ion mode showed a molecular ion at *m/z* 285.0602 $[M-H]^-$ (calculated *m/z* 285.0611 $[M-H]^-$), suggesting a molecular formula $C_{12}H_{14}O_8$. The loss of one pentose was observed through the fragment at *m/z* 152.0105 $([M-H]-H_2O-132\ Da)^-$ with a further loss of -COOH evidenced for the fragment at *m/z* 108.0210 $([M-H]-44\ Da)^-$. Acid hydrolysis of **7** furnished D-xylose, which was identified by comparison of the HPLC retention times of thiocarbamoyl thiazolidine derivatives prepared from sugar standards as previously described. [142] ^{1}H NMR data showed two main groups of signals, one related to an aromatic region and the second one due to sugar region. The aromatic protons exhibited a typical ABX substitution pattern, δ_H 6.86 d, (*J*= 9.0 Hz), 7.24 dd (*J*=9.0 and 3.0 Hz) and 7.54 d

(*J*=3.0 Hz). An anomeric proton was also observed at δ_H 4.73 ppm with a beta linkage due to the large coupling constant. DQFCOSY showed two aromatic spin systems through correlation among the three aromatic protons and also among the sugar protons. The HMQC spectra was used to assign direct C-H correlations (**Figure 8A**), indicating δ_C 114.1; 151.1 and 158.9 ppm as quaternary carbons and 173.3 ppm as a carbonyl group from a carboxylic acid, according to HR-ESI-MS/MS. Cross-peak ^{3}J HMBC correlations were used to assign the aromatic ring, 7.54 ppm showed correlations with 158.9 ppm and the carbonyl group at 173.3 ppm, indicating that the carboxylic acid group is *ortho* to H-6. In the same way, 7.24 ppm (H-4) showed ^{3}J HMBC correlations with 119.1 (C-6) and 158.9 ppm (C-2), and 6.86 showed ^{3}J HMBC correlation with 114.1 ppm (C-1) and 151 ppm (C-5) (**Figure 8B**). The xylose was found to be attached at δ_C 151 ppm due to the HMBC cross-peak with the anomeric proton (4.73 ppm). DQFCOSY showed the correlation between the anomeric proton and 3.40 ppm (74.8 ppm) and 3.92 ppm (H-5) with 3.59 ppm (H-4). Additionally, ^{3}J HMBC correlation between 77.8 ppm with 3.92 ppm corroborated the position 3 of the sugar. Thus, compound 7 was named as 2-hydroxy-5-*O*-β-D-xylopyranosyl benzoic acid, shown in **Figure 9**. HPLC-UV, HRESIMS, fully assigned 1D, 2D NMR data for compound **7** were shown in **Figure A30-A34**. ^{1}H and ^{13}C chemical shifts are presented in **Table 5** and **6** respectively. This is the first report on the isolation and structure elucidation of compound **7**.

Table 5 ^{1}H NMR data for compounds (1-7) from acetone extract of Momordica charantia, (MeOD, 400 MHz, δ in ppm)

	1	**2**	**3**	**4**	**5**	**6**	**7**
1	1.39;1.39 m	1.40;1.40 m	1.63 m;1.63 m	1.44; 1.13 m	0.92; 1.42 m	1.45; 1.45	-
2	0.93;1.01 m	1.76;2.12 m	1.69m; 1.69m	2.16; 1.79 m	2.12; 2.16 m	2.75; 1.78	-
3	3.37 s	3.39 br s	3.55 br s	3.40 m br s	3.39 br s	3.41 br s	6.86 d (*J*=9.0 Hz)
4							7.24 dd (*J*=9.0; 3.0 Hz)
6	6.02 dd (*J*=9.9;1.9 Hz)	6.09 dd (*J*=9.8; 1.8 Hz	5.97 d (*J*=4.4 Hz)	5.65 m	5.63 m	6.09 d (1H, *J*=9.3 Hz)	7.54 d (*J*=3.0 Hz)
7	5.55 dd (*J*=9.8;3.8 Hz)	5.63 dd (*J*=9.9; 3.8 Hz)	4.18 d (*J*=5.6 Hz)	6.10 d (*J*=10 Hz, 1H)	6.09 d (*J*=10 Hz, 1H)	5.63 dd (*J*=3.9, 9.5 Hz)	-
8	2.33 m	2.40 m	1.60 m	2.40 br s	2.38 br s	2.42 br s	-
10	2.24 (*J*=10.6, 3.9Hz)	2.26 m	2.57 dd (*J*=4.4 Hz,4 Hz)	2.29 m	2.26 m	2.31 m	-
11	1.49; 1.69 m	1.72; 1.77 m	1.45 m; 1.45 m	1.74; 1.74 m	1.71; 1.75 m	1.75; 1.53 m	-
12	1.56; 1.72 m	1.62;1.74 m	1.26 m; 1.26 m	1.64; 1.77 m	1.57; 1.72 m	1.69; 1.69 m	-
14							-
15	1.32; 1.32 m	1.35; 1.35 m	1.40 m; 1.40 m	1.36; 1.36	1.32; 1.34 m	1.37; 1.37 m	-
16	0.86; 1.23 m	1.36;1.36 m	1.39 m; 1.39 m	1.30; 1.30	1.27; 1.27 m	2.04; 1.51 m	-
17	1.51 m	1.53 m	2.10 m	1.55 m	1.49 m	1.49 m	-
18	0.84 m	0.93 m	0.94 s	0.93 s	0.91 s	0.96	-
19	3.14; 3.46 m	3.52 d (*J*=8.0 Hz); 3.65 m	9.85 s	3.53; 3.66 m	3.49; 3.63 m	3.67; 3.53 d (*J*=7.9 Hz)	-
20	1.50 m	1.59 m	1.58 m	1.54 m	1.59 m	1.75 m	
21	0.86 s	0.93 m	0.96 d (*J*=4 Hz)	0.95 m	0.92 m	0.99 (*J*=6.3 Hz)	-
22	2.13; 2.09 m	1.80;1.88 m	2.26 m; 2.20 m	1.82; 2.21 m	1.86; 2.19 m	1.94; 0.95 m	-
23	5.50 m	5.57 dd (*J*=8.7;5.8 Hz)	5.59 m	5.59 m	5.58 dd (*J*= 16 Hz, 4 Hz, 1H)	4.06 (1H, ddd like)	-
24	5.50 m	5.37 d (J=15.8 Hz)	5.40 d (*J*=16 Hz)	5.6 (*J*=14.9 Hz)	5.46 d (*J*= 16 Hz, 1H)	3.05 (1H, d - like)	-
26	1.18 s	0.93 m	1.25 s	1.27 s	1.24 s	1.27 s	-
27	1.18 s	1.24 s	1.25 s	1.27 s	1.23 s	0.95 s	-
28	0.84 m	1.12 s	1.25 s	1.28 s	1.11 s	0.95 s	-
29	1.17 s	0.93 m	1.09 s	0.95 s	0.92 s	1.24 s	-
30	1.05 s	0.93 m	0.83 s	0.92 s	0.89 s	1.14 s	-
OCH_3			3.14 s		3.13 s		-
			7-O-β-Glc	3-O-β-All	3-O-β-All	3-O-β-All	-
1'	4.2 d (J= 8.0 Hz)	4.23 d (*J*=8.0 Hz)	4.24 d (*J*=8 Hz)	4.63 d (*J*=8 Hz, 1H)	4.64 d (*J*=8 Hz, 1H)	4.64 d (*J*=7.9 Hz, 1H)	4.73 d (*J*= 8.0Hz)
2'	3.19 m	3.20 m	3.14 m	3.34	3.32	4.08	3.40 m
3'	3.20 m	3.22 m	3.24 m	4.07	4.04	3.35	3.40 m
4'	3.29 m	3.32 m	3.25 m	3.46	3.47	3.48	3.59 m
5'	3.32 m	3.35 m	3.35 m	3.67	3.64	3.68	3.92; 3.31
6'	3.77; 3.60 m	3.86; 3.64 dd (J=11.6;2.4 Hz)	3.90 dd; 3.64 m (J=12 Hz, J=2.1 Hz)	3.64; 3.86 m	3.61; 3.81 m	3.81; 3.65 m	-

Table 6 ^{13}C NMR data for compounds (1-7) from acetone extract of Momordica charantia (MeOD, 100 MHz, δ in ppm)

Position	**1**	**2**	**3**	**4**	**5**	**6**	**7**
1	19.6	19.6	22.5	19.6	19.6	19.6	114.1
2	28.3	28.3	30.3	28.3	28.2	28.3	158.9
3	87.2	87.1	77.2	87.2	87.2	87.2	119.0
4	39.9	39.9	42.5	39.8	39.8	39.8	127.1
5	87.9	87.9	148.1	87.9	87.9	87.9	151.1
6	134.0	134.0	123.5	131.6	131.6	134.1	119.1
7	131.7	131.6	73.6	134.1	134.1	131.7	-
8	53.5	53.4	51.4	53.5	53.5	53.5	-
9	46.6	46.6	51.4	50.0	50.0	46.1	-
10	41.1	41.1	37.5	41.1	41.1	41.1	-
11	24.8	24.7	23.3	24.8	24.8	24.8	-
12	32.1	32.1	30.0	32.1	32.1	32.4	-
13	46.1	46.1	47.1	46.1	46.1	46.7	-
14	50.0	50.0	48.5	46.6	46.6	50.0	-
15	34.5	34.5	35.9	34.5	34.5	34.4	-
16	29.2	29.2	28.5	30.9	30.9	29.3	-
17	51.4	51.4	46.8	51.4	51.4	52.7	-
18	15.6	15.6	15.6	15.6	15.6	15.6	-
19	80.9	80.9	210.3	80.9	80.9	80.9	-
20	37.7	37.5	37.6	37.7	37.9	33.5	-
21	19.3	19.4	19.4	19.3	19.3	19.2	-
22	40.4	40.6	40.6	40.5	40.6	43.5	-
23	126.0	130.1	130.2	126	130.2	68.6	-
24	141.0	137.8	137.8	141	137.8	80.3	-
25	71.3	76.6	76.6	71.3	76.7	74.7	-
26	30.3	26.7	26.6	30.3	26.3	27.5	-
27	30.2	26.4	26.4	30.2	20.6	26.4	-
28	20.8	20.5	26.2	29.2	26.3	20.8	-
29	26.4	26.2	28.0	26.4	26.4	26.3	-
30	20.5	20.8	19.0	20.8	20.8	20.6	-
25-OCH_3		76.6	76.6		50.7		-
Sugar	3-O-β-Glc	3-O-β-Glc	7-O-β-Glc	3-O-β-All	3-O-β-All	3-O-β-All	-
1′	107.8	107.8	102.3	105.1	105.1	105.1	104.3
2′	75.4	75.4	75.1	72.6	72.6	73.0	74.8
3′	77.9	77.9	78.3	73.0	73.0	72.6	77.8
4′	71.9	71.9	71.8	69.1	69.2	69.2	71.1
5′	77.7	77.7	78.2	75.4	75.4	75.4	67.0
6′	63.0	63.0	63.0	63.4	63.4	63.4	-
-COOH							173.3

Compounds **8-10** were isolated from methanol extract and identified using HR-ESIMS and NMR; results were compared with published literature. [143, 144] Based on these data, compounds **8-10** were identified as benzoic acid (**8**), quercetin 7-*O*-β-glucopyranoside (**9**) and phenylalanine (**10**) respectively.

4.4.2 In vitro inhibition activity of α-amylase and α-glucosidase

Anti-diabetic compounds often inhibit carbohydrate-degrading enzymes; therefore we tested compounds **1-7** for inhibition of α-amylase and α-glucosidase activity, compared with the known inhibitor acarbose. In the α-amylase inhibition assay, purified compounds **1-7** exhibited significant inhibition of α-amylase at 0.43 mM and 0.87 mM, ranging between 63-70 % but lower than acarbose (88% inhibition at 0.13 mM). However, higher inhibition was observed at 0.87 mM. Among momordicoside G (**5**) showed highest α-amylase inhibitory activity (70.5%), followed by momordicoside K (**3**) (69.0%), karaviloside XI (**6**) (66.4%), momordicoside I (1) (64.2%), momordicoside F_2 (**4**) 63.7%), momordicoside F_1 (**2**) (63.5%), and 2-hydroxy-5-*O*-β-D-xylopyranosyl benzoic acid (**7**) (60.7%) (**Figure 10A**).

Similarly, the purified compounds **1–7** showed moderate inhibition of α-glucosidase at 0.67 and 1.33 mM. Among the tested compounds, 2-hydroxy-5-*O*-β-D-xylopyranosyl benzoic acid (**7**) showed maximum (56.4%) inhibition followed by karaviloside XI (6) (49.4%), momordicoside G (**5**) (48.5%), momordicoside K (**3**) (47.5%), momordicoside F_2 (**4**) (42.4%), momordicoside F_1 (2) (35.9%), and

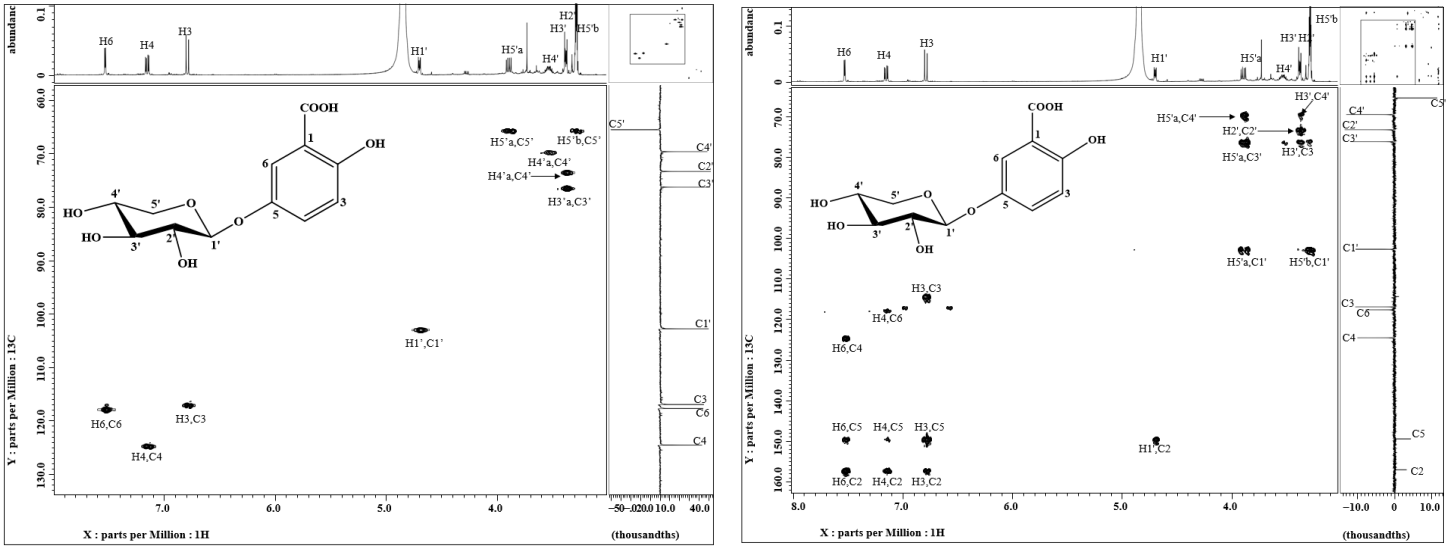

Figure 8 Complete assignments of (A). HMQC spectra, traces of one-dimensional 1H spectrum and 13C DEPT-135 spectrum (CH negative C and CH2 negative) are also shown, (B). HMBC spectra and 1H-NMR on X-axis and APT is on Y-axis of the spectrum of 2-hydroxy-5-O-β-D-xylopyranosyl benzoic acid. Spectra were recorded in MeOD.

momordicoside I (**1**) (35.1%) at 1.33 mM. In both enzymatic assays, momordicoside G (**5**) and karaviloside XI (**6**) showed maximum inhibition. (**Figure 10B**). In both enzymatic assays, momordicoside G (**5**) and karaviloside XI (**6**) showed relative maximum inhibition.

Bitter melon has gained much attention for the treatment of diabetes mellitus. The inhibition of the carbohydrate digesting enzymes helps in reducing post-prandial blood glucose by delaying starch hydrolysis. The beneficial effects of the bitter melon extracts and the mechanism with which it treats diabetes mellitus have been extensively studied. [145, 146] A previous study reported momordicoside G, I, F_1 and F_2 as weak α-glucosidase inhibitors. In the same study, more polar compounds, momordicoside A and M, which have two sugar moieties at the C-3 position and multiple hydroxyl groups, showed stronger α-glucosidase inhibitory activity (21.71% and 18.63% inhibition at the concentration of 50 μM). [126]

Karaviloside XI has a sugar moiety at C-3 and three hydroxyl groups at position C-24, 25 and 26 showed strong α-glucosidase inhibitory activity compared to other cucurbitane mono glycosides. Another study on α-glucosidase inhibitory activity demonstrated that compounds bearing a *β*-D-allopyranosyl group at C-3 exhibited higher inhibitory activity than compounds bearing a *β*-D-glucopyranosyl group at C-3. Interestingly, we observed a similar trend in our study where momordicoside G (**5**) and karaviloside XI (**6**) were the most active compounds against both the enzymes (**Figure 10**). The higher inhibitory activity of momordicoside G and karaviloside XI compared to other compounds suggested that attachment of the *β*-D-allopyranosyl group at C-3 has a

notable effect on the inhibitory activity against both the enzymes. Also, momordicoside F_1, K, I and G showed weaker α-amylase activity compared to acarbose at 100 µM. [147] However, in the present study, all compounds **1-7** showed significant effects and exhibited the same potency of α-amylase inhibition at 0.87 mM.

4.4.3 Molecular docking study

4.4.3.1 Virtual screening of α-amylase inhibitors

Molecular docking uses chemometrics methods to simulate, identify and predict the structure of receptor-ligand complex according to the lock and key principle of .[148] Therefore, we used *in silico* by molecular docking to examine the inhibitory activity of compounds **1–7** towards α-amylase and α-glucosidase.

Molecular docking for α-amylase was conducted with the crystal structure of porcine pancreatic α-amylase (PDB ID:1OSE), downloaded from the protein data bank. The refined α -amylase structure is well characterized and has a network of water molecules occupying the cleft of the active sites and hydrogen-bonding with polar side chains of Asp300, Glu233, and Aspl97, with the chloride ligand Asn298, and with the main chain through Ala307 N and Trp59. Also, the binding cleft is characterized by aromatic residues such as Trp58, Trp59, Tyr62, His101, Pro163, Ile235, Tyr258, His305, and Ala307. [149]

Binding energies of compounds **1-7** ranged from -8.23 to -11.83 kcal/mol. The likeliest docked poses of compounds with best binding affinity for α-amylase at the catalytic site were selected and are shown in **Figure 11(A-G)**. Momordicoside K (**3**) showed the lowest binding energy (-11.83 kcal/mol), followed by momordicoside G (**5**) (-10.76 kcal/mol), karaviloside XI (**6**) (-10.48 kcal/mol), momordicoside I (**1**) (-10.27 kcal/mol), momordicoside F_1 (**2**) (-10.11 kcal/mol), momordicoside F_2 (**4**), and 2-hydroxy-5-*O*-β-D-xylopyranosyl benzoic acid (**7**) (-8.23 kcal/mol). Lower binding energy corresponds to easier binding of a ligand to the protein. Hence momordicoside K is most favorable to bind with the α-amylase. Furthermore, a detailed analysis of the docked poses regarding ligand-protein binding energy, the number of H-bonds, and the inhibition constant are shown in Table 3. In **Figure 11 (A-G)** the ligand in the active site of α-amylase is displayed as a stick model and colored green. The carbon, hydrogen and oxygen atoms on an amino acid residue are displayed as white, blue and red, respectively. The hydrogen bonds are shown in yellow dashed lines to judge interaction between receptor and ligand.

As shown in **Figure 11(A-G)** and **Figure A35 (A-G),** compound **1-7** were surrounded by crucial amino acid residues including Asp300, Glu233, Asp197, Gly308, Gly306, Gly238, Trp58, His305, Trp59, Val163, Leu162, Lys200, His201, Ile235, and Glu240 in domain A of α-amylase. The docking result **Figure 11(A-G**) showed that the binding site on α-amylase for momordicoside I, F_1 K, F_2, G, karaviloside XI, and 2-hydroxy-5-*O*-β-D-xylopyranosyl benzoic acid were same as the binding site of acarbose from the previous research. Indeed, acarbose, a standard antidiabetic drug to treat Type II

diabetes via inhibiting α-amylase, was found to be an anchor at enzymatic pocket (domain A) of α-amylase and bound to residues including Asp197, Glu233, and Asp300, resulting in potent inhibition of α-amylase [150]. These residues are believed to play crucial roles in the catalytic mechanism of α-amylase. Moreover, it was observed that the binding site for compounds **1-7** was inside the binding site pocket of α-amylase by forming various hydrogen bonds. Momodicoside I (**1**) was surrounded by Glu233, Arg195, Gly306, Gly308, Asp300, and His305 respectively. Similarly, the refined docking of momordicoside F_1 (**2**) with α-amylase (**Figure 11B** and **Figure A35B**) generated the best pose with minimum inhibition constant of 39.1 nM. Momordicoside F_1 was surrounded by Asp197, Asp300, Gly308, and His307 respectively. We also observed strong Van der Waals bonding with amino acid residues including Glu233, Leu162, and Glu240.

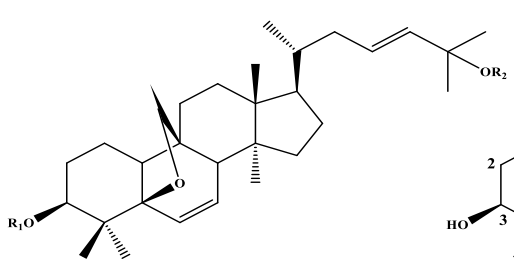

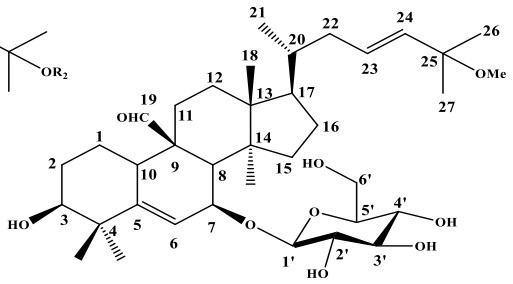

1. R_1=Glc R_2=OH (momordicoside I)
2. R_1=Glc R_2=OMe (momordicoside F_1)
4. R_1=All R_2=OH (momordicoside F_2)
5. R_1=All R_2=OMe (momordicoside G)

3. momordicoside K

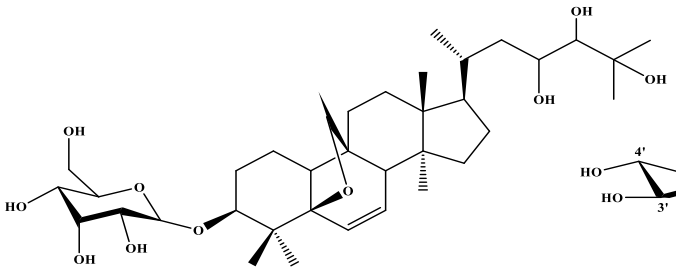

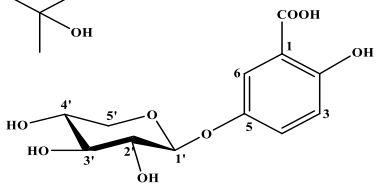

6. karaviloside XI

7. 2-hydroxy-5-*O*-*β*-D-xylopyranosyl benzoic acid

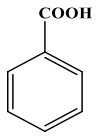

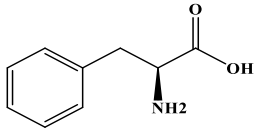

8. benzoic acid

9. phenylalanine

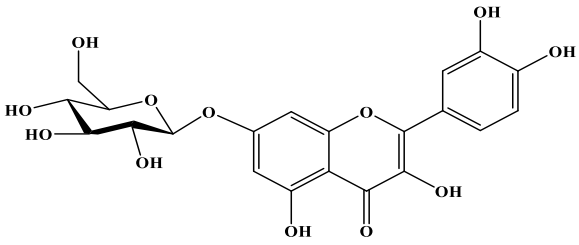

10. quercetin-7-*O*-*β*-D-glucopyranoside

Figure 9 Chemical structures of isolated compounds (1–10) from the acetone extract of Momordica charantia

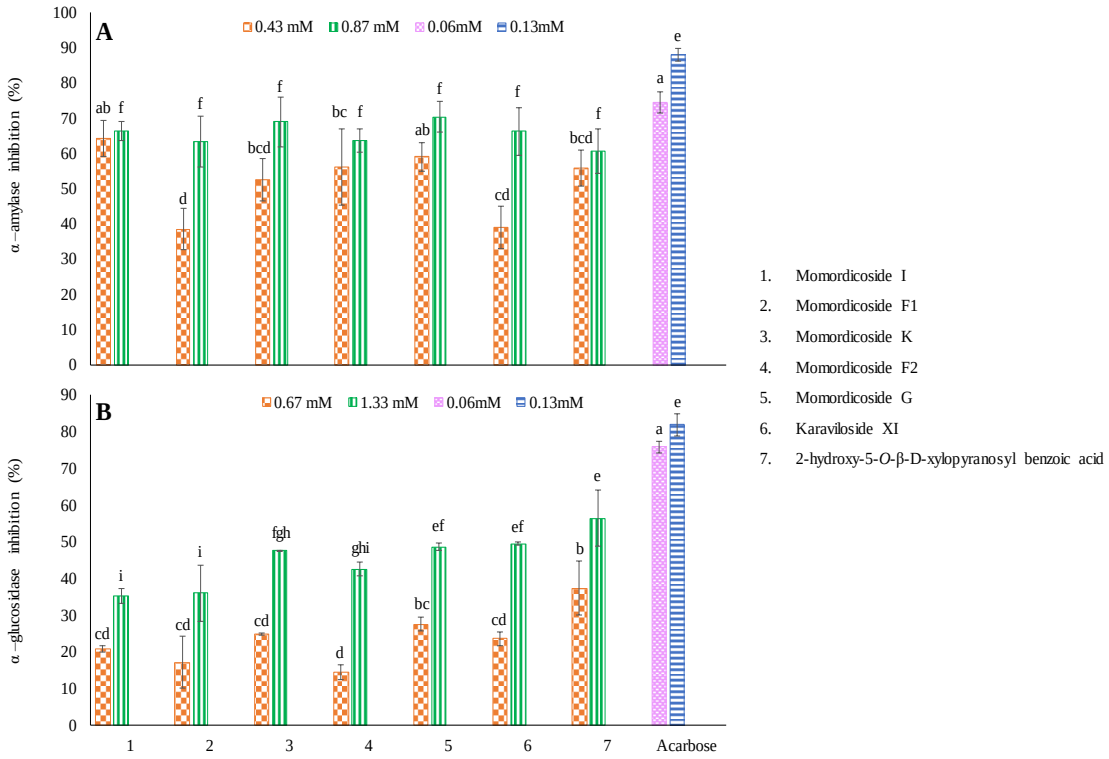

Figure 10 Effect of purified compounds (1-7) on the inhibition of (A). α-amylase (B). α-glucosidase. Acarbose was used as a positive control, and all the experiments were conducted in (n=3), biological replications), (n=3) test replications and analyzed by one-way ANOVA. The results are represented as means ± SD and analyzed by one-way ANOVA. Identical letters at each concentration are not significantly different at $p \leq 0.001$.

Moreover, its docking score was -10.11 kcal/mol, having a notable *in vitro* inhibition activity of α-amylase (63.5 %). On the other hand, momordicoside K (**3)** showed a potential inhibition activity of amylase (68.98%), and its docking score on this enzyme is the first among the other six scores (-11.83 kcal/mol). It was entirely wrapped in the active site of α-amylase by surrounding Asp197, Glu233, His201, Gly306, His101, Arg195, Tyr151, and Gly104 and His305. Momordicoside F_2 (**4**) formed four hydrogen bonding with the α-amylase enzyme and had the binding energy of -9.58 kcal/mol which was the second least among the other six compounds. MomordicosideF_2 (**4)** was surrounded by Asp300, Gly238, Gly306 respectively (**Figure 11D** and **Figure A35D**). Moreover, momordicoside F_2 (**4)** showed comparable inhibition activity of 63.65% with compound **2**. Momordicoside G (**5**) with the binding energy of -10.76 kcal/mol occupied the active region of α-amylase by making two hydrogen bonds between Asp300 and Asp197 and C-6', C-2' respectively. (**Figure 11E** and **Figure A35E**). These hydrogen bonds overtly strengthened the interaction between momordicoside G and the enzyme catalytic site. Also, momordicoside G showed an excellent % α-amylase inhibition activity (70.46%) which was the highest among the other six compounds. Similarly, karaviloside XI (**6**) was bound to the active site of α-amylase with a binding energy of -10.48 kcal/mol. Karaviloside XI (**6)** was surrounded by Asp197, Asp300, Glu240 respectively **(Figure 11F** and **Figure A29F**). These strong hydrogen bonds with the enzyme catalytic site were responsible for inhibiting the activity of α-amylase. **Figure 11G** and **Figure A35G** shows the binding mode of 2-hydroxy-5-*O*-β-D-xylopyranosyl benzoic acid (**7**) in the active site of α-amylase with an inhibition constant of 925.37 nM. The ligand was stabilized in the

active site of an enzyme by interacting with key amino acid residues Glu233, Ile235, Asp197, Arg195, His299, Tyr62, and Asp300. Based on the previous investigations, the present molecular docking, and *in vitro* assay study results, we concluded that the robust *in vitro* α-amylase inhibitory activity of compounds **1-7** might be due to binding to the side chain of Glu233, or Asp 197, and Asp 300 of α-amylase. In docking studies between flavonoids and human pancreatic α-amylase Asp197, Glu233, and His305 were reported to be the essential amino acid residues in forming hydrogen bonds and inhibition of α-amylase. [151] In the present study, we noticed that hydroxyl groups on sugar moiety of compounds **1-7** are favorable for the ligand to interact with the amino acid residues of the binding pocket, mostly with Glu233, Asp197, and Asp300 and enhancing the activity of particular ligands.

Among seven compounds, karaviloside XI formed nine hydrogen bonds with the enzyme and whose binding energy was second highest among the seven compounds (**Table 7**). This could be the due to the presence of multiple hydroxyl groups on the side chain and a sugar moiety. A 2-hydroxy-5-*O*-β-D-xylopyranosyl benzoic acid formed eight hydrogen bonds with the enzyme. However, we observed lower binding energy of -8.23 kcal/mol. Similarly, momordicoside I and momordicoside G formed seven hydrogen bonds followed momordicoside K, momordicoside F_1, momordicoside F_2 which formed six, five and four hydrogen bonds with the enzyme respectively. Furthermore, we also observed the altered docking pose for momordicoside G, and Karaviloside XI compared to other compounds. Also, to support this, momordicoside G and Karaviloside XI showed better inhibition activity compared to other compounds. Therefore, interactions between

different sugar moieties attached to the compounds and enzyme active pocket play an important role in determining binding energy and inhibitory activity.

Table 7 Binding free energy of the ligand-receptor complex; the number of hydrogen bonds between compounds and the active site of the enzymes; of purified compound (**1**–**7**) with porcine pancreatic α-amylase (PDB ID: 1OSE) and α-glucosidase (PDB ID: 3A4A)

Receptor	Compounds	Binding energies (kcal/mol)	Hydrogen bonds	Interactions	Hydrogen bonds in Å	Inhibition constant (nM)
α-amylase (PDB ID:1OSE)	Momordicoside I	-10.27	7	His305, Asp300, Arg195, Glu233, Gly306, Gly308, Ala307, Ile235, Tyr151, His201, Ala198, Lys200, Leu162	His305 (2.1) Asp300 (2.2 and 1.9), Glu233 (2.3), Arg195 (2.2), Gly306 (2.1), Gly308 (2.1)	29.57
	Momordicoside F_1	-10.11	5	His305, Asp300, Asp197, Gly308, Ala307, Tyr151, Lys200, Ile235, His201, Ala198, Leu162	His 305 (2.1), Asp 300 (1.9 and 2.2), Asp 197 (2.4), Gly 308 (1.9)	39.1
	Momordicoside K	-11.83	6	Asp197, Glu233, His201, Ile235, Asp300, Leu165, Trp59, Val163, Leu162, His305, Gly306, Tyr151	Asp 197 (1.9 and 2.7), Glu 233 (2.1), His 201 (1.9), Gly 306 (2.9), His 305 (2.1)	2.15
	Momordicoside F_2	-9.58	4	Val163, Gly306, Asp300, Ala307, Ile235, Gly238, Lys200, Tyr151, Leu162, His201,	Gly 306 (2.6), Asp 300 (2.0 and 2.5), Gly 238 (2.1)	95.02
	Momordicoside G	-10.76	7	Ala107, Val51, Ile49, Trp59, TRp58, Asp197, Glu233, Gly306, Asp300, Ile235, Leu165, Val163	Asp 197 (1.9, 2.0, and 2.3), Asp 300 (2.0, 2.8, 3.1 and 3.2)	12.9
	Karaviloside XI	-10.48	9	Glu240, Tyr151, Ile235, Val163, Leu162, Asp197, Asp300, Leu237, Ala307	Asp300 (2.0, 2.0 and 2.1), Glu240 (1.9 and 2.3), Asp197 (2.0, 2.1 and 2.5), His101(2.0)	20.78
	2-hydroxy-5-*O*-*β*-D-xylopyranosyl benzoic acid	-8.23	8	Ser199, Val234, His201, Glu233, His101, Tyr62, Asp197, Arg195, His299, Ala198, Asp300	Glu233 (1.9,2.1 and 2.3), Ile235(2.8), His201 (3.3), Asp197(2.1), Arg195(2.3), His299(3.4)	925.37
α-glucosidase (PDB ID:3A4A)	Momordicoside I	-10.4	5	His280, Ser157, Tyr158, Phe178, Arg442, Asp69, Phe303, Arg315, Pro312	Arg442 (2.0), Asp69 (1.8), Ser157 (2.0 and 1.9), Pro312 (3.2)	23.99
	Momordicoside F_1	-12.08	5	Ser240, Leu313, Phe303, Asp352, Glu237, Arg315, Tyr158, Phe314, Lys156,	Ser240 (2.5), Leu313 (2.0 and 1.9), Glu277 (1.9), Asp352 (2.6)	1.39
	Momordicoside K	-10.69	6	His280, Arg315, Tyr158, Arg442, Asp352, Phe178, Phe159, Ser240, Leu313, Lys156, Ser157	Arg442(3.5), Asp352 (2.6), Glu277 (1.9), Ser240 (2.3), Leu313 (2.0), Lys156 (2.5), Ser157 (2.4)	14.64
	Momordicoside F_2	-11.43	5	Pro243, Pro312, Tyr158, Phe303, Glu277, Asp352, Arg315, Phe314, Leu313, Lys156, Pro243	Pro312 (3.2), Glu277 (2.0), Asp352 (2.9), Ser240 (1.9), Asp242 (3.4)	4.22
	Momordicoside G	-9.9	5	Asn302, Ala281, His280, Ser157, Asn415, Tyr158, Pro312,	Asn302 (2.3), Ala281 (2.0), Gly160 (2.5), Ser157 (3.2 and 1.9)	55.65
	Karaviloside XI	-12.19	5	Asp315, Glu277, Asp352, Phe303, Tyr158, Arg315, His305, Leu313, Phe159	Glu277 (2.0 and 2.0), Asp215 (1.9), Asp352 (1.9), Leu313 (2.0)	1.16
	2-hydroxy-5-*O*-β-D-xylopyranosyl benzoic acid	-7.97	5	Ser241, Asp242, Tyr158, Pro312, Leu313, Val232, Asp233, Lys156, Ser240, Gln239, Ser157,	Asp242 (3.9,3.6), Ser241 (2.9), Ser240 (3.3), Lys156 (2.4)	1.45 µM

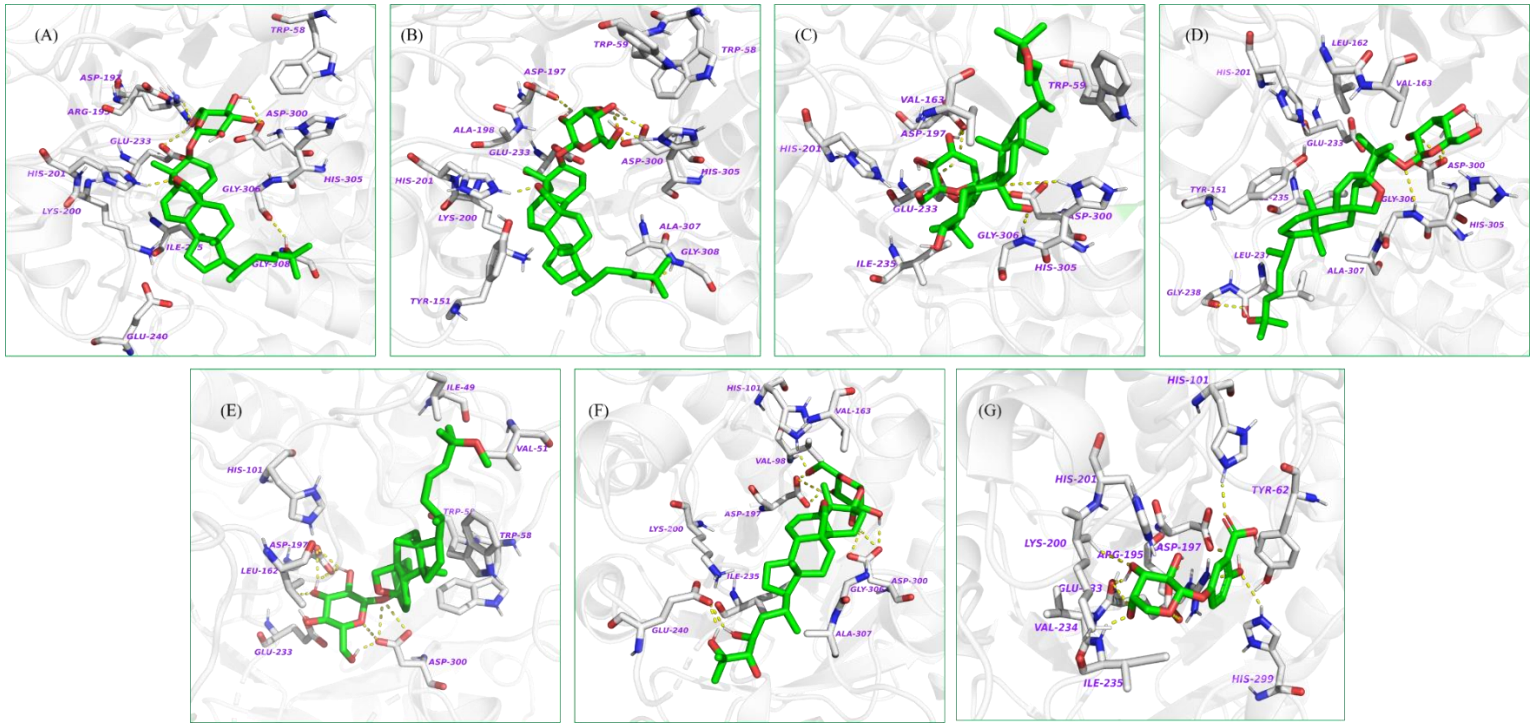

Figure 11 The 3D ligand-protein interactions for (A). momordicoside I, (B) momordicoside F1, (C). momordicoside K (D). momordicoside F2 (E). momordicoside G, (F). karaviloside XI and (G). 2-hydroxy-5-O-β-D-xylopyranosyl benzoic acid in the binding pocket of α-amylase respectively. The ligands in the 3D structure are shown in light sea green color and hydrogen bonds are shown in yellow color.

4.4.3.2 Virtual screening of isomaltase inhibitors

The binding energy and the inhibition constants for α-glucosidase docking study are shown in Table 3. The 3D and 2D interactions found for the best poses are depicted in **Figure 12A-12G** and **Figure A36A-A36G,** respectively. To date, the crystal structure of α-glucosidase from *S. cerevisiae* (the enzyme used for the biological assay) has not been resolved. Therefore, the compounds were docked to the isomaltase crystal structure (PDB ID:3A4A) downloaded from the Protein Data Bank. [152] From the docking study, it was observed that all the compounds were well accommodated inside the active site of isomaltase.

Binding energies of compounds (**1-7**) are ranging from -7.97 to -12.19 kcal/mol. The likeliest docked poses of compounds (**1-7**) with best binding affinity for isomaltase at the catalytic site were selected and are shown in **Figure 12A-12G**. Karaviloside XI (**6**) exhibited the lowest binding energy (-12.19 kcal/mol), followed by momordicoside F_1 (**1**) (-12.08 kcal/mol), momordicoside F_2 (**4**) (-11.43 kcal/mol), momordicoside K (**3**) (-10.69 kcal/mol), momordicoside I (**1**) (-10.4 kcal/mol), momordicoside G (**5**) (-9.9 kcal/mol), and 2-hydroxy-5-*O*-β-D-xylopyranosyl benzoic acid (**7**) (-7.97 kcal/mol).

As shown in **Figure 12(A-G)** and **Figure A36(A-G),** compound **1-7** were surrounded by crucial amino acid residues including Ser157, Glu277, Glu411, Asp307, Gly353, Arg442, Asp69, His351, Asp352, Arg213, and Tyr347 of α-glucosidase. Furthermore, a detailed analysis of the docked poses regarding ligand-protein binding energy, the number of H-bonds, and the inhibition constant are shown in **Table 7.**

In the isomaltase molecular docking study, momordicoside I (**1**) (**Figure 12A** and **Figure A36A)** was buried inside the active pocket site of isomaltase by surrounding with residues Ser157, Arg442, Asp69, Arg315, Phe303, His280, Tyr158, Arg442, and Phe178. **Figure 12B** and **Figure A36B** showed the binding mode of momordicoside F_1 (**2**) in the active site of isomaltase. The ligand was stabilized in the active site of an enzyme by surrounding key amino acid residues including Glu277, Asp252, Leu313, and Ser240. The docked momordicoside F_1 was buried entirely in the α-glucosidase binding pocket with part of the molecule reaching the catalytic center comprised of Glu277, Arg442, and Asp352, which adequately explains the competitive nature of momordicoside F_1; the remaining portion of the momordicoside F_1 extended towards the protein surface. Momordicoside F_1 showed a potential inhibition activity of amylase (68.98%), and its docking score on this enzyme is the first among the other six scores (-12.08 kcal/mol). The 3D docking mode (**Figure 12D**) and 2D schematic (**Figure A36D**) of momordicoside F_2 and isomaltase clearly showed that the momordicoside F_2 (**4**) inserted into the cavity of isomaltase by surrounding Asp352, Glu277, Pro312, Lys156, Phe314, Arg315, Tyr158, and Phe303. These interactions overtly strengthened the interactions between momordicoside F_2 and isomaltase, resulted in the binding energy of (-11.43 kcal/mol). Momordicoside G bound to the active site of isomaltase with binding energy -9.9 kcal/mol. As shown in **Figure 12E** and **Figure A36E**, momordicoside G (**5**) interacted with crucial amino acid residues including Ser157 and Ala281, Asn312, Asn415 in the catalytic site of isomaltase.

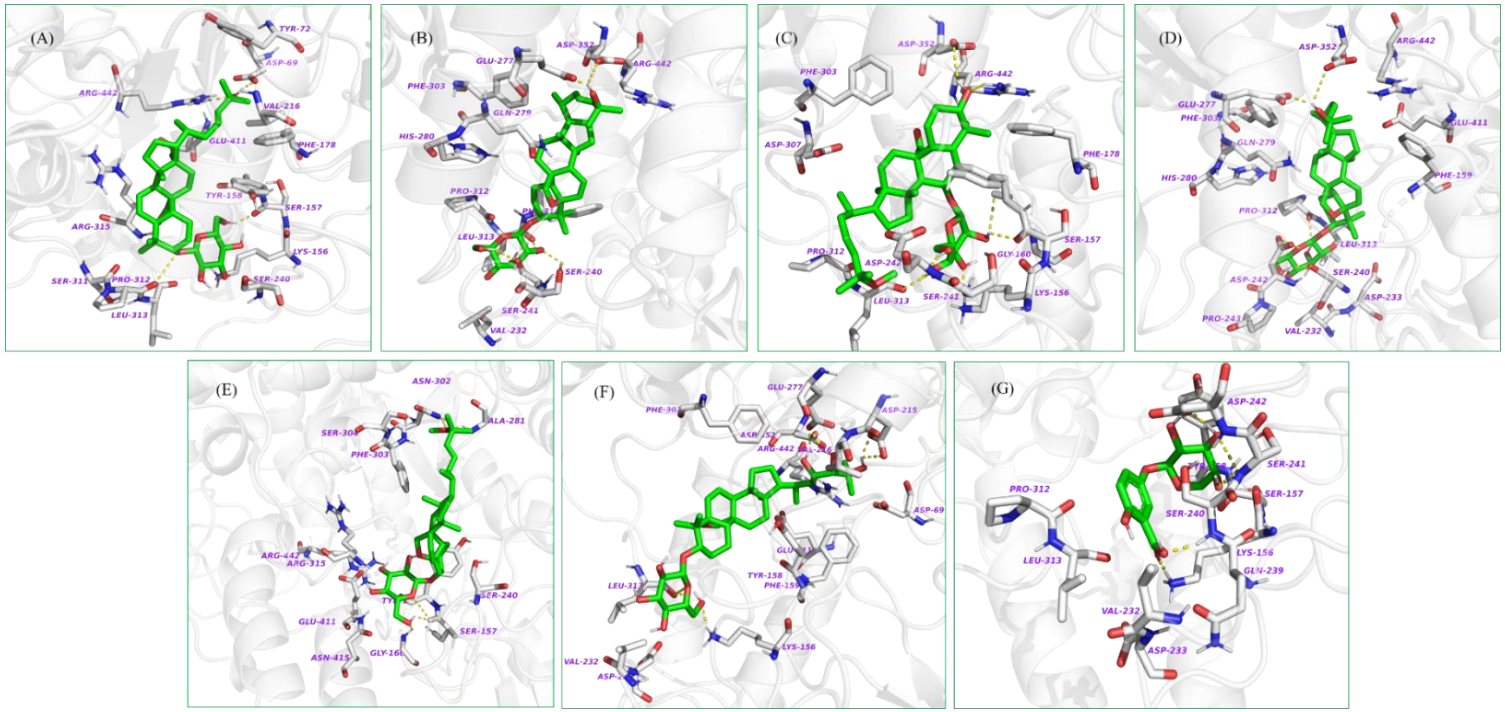

Figure 12 The 3D ligand-protein interactions for (A). momordicoside I, (B). momordicoside F1, (C). momordicoside K (D). momordicoside F2, (E). momordicoside G, (F). karaviloside XI, and (G). 2-hydroxy-5-O-β-D-xylopyranosyl benzoic acid in the binding pocket of α-glucosidase respectively. The ligands in the 3D structure are shown in green color and hydrogen bonds are shown in yellow color.

However, the attachment of allose sugar moiety at C-3 and attachment of OMe group at C-25 in momordicoside G resulted in an altered docking pose compared to other compounds. Also, Karaviloside XI (**6**) with the binding energy of -9.45 kcal/mol occupied the active region of isomaltase by interacting with amino acids including Asp 215, Glu277, Asp352, and Leu313. Besides, karaviloside XI was utterly inserted in the binding pocket of the enzyme by making additional hydrophobic interactions with amino acids residues including Phe159, Tyr158, Phe303, Arg315, and His280. All these interactions affected the enzyme inhibitory activity significantly and resulted in the binding energy of -12.19 kcal/mol.

The refined docking of 2-hydroxy-5-*O*-β-D-xylopyranosyl benzoic acid (**7**) with isomaltase generated the best pose with a minimum binding energy of -7.97 kcal/mol. The 3D interactions in **Figure 12G** and 2D schematic **Figure A36G** shows that compound **7** established seven hydrogen bonds within the isomaltase enzymatic pocket. The C-1 (carboxylic acid) formed two hydrogen bonds with Lys156 and Ser240 respectively. Similarly, hydroxyl groups at C-3' and C-4' of pentose sugar formed conventional hydrogen bonds with Ser241 and Asp242 (two hydrogen bonds) respectively. Also, 2-hydroxy-5-*O*-β-D-xylopyranosyl benzoic acid (**7**) showed the highest % inhibition of α-amylase of 60.67%.

4.4.4 In vitro anti-inflammatory activity

Purified compounds (**1-7**) were tested for anti-inflammatory activity in RAW 264.7 macrophages, using the bacteria toxin LPS to induce acute inflammation. As expected, LPS significantly increased expression of pro-inflammatory genes *IL-1β*, *Cox-2*, *IL-6*, *iNOS*, *TNF-α*, and *NF-κB,* compared to control (**Figure 13**). All of the compounds tested differentially affected the expression of *IL-1β*, *Cox-2*, *IL-6*, *iNOS*, *TNF-α*, and *NF-κB*. Also, compounds (**1-7**) significantly decreased expression of *IL-1β* when compared to the LPS group (p<0.001). It is worth noting that momordicoside G (**5**), at the concentration of 25 µM, was most potent at decreasing the expression of *IL-1β*. Similarly, in case of *Cox-2*, compounds **1**, **2**, **3**, **6**, and **7** significantly suppressed LPS stimulated *Cox-2* expression at 25 µM (p<0.001). Among them, we observed compounds **1**, **6** and **7** to be potent suppressing agents for the expression of *Cox-2*. Pre-treatment with compounds **1-7** significantly suppressed the LPS-stimulated expression of *iNOS* and *NF-κB* mRNA compared to the LPS treatment group (p<0.001). Momordicoside F_1(**2**) was most potent at suppressing the expression of *iNOS* (p< 0.001), compared to the LPS group. As seen in **Figure 13**, compounds **1, 6** and **7** significantly down-regulated the expression of *IL-6*, compared to the LPS-treated group at 25 µM concentration. Conversely, compound **3** did not reduce the expression of IL-6 at 25 µM concentration significantly. Compounds (**2**), (**5**) significantly suppressed the expression of TNF-α at 25 µM concentration (p< 0.001), while the remaining compounds showed moderate suppression of TNF-α expression.

To date, many natural products have been identified as potential anti-inflammatory agents. These natural products, such as triterpenes, could strongly inhibit/attenuate inflammatory mediators. Triterpenoids, major bioactive constituents in *M. charantia*, are widely distributed in plants and maybe responsible for bitter melons' anti-inflammatory effects. [153] However, studies relating specific natural compounds of bitter melon to the bioactivities of the plant and exploring the underlying mechanisms are limited. In earlier studies, compound 5β, 19-epoxy-25-methoxycucurbita-6, 23-diene-3β, 19-diol (16, EMCD) isolated from *M. charantia* was evaluated for anti-inflammatory activities against *TNF-α* induced inflammation via AMPK in FL83B cells. EMCD inhibits *TNF-α* induced expression of *iNOS*, *NF-κB*, protein-tyrosine phosphatase-1B, *TNF-α*, and *IL-1β*. [154] In another study, the active constituents of *M. charantia,* 1-α-linolenoyl-lysophosphatidylcholine (LPC) and 1-linoleoyl-LPC suppressed the LPS-induced *TNF-α* production in RAW 264.7 cells at a concentration of 10 μg/mL [107]. In the present study, momordicoside I (**1**), momordicoside K (**3**), karaviloside XI (**6**) and 2-hydroxy-5-*O*-β-D-xylopyranosyl benzoic acid (**7**) were determined as the most potent anti-inflammatory compounds by demonstrating their effects on the levels of the pro-inflammatory markers, including *IL-1β, Cox-2, IL-6, iNOS* and *NF-κB* in LPS-stimulated RAW 264.7 cells.

NF-kB is a key transcriptional regulator of the inflammatory response and plays a vital role in the development of the inflammatory process and cellular injuries. It is activated in response to different extracellular stimuli, including oxidative stress, LPS, and cytokines. [155] NF-kB enters the nucleus and activates the transcription of pro-inflammatory factors including *TNF-α, IL-1β, IL-6*, the subunits of NF-kB, *iNOS* and

COX-2, resulting in inflammation. In the present study, LPS could induce the translocation of *NF-κB* and promotes expression of pro-inflammatory factors, whereas all tested compounds significantly reduced the expression of *NF-κB* compared to LPS treatment group, subsequently attenuating expression of pro-inflammatory genes. To the best of our knowledge, this is the first-time anti-inflammatory activity by cucurbitane-type triterpene glycosides from the fruits of bitter melon has been observed.

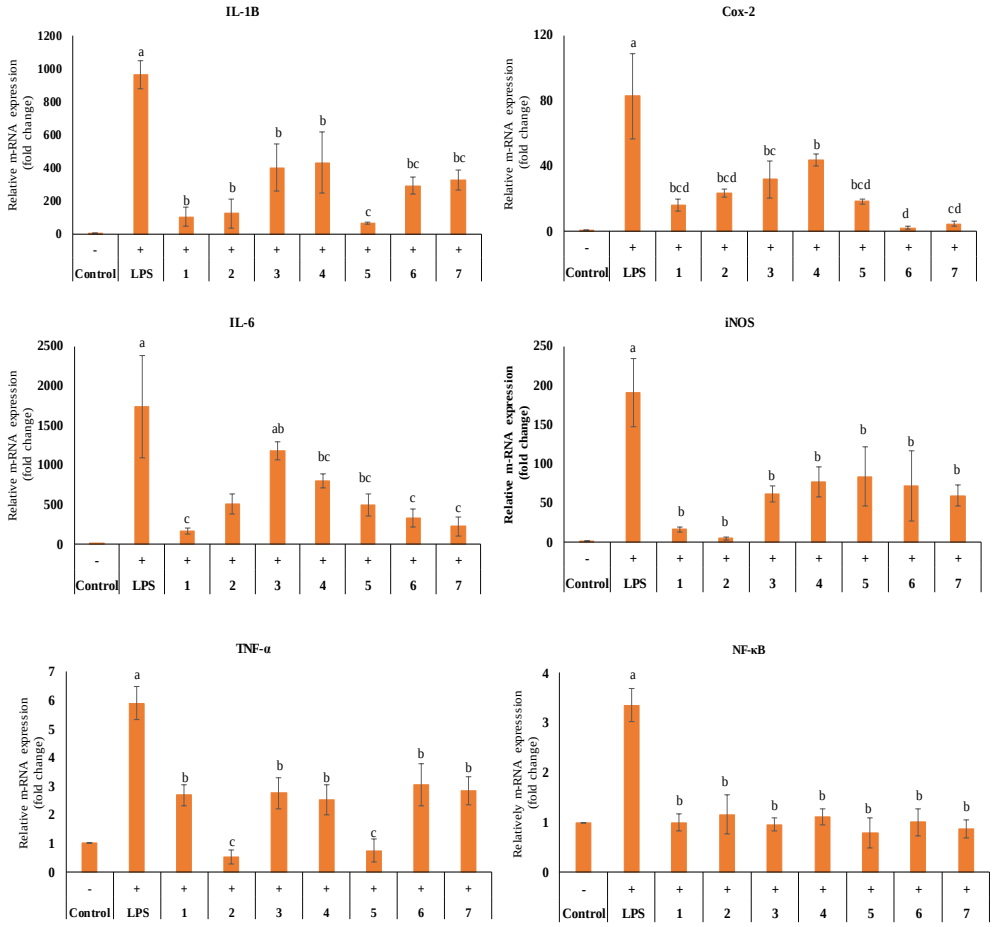

Figure 13 Effect of purified compounds (1-7) at on mRNA expression of IL-1β, IL-6, TNF-α, INOS, NF-κB and Cox-2 on LPS induced murine macrophage RAW 264.7 cells. The cells were pretreated with 25 µM compounds 1. momordicoside I, 2. momordicoside F_1, 3. momordicoside K, 4. momordicoside F_2, and 5. momordicoside G, 6. karaviloside XI and 7. 2-hydroxy-5-*O*-β-D-xylopyranosyl benzoic acid then LPS (1µg/ml) was added and incubated for 18 h. Data are expressed as mean ± SD (n=9), and analyzed by one-way ANOVA. Different letters within the same panel indicate there were significant differences at $p<0.001$

4.5 Conclusions

In this study, ten compounds were isolated from the fruit of *M. charantia*. Compounds **1-7** showed variable α-amylase and α-glucosidase inhibitory activities, ranging from 35–75%. Molecular docking studies showed that compounds **1-7** had a high affinity close to the active site of both enzymes by interacting with key amino acid residues. Also, the anti-inflammatory activities of compounds (**1-7**) demonstrated that momordicoside I (**1**), momordicoside K (**3**), karaviloside XI (**6**) and 2-hydroxy-5-*O*-β-D-xylopyranosyl benzoic acid (**7**) are the most effective anti-inflammatory agents, suppressing the expression of pro-inflammatory markers *IL-1β, Cox-2, IL-6, iNOS, TNF-α* and *NF-κB* in LPS-stimulated RAW 264.7 cells. Overall, the results presented here indicated that compounds isolated from bitter melon are worthy of further investigation in the development of new antidiabetic and anti-inflammatory drugs of natural origin.

CHAPTER 5

SUMMARY AND CONCLUSIONS

Existing literature suggests that *M. charantia* consists of an array of natural compounds, which makes it functional food, especially in the reducing risk from diabetes. However, the exact role of each of these compounds in the overall observed antidiabetic and anti-inflammatory potential of *M. charantia* is still obscure. In the present study, 14 bioactive compounds were isolated from the medium polar and polar extracts of *M. charantia.* The structures of the isolated compounds were characterized by 1D and 2D NMR and high-resolution mass spectroscopic data. Charantoside XI and 2-hydroxy-5-*O*-β-D-xylopyranosyl benzoic acid were the two purified novel compounds from *M. charantia.* Charantoside XI is the first example of cucurbitane triterpene containing carboxylic group at position 3. Also, TCD and charantal were purified first time from the edible part of *M. charantia.*

Similarly, momordicoside I, F_1, K, F_2, and G were previously isolated from the fruit of *M. charantia*. However, there is no precise, complete NMR data available for these compounds. Hence, this study presented complete NMR data for these compounds. In case of bioactivity, IDG was the most potent compound and exhibited higher inhibition of carbolytic enzymes compared to the other compounds and comparable activity to that of acarbose. Similarly, triterpene glycosides momordicoside G and K showed potent α-amylase inhibitory activity. Novel compound, 2-hydroxy-5-*O*-β-D-xylopyranosyl benzoic acid exhibited moderate α-glucosidase inhibition compared to other compounds. The

inhibition of these enzymes in the pancreas and brush border membrane of small intestine regulates the digestion of complex carbohydrates, which in turn controls the blood glucose. Also, The inhibitory mechanism of these compounds significantly varied due to conformational changes derived from the presence of a sugar moiety in some of the compounds.

Similarly, in the present study, polar compounds karaviloside XI has a sugar moiety and having multiple hydroxyl groups showed strong α-glucosidase inhibitory activity compared to other cucurbitane mono glycosides. Interestingly we also observed in α-glucosidase inhibitory activity compounds bearing a *β*-D-allopyranosyl group at C-3 exhibited higher inhibitory activity than compounds bearing a *β*-D-glucopyranosyl group at C-3.

Antidiabetic activity was further confirmed by SAR through the help of molecular docking studies. The elven compounds from *M. chrantia* all showed competitive inhibition against porcine pancreatic α-amylase and isomaltase. They demonstrated different inhibition activities, among which IDG had the highest one. The molecular docking study showed that all the eleven purified compounds occupied the active site of porcine pancreatic α-amylase and isomaltase forming hydrogen, pi-alkyl bonds. In the case of α-amylase GLU233, ASP300 and ASP197 were found to be the common key residues for imparting the inhibition activity of all the eleven compounds. In the case of isomaltase molecular docking studies, compounds were able to form hydrogen bonds key amino acid residues on isomaltase including ARG442 and GLU277. Overall, results obtained from this study would help to reveal the structure-activity relationships purified

compounds from bitter melon to better design novel functional foods with slow-releasing sugars, thereby lowering the risk of postprandial hyperglycemia which is characterized as early Type II diabetes.

Meanwhile, TCD (**1**) and charantoside XI, momordicoside I, momordicoside K, karaviloside XI, and 2-hydroxy-5-*O*-β-D-xylopyranosyl benzoic acid were determined as the most potent anti-inflammatory compounds by demonstrating their effects on the levels of the pro-inflammatory markers, including *IL-1β*, *Cox-2*, *IL-6*, *iNOS* and *NF-κB* in LPS-stimulated RAW 264.7 cells. Our findings suggest that these compounds purified from bitter melon have potential anti-inflammatory activities and therefore hold promise for the development of plant-based treatments for inflammatory conditions.

REFERENCES

[1] J. Grover, S. Yadav, V. Vats, Medicinal plants of India with anti-diabetic potential, Journal of ethnopharmacology, 81 (2002) 81-100.

[2] Z.K. Bagewadi, R. Siddanagouda, P.G. Baligar, Phytochemical screening and evaluation of antimicrobial activity of Semecarpus anacardium nuts, International Journal of Pharmacology and Pharmaceutical Technology, 1 (2012) 68-74.

[3] E. Basch, S. Gabardi, C. Ulbricht, Bitter melon (Momordica charantia): a review of efficacy and safety, American Journal of Health-System Pharmacy, 60 (2003) 356-359.

[4] T. Behera, Heterosis in bittergourd, Journal of New Seeds, 6 (2005) 217-221.

[5] M.J. Davies, D.A. D'Alessio, J. Fradkin, W.N. Kernan, C. Mathieu, G. Mingrone, P. Rossing, A. Tsapas, D.J. Wexler, J.B. Buse, Management of hyperglycaemia in type 2 diabetes, 2018. A consensus report by the American Diabetes Association (ADA) and the European Association for the Study of Diabetes (EASD), Diabetologia, 61 (2018) 2461-2498.

[6] H.-L. Cheng, H.-K. Huang, C.-I. Chang, C.-P. Tsai, C.-H. Chou, A cell-based screening identifies compounds from the stem of Momordica charantia that overcome insulin resistance and activate AMP-activated protein kinase, Journal of Agricultural and Food Chemistry, 56 (2008) 6835-6843.

[7] B. Joseph, D. Jini, Antidiabetic effects of Momordica charantia (bitter melon) and its medicinal potency, Asian Pacific Journal of Tropical Disease, 3 (2013) 93-102.

[8] A.P. Jayasooriya, M. Sakono, C. Yukizaki, M. Kawano, K. Yamamoto, N. Fukuda, Effects of Momordica charantia powder on serum glucose levels and various lipid parameters in rats fed with cholesterol-free and cholesterol-enriched diets, Journal of ethnopharmacology, 72 (2000) 331-336.

[9] X. Wang, W. Sun, J. Cao, H. Qu, X. Bi, Y. Zhao, Structures of new triterpenoids and cytotoxicity activities of the isolated major compounds from the fruit of Momordica charantia L, J. Agric. Food Chem., 60 (2012) 3927-3933.

[10] T. Akihisa, N. Higo, H. Tokuda, M. Ukiya, H. Akazawa, Y. Tochigi, Y. Kimura, T. Suzuki, H. Nishino, Cucurbitane-type triterpenoids from the fruits of Momordica charantia and their cancer chemopreventive effects, J. Nat. Prod., 70 (2007) 1233-1239.

[11] M.-J. Tan, J.-M. Ye, N. Turner, C. Hohnen-Behrens, C.-Q. Ke, C.-P. Tang, T. Chen, H.-C. Weiss, E.-R. Gesing, A. Rowland, Antidiabetic activities of triterpenoids isolated from bitter melon associated with activation of the AMPK pathway, Chem. Biol., 15 (2008) 263-273.

[12] H.-L. Cheng, H.-K. Huang, C.-I. Chang, C.-P. Tsai, C.-H. Chou, A cell-based screening identifies compounds from the stem of Momordica charantia that overcome insulin resistance and activate AMP-activated protein kinase, J. Agric. Food Chem., 56 (2008) 6835-6843.

[13] A. Parkash, T. Ng, W. Tso, Purification and characterization of charantin, a napin-like ribosome-inactivating peptide from bitter gourd (Momordica charantia) seeds, Chemical Biology & Drug Design, 59 (2002) 197-202.

[14] H.-Y. Wang, W.-C. Kan, T.-J. Cheng, S.-H. Yu, L.-H. Chang, J.-J. Chuu, Differential anti-diabetic effects and mechanism of action of charantin-rich extract of Taiwanese Momordica charantia between type 1 and type 2 diabetic mice, Food and chemical toxicology, 69 (2014) 347-356.

[15] J. Efird, Y. Choi, S. Davies, S. Mehra, E. Anderson, L. Katunga, Potential for improved glycemic control with dietary Momordica charantia in patients with insulin resistance and pre-diabetes, Int J Environ Res Public Health, 11 (2014) 2328-2345.

[16] B. Joseph, D. Jini, Antidiabetic effects of Momordica charantia (bitter melon) and its medicinal potency, Asian Pac J Trop Dis, 3 (2013) 93-102.

[17] A.M.L. Dans, M.V.C. Villarruz, C.A. Jimeno, M.A.U. Javelosa, J. Chua, R. Bautista, G.G.B. Velez, The effect of Momordica charantia capsule preparation on glycemic control in type 2 diabetes mellitus needs further studies, Journal of clinical epidemiology, 60 (2007) 554-559.

[18] Q. Chen, L.L. Chan, E.T. Li, Bitter melon (Momordica charantia) reduces adiposity, lowers serum insulin and normalizes glucose tolerance in rats fed a high fat diet, The Journal of nutrition, 133 (2003) 1088-1093.

[19] P. Chaturvedi, S. George, M. Milinganyo, Y. Tripathi, Effect of Momordica charantia on lipid profile and oral glucose tolerance in diabetic rats, Phytotherapy Research, 18 (2004) 954-956.

[20] L. Ma, A.-H. Yu, L.-L. Sun, W. Gao, M.-M. Zhang, Y.-L. Su, H. Liu, T. Ji, Two new bidesmoside triterpenoid saponins from the seeds of Momordica charantia L, Molecules, 19 (2014) 2238-2246.

[21] J.-R. Weng, L.-Y. Bai, C.-F. Chiu, J.-L. Hu, S.-J. Chiu, C.-Y. Wu, Cucurbitane triterpenoid from Momordica charantia induces apoptosis and autophagy in breast cancer cells, in part, through peroxisome proliferator-activated receptor γ activation, Evidence-Based Complementary and Alternative Medicine, 2013 (2013).

[22] L. Leung, R. Birtwhistle, J. Kotecha, S. Hannah, S. Cuthbertson, Anti-diabetic and hypoglycaemic effects of Momordica charantia (bitter melon): a mini review, British Journal of Nutrition, 102 (2009) 1703-1708.

[23] K. Abascal, E. Yarnell, Using bitter melon to treat diabetes, Alternative & Complementary Therapies, 11 (2005) 179-184.

[24] R. Bakare, O. Magbagbeola, O. Okunowo, Nutritional and chemical evaluation of Momordica charantia, Journal of Medicinal Plants Research, 4 (2010) 2189-2193.

[25] J. Kubola, S. Siriamornpun, Phenolic contents and antioxidant activities of bitter gourd (Momordica charantia L.) leaf, stem and fruit fraction extracts in vitro, Food chemistry, 110 (2008) 881-890.

[26] D.S. Kumar, K.V. Sharathnath, P. Yogeswaran, A. Harani, K. Sudhakar, P. Sudha, D. Banji, A medicinal potency of Momordica charantia, (2010).

[27] E. Yeşilada, I.l. Gürbüz, H. Shibata, Screening of Turkish anti-ulcerogenic folk remedies for anti-Helicobacter pylori activity, Journal of Ethnopharmacology, 66 (1999) 289-293.

[28] B. Reyes, N. Bautista, N. Tanquilut, R. Anunciado, A. Leung, G. Sanchez, R. Magtoto, P. Castronuevo, H. Tsukamura, K.-I. Maeda, Anti-diabetic potentials of Momordica charantia and Andrographis paniculata and their effects on estrous cyclicity of alloxan-induced diabetic rats, Journal of ethnopharmacology, 105 (2006) 196-200.

[29] P. Budrat, A. Shotipruk, Enhanced recovery of phenolic compounds from bitter melon (Momordica charantia) by subcritical water extraction, Separation and Purification Technology, 66 (2009) 125-129.

[30] J.G.M. Costa, E.M. Nascimento, A.R. Campos, F.F. Rodrigues, Antibacterial activity of Momordica charantia (Curcubitaceae) extracts and fractions, Journal of basic and clinical pharmacy, 2 (2010) 45.

[31] V. Pongthanapisith, K. Ikuta, P. Puthavathana, W. Leelamanit, Antiviral protein of Momordica charantia L. inhibits different subtypes of influenza A, Evidence-Based Complementary and Alternative Medicine, 2013 (2013).

[32] C.-K. Lii, H.-W. Chen, W.-T. Yun, K.-L. Liu, Suppressive effects of wild bitter gourd (Momordica charantia Linn. var. abbreviata ser.) fruit extracts on inflammatory responses in RAW 264.7 macrophages, Journal of Ethnopharmacology, 122 (2009) 227-233.

[33] M. Kobori, J. Amemiya, M. Sakai, M. Shiraki, H. Sugishita, N. Sakaue, Y. Hoshi, C. Yukizaki, Bitter gourd induces apoptosis in HL60 human leukemia cells and suppresses the production of inflammatory cytokine in RAW264. 7 macrophage like cells, JOURNAL OF THE JAPANESE SOCIETY FOR FOOD SCIENCE AND TECHNOLOGY-NIPPON SHOKUHIN KAGAKU KOGAKU KAISHI, 53 (2006) 408-415.

[34] S. Umukoro, R. Ashorobi, Evaluation of anti-inflammatory and membrane stabilizing property of aqueous leaf extract of Momordica charantia in rats, African Journal of Biomedical Research, 9 (2006).

[35] I. Ahmed, M. Lakhani, M. Gillett, A. John, H. Raza, Hypotriglyceridemic and hypocholesterolemic effects of anti-diabetic Momordica charantia (karela) fruit extract in streptozotocin-induced diabetic rats, Diabetes Research and Clinical Practice, 51 (2001) 155-161.

[36] P. Pitchakarn, K. Ogawa, S. Suzuki, S. Takahashi, M. Asamoto, T. Chewonarin, P. Limtrakul, T. Shirai, Momordica charantia leaf extract suppresses rat prostate cancer progression in vitro and in vivo, Cancer Science, 101 (2010) 2234-2240.

[37] R.B. Ray, A. Raychoudhuri, R. Steele, P. Nerurkar, Bitter melon (Momordica charantia) extract inhibits breast cancer cell proliferation by modulating cell cycle regulatory genes and promotes apoptosis, Cancer Research, 70 (2010) 1925-1931.

[38] J.L. Perez, G.K. Jayaprakasha, K. Crosby, B.S. Patil, Evaluation of bitter melon (Momordica charantia) cultivars grown in Texas and levels of various

phytonutrients, Journal of the Science of Food and Agriculture, 99 (2019) 379-390.

[39] G. Nagarani, A. Abirami, P. Siddhuraju, Food prospects and nutraceutical attributes of Momordica species: a potential tropical bioresources–a review, Food Science and Human Wellness, 3 (2014) 117-126.

[40] S.H. Lee, Y.S. Jeong, J. Song, K.-A. Hwang, G.M. Noh, I.G. Hwang, Phenolic acid, carotenoid composition, and antioxidant activity of bitter melon (Momordica charantia L.) at different maturation stages, International Journal of Food Properties, 20 (2017) S3078-S3087.

[41] S.P. Tan, T.C. Kha, S.E. Parks, P.D. Roach, Bitter melon (Momordica charantia L.) bioactive composition and health benefits: A review, Food Reviews International, 32 (2016) 181-202.

[42] J.C. Chen, M.H. Chiu, R.L. Nie, G.A. Cordell, S.X. Qiu, Cucurbitacins and cucurbitane glycosides: structures and biological activities, Natural product reports, 22 (2005) 386-399.

[43] A. Falasca, A. Gasperi-Campani, A. Abbondanza, L. Barbieri, F. Stirpe, Properties of the ribosome-inactivating proteins gelonin, Momordica charantia inhibitor, and dianthins, Biochemical Journal, 207 (1982) 505-509.

[44] S. Lee-Huang, P.L. Huang, A. Bourinbaiar, H. Chen, H. Kung, Inhibition of the integrase of human immunodeficiency virus (HIV) type 1 by anti-HIV plant proteins MAP30 and GAP31, Proceedings of the National Academy of Sciences, 92 (1995) 8818-8822.

[45] J. Singh, E. Cumming, G. Manoharan, H. Kalasz, E. Adeghate, Suppl 2: Medicinal chemistry of the anti-diabetic effects of *Momordica charantia*: active constituents and modes of actions, Open J Med Chem, 5 (2011) 70.

[46] Y. Kimura, T. Akihisa, N. Yuasa, M. Ukiya, T. Suzuki, M. Toriyama, S. Motohashi, H. Tokuda, Cucurbitane-Type Triterpenoids from the Fruit of Momordica c harantia, Journal of natural products, 68 (2005) 807-809.

[47] C.-I. Chang, C.-R. Chen, Y.-W. Liao, H.-L. Cheng, Y.-C. Chen, C.-H. Chou, Cucurbitane-Type Triterpenoids from Momordica c harantia, Journal of natural products, 69 (2006) 1168-1171.

[48] L. Harinantenaina, M. Tanaka, S. Takaoka, M. Oda, O. Mogami, M. Uchida, Y. Asakawa, Momordica charantia constituents and antidiabetic screening of the isolated major compounds, Chemical and Pharmaceutical Bulletin, 54 (2006) 1017-1021.

[49] S. Nakamura, T. Murakami, J. Nakamura, H. Kobayashi, H. Matsuda, M. Yoshikawa, Structures of new cucurbitane-type triterpenes and glycosides, karavilagenins and karavilosides, from the dried fruit of Momordica charantia L. in Sri Lanka, Chemical and pharmaceutical bulletin, 54 (2006) 1545-1550.

[50] T. Akihisa, N. Higo, H. Tokuda, M. Ukiya, H. Akazawa, Y. Tochigi, Y. Kimura, T. Suzuki, H. Nishino, Cucurbitane-type triterpenoids from the fruits of Momordica charantia and their cancer chemopreventive effects, Journal of natural products, 70 (2007) 1233-1239.

[51] Q.Y. Li, H.B. Chen, Z.M. Liu, B. Wang, Y.Y. Zhao, Cucurbitane triterpenoids from Momordica charantia, Magnetic Resonance in Chemistry, 45 (2007) 451-456.

[52] C.-I. Chang, C.-R. Chen, Y.-W. Liao, H.-L. Cheng, Y.-C. Chen, C.-H. Chou, Cucurbitane-type triterpenoids from the stems of Momordica charantia, Journal of natural products, 71 (2008) 1327-1330.

[53] J.C. Chen, L. Lu, X.M. Zhang, L. Zhou, Z.R. Li, M.H. Qiu, Eight New Cucurbitane Glycosides, Kuguaglycosides A–H, from the Root of Momordica charantia L, Helvetica Chimica Acta, 91 (2008) 920-929.

[54] J. Chen, R. Tian, M. Qiu, L. Lu, Y. Zheng, Z. Zhang, Trinorcucurbitane and cucurbitane triterpenoids from the roots of Momordica charantia, Phytochemistry, 69 (2008) 1043-1048.

[55] Y. Liu, Z. Ali, I.A. Khan, Cucurbitane-type triterpene glycosides from the fruits of Momordica charantia, Planta medica, 74 (2008) 1291-1294.

[56] M.-J. Tan, J.-M. Ye, N. Turner, C. Hohnen-Behrens, C.-Q. Ke, C.-P. Tang, T. Chen, H.-C. Weiss, E.-R. Gesing, A. Rowland, Antidiabetic activities of triterpenoids isolated from bitter melon associated with activation of the AMPK pathway, Chemistry & biology, 15 (2008) 263-273.

[57] J.-C. Chen, W.-Q. Liu, L. Lu, M.-H. Qiu, Y.-T. Zheng, L.-M. Yang, X.-M. Zhang, L. Zhou, Z.-R. Li, Kuguacins F–S, cucurbitane triterpenoids from Momordica charantia, Phytochemistry, 70 (2009) 133-140.

[58] N.X. Nhiem, P.V. Kiem, C.V. Minh, N.K. Ban, N.X. Cuong, L.M. Ha, B.H. Tai, T.H. Quang, N.H. Tung, Y.H. Kim, Cucurbitane-type triterpene glycosides from

the fruits of Momordica charantia, Magnetic Resonance in Chemistry, 48 (2010) 392-396.

[59] C.-I. Chang, C.-R. Chen, Y.-W. Liao, W.-L. Shih, H.-L. Cheng, C.-Y. Tzeng, J.-W. Li, M.-T. Kung, Octanorcucurbitane triterpenoids protect against tert-butyl hydroperoxide-induced hepatotoxicity from the stems of Momordica charantia, Chemical and Pharmaceutical Bulletin, 58 (2010) 225-229.

[60] C.R. Chen, Y.W. Liao, W.L. Shih, C.Y. Tzeng, H.L. Cheng, W.T. Kao, C.I. Chang, Triterpenoids from the stems of Momordica charantia, Helvetica Chimica Acta, 93 (2010) 1355-1361.

[61] C.-H. Liu, M.-H. Yen, S.-F. Tsang, K.-H. Gan, H.-Y. Hsu, C.-N. Lin, Antioxidant triterpenoids from the stems of Momordica charantia, Food chemistry, 118 (2010) 751-756.

[62] A.C. Keller, J. Ma, A. Kavalier, K. He, A.-M.B. Brillantes, E.J. Kennelly, Saponins from the traditional medicinal plant *Momordica charantia* stimulate insulin secretion in vitro, Phytomedicine, 19 (2011) 32-37.

[63] J.Q. Cao, Y. Zhang, J.M. Cui, Y.Q. Zhao, Two new cucurbitane triterpenoids from Momordica charantia L, Chinese Chemical Letters, 22 (2011) 583-586.

[64] C. Hsu, C.-L. Hsieh, Y.-H. Kuo, C.-j. Huang, Isolation and identification of cucurbitane-type triterpenoids with partial agonist/antagonist potential for estrogen receptors from Momordica charantia, Journal of agricultural and food chemistry, 59 (2011) 4553-4561.

[65] Y.W. Liao, C.R. Chen, J.L. Hsu, H.L. Cheng, W.L. Shih, Y.H. Kuo, T.C. Huang, C.I. Chang, Sterols from the Stems of Momordica charantia, Journal of the Chinese Chemical Society, 58 (2011) 893-898.

[66] L. Peng, L. Jian-Feng, K. Li-Ping, Y. He-Shui, L.-J. ZHANG, S. Xin-Bo, M. Bai-Ping, A new C30 sterol glycoside from the fresh fruits of Momordica charantia, Chinese journal of natural medicines, 10 (2012) 88-91.

[67] X. Wang, W. Sun, J. Cao, H. Qu, X. Bi, Y. Zhao, Structures of new triterpenoids and cytotoxicity activities of the isolated major compounds from the fruit of Momordica charantia L, Journal of agricultural and food chemistry, 60 (2012) 3927-3933.

[68] J. Zhang, Y. Huang, T. Kikuchi, H. Tokuda, N. Suzuki, K.i. Inafuku, M. Miura, S. Motohashi, T. Suzuki, T. Akihisa, Cucurbitane triterpenoids from the leaves of Momordica charantia, and their cancer chemopreventive effects and cytotoxicities, Chemistry & biodiversity, 9 (2012) 428-440.

[69] P.H. Yen, D.T. Dung, N.X. Nhiem, H.T. Anh, D. Hang, D. Yen, N. Cuc, N.K. Ban, C. Van Minh, P. Van Kiem, Cucurbitane-type triterpene glycosides from the fruits of Momordica charantia, Natural product communications, 9 (2014) 383-386.

[70] Z.J. Li, J.C. Chen, Y.Y. Deng, N.L. Song, M.Y. Yu, L. Zhou, M.H. Qiu, Two new cucurbitane triterpenoids from immature fruits of Momordica charantia, Helvetica Chimica Acta, 98 (2015) 1456-1461.

[71] Y. Jiang, X.-R. Peng, M.-Y. Yu, L.-S. Wan, G.-L. Zhu, G.-T. Zhao, L. Zhou, M.-H. Qiu, J. Liu, Cucurbitane-type triterpenoids from the aerial parts of Momordica charantia L, Phytochemistry Letters, 16 (2016) 164-168.

[72] C.J. Bailey, C. Day, Traditional plant medicines as treatments for diabetes, Diabetes care, 12 (1989) 553-564.

[73] M. Modak, P. Dixit, J. Londhe, S. Ghaskadbi, T.P.A. Devasagayam, Recent advances in Indian herbal drug research guest editor: Thomas Paul Asir Devasagayam Indian herbs and herbal drugs used for the treatment of diabetes, Journal of clinical biochemistry and nutrition, 40 (2007) 163-173.

[74] P. Meir, Z. Yaniv, An *in vitro* study on the effect of *Momordica charantia* on glucose uptake and glucose metabolism in rats, Planta Med., 51 (1985) 12-16.

[75] B.W. Roffey, A.S. Atwal, T. Johns, S. Kubow, Water extracts from *Momordica charantia* increase glucose uptake and adiponectin secretion in 3T3-L1 adipose cells, J. Ethnopharmacol., 112 (2007) 77-84.

[76] I. Ahmed, E. Adeghate, A. Sharma, D. Pallot, J. Singh, Effects of *Momordica charantia* fruit juice on islet morphology in the pancreas of the streptozotocin-diabetic rat, Diabetes Res. Clin. Pract., 40 (1998) 145-151.

[77] S.N. Nivitabishekam, M. Asad, V.S. Prasad, Pharmacodynamic interaction of *Momordica charantia* with rosiglitazone in rats, Chem.-Biol. Interact., 177 (2009) 247-253.

[78] D.G. Popovich, L. Li, W. Zhang, Bitter melon (*Momordica charantia*) triterpenoid extract reduces preadipocyte viability, lipid accumulation and adiponectin expression in 3T3-L1 cells, Food Chem. Toxicol., 48 (2010) 1619-1626.

[79] H.-L. Cheng, C.-Y. Kuo, Y.-W. Liao, C.-C. Lin, EMCD, a hypoglycemic triterpene isolated from Momordica charantia wild variant, attenuates TNF-α-induced inflammation in FL83B cells in an AMP-activated protein kinase-independent manner, European journal of pharmacology, 689 (2012) 241-248.

[80] Z. Ahmad, K.F. Zamhuri, A. Yaacob, C.H. Siong, M. Selvarajah, A. Ismail, M.N. Hakim, In vitro anti-diabetic activities and chemical analysis of polypeptide-k and oil isolated from seeds of Momordica charantia (bitter gourd), Molecules, 17 (2012) 9631-9640.

[81] K. Zeng, Y.-N. He, D. Yang, J.-Q. Cao, X.-C. Xia, S.-J. Zhang, X.-L. Bi, Y.-Q. Zhao, New compounds from acid hydrolyzed products of the fruits of Momordica charantia L. and their inhibitory activity against protein tyrosine phosphatas 1B, European journal of medicinal chemistry, 81 (2014) 176-180.

[82] V. Baldwa, C. Bhandari, A. Pangaria, R. Goyal, Clinical trial in patients with diabetes mellitus of an insulin-like compound obtained from plant source, Upsala journal of medical sciences, 82 (1977) 39-41.

[83] B. Leatherdale, R. Panesar, G. Singh, T. Atkins, C. Bailey, A. Bignell, Improvement in glucose tolerance due to Momordica charantia (karela), Br Med J (Clin Res Ed), 282 (1981) 1823-1824.

[84] Y. Srivastava, H. Venkatakrishna-Bhatt, Y. Verma, K. Venkaiah, B. Raval, Antidiabetic and adaptogenic properties of Momordica charantia extract: an experimental and clinical evaluation, Phytotherapy Research, 7 (1993) 285-289.

[85] J. Welihinda, E. Karunanayake, M. Sheriff, K. Jayasinghe, Effect of Momordica charantia on the glucose tolerance in maturity onset diabetes, Journal of Ethnopharmacology, 17 (1986) 277-282.

[86] C.-H. Tsai, E.C.-F. Chen, H.-S. Tsay, C.-j. Huang, Wild bitter gourd improves metabolic syndrome: a preliminary dietary supplementation trial, Nutrition Journal, 11 (2012) 4.

[87] I. Hasan, S. Khatoon, Effect of Momordica charantia (bitter gourd) tablets in diabetes mellitus: Type 1 and Type 2, Prime Res Med (PROM), 2 (2012) 72-74.

[88] A. Fuangchan, P. Sonthisombat, T. Seubnukarn, R. Chanouan, P. Chotchaisuwat, V. Sirigulsatien, K. Ingkaninan, P. Plianbangchang, S.T. Haines, Hypoglycemic effect of bitter melon compared with metformin in newly diagnosed type 2 diabetes patients, Journal of ethnopharmacology, 134 (2011) 422-428.

[89] A. Tongia, S.K. Tongia, M. Dave, Phytochemical determination and extraction of Momordica charantia fruit and its hypoglycemic potentiation of oral hypoglycemic drugs in diabetes mellitus (NIDDM), Indian journal of physiology and pharmacology, 48 (2004) 241-244.

[90] A. John, R. Cherian, H. Subhash, A. Cherian, Evaluation of the efficacy of bitter gourd (momordica charantia) as an oral hypoglycemic agent--a randomized

controlled clinical trial, Indian journal of physiology and pharmacology, 47 (2003) 363-365.

[91] M.S. Akhtar, Trial of Momordica charantia Linn (Karela) powder in patients with maturity-onset diabetes, J Pak Med Assoc, 32 (1982) 106-107.

[92] P. Khanna, S. Jain, A. Panagariya, V. Dixit, Hypoglycemic activity of polypeptide-p from a plant source, Journal of Natural Products, 44 (1981) 648-655.

[93] J. Patel, M. Dhirawani, J. Doshi, Karelia" in the treatment of diabetes mellitus, Indian journal of medical sciences, 22 (1968) 30-32.

[94] M.J. Firdhouse, P. Lalitha, Maestro 9.4 as a Tool in the Structure Based Screening of Glycoalkaloids and Related Compounds, Targeting Aldose Reductase, Trends in Bioinformatics, 8 (2015) 26.

[95] L. Flores-Bocanegra, A. Pérez-Vásquez, M. Torres-Piedra, R. Bye, E. Linares, R. Mata, α-Glucosidase inhibitors from *Vauquelinia corymbosa*, Molecules, 20 (2015) 15330-15342.

[96] P. Rathinavelusamy, P.M. Mazumder, D. Sasmal, V. Jayaprakash, Evaluation of in silico, in vitro α-amylase inhibition potential and antidiabetic activity of Pterospermum acerifolium bark, Pharm. Biol., 52 (2014) 199-207.

[97] K.-T. Kim, L.-E. Rioux, S.L. Turgeon, Alpha-amylase and alpha-glucosidase inhibition is differentially modulated by fucoidan obtained from Fucus vesiculosus and Ascophyllum nodosum, Phytochemistry, 98 (2014) 27-33.

[98] J. Grover, S. Yadav, Pharmacological actions and potential uses of Momordica charantia: a review, J Ethnopharmacol, 93 (2004) 123-132.

[99] T.A. Pearson, G.A. Mensah, R.W. Alexander, J.L. Anderson, R.O. Cannon III, M. Criqui, Y.Y. Fadl, S.P. Fortmann, Y. Hong, G.L. Myers, Markers of inflammation and cardiovascular disease: application to clinical and public health practice: a statement for healthcare professionals from the Centers for Disease Control and Prevention and the American Heart Association, circulation, 107 (2003) 499-511.

[100] B.B. Duncan, M.I. Schmidt, J.S. Pankow, C.M. Ballantyne, D. Couper, A. Vigo, R. Hoogeveen, A.R. Folsom, G. Heiss, Low-grade systemic inflammation and the development of type 2 diabetes: the atherosclerosis risk in communities study, Diabetes, 52 (2003) 1799-1805.

[101] M. Shahinozzaman, N. Taira, T. Ishii, M. Halim, M. Hossain, S. Tawata, Anti-Inflammatory, Anti-Diabetic, and Anti-Alzheimer's Effects of Prenylated Flavonoids from Okinawa Propolis: An Investigation by Experimental and Computational Studies, Molecules, 23 (2018) 2479.

[102] S.-S. Huang, S.-Y. Su, J.-S. Chang, H.-J. Lin, W.-T. Wu, J.-S. Deng, G.-J. Huang, Antioxidants, anti-inflammatory, and antidiabetic effects of the aqueous extracts from Glycine species and its bioactive compounds, Bot Stud, 57 (2016) 38.

[103] S. Himaya, B. Ryu, Z.-J. Qian, S.-K. Kim, Paeonol from Hippocampus kuda Bleeler suppressed the neuro-inflammatory responses in vitro via NF-κB and MAPK signaling pathways, Toxicol In Vitro, 26 (2012) 878-887.

[104] C.P. Domingueti, L.M.S.A. Dusse, M. das Graças Carvalho, L.P. de Sousa, K.B. Gomes, A.P. Fernandes, Diabetes mellitus: the linkage between oxidative stress,

inflammation, hypercoagulability and vascular complications, J. Diabetes Complications, 30 (2016) 738-745.

[105] C.-C. Liaw, H.-C. Huang, P.-C. Hsiao, L.-J. Zhang, Z.-H. Lin, S.-Y. Hwang, F.-L. Hsu, Y.-H. Kuo, 5β,19-epoxycucurbitane triterpenoids from *Momordica charantia* and their anti-inflammatory and cytotoxic activity, Planta Med., 81 (2015) 62-70.

[106] T.-H. Tsai, W.-C. Huang, H.-T. Ying, Y.-H. Kuo, C.-C. Shen, Y.-K. Lin, P.-J. Tsai, Wild bitter melon leaf extract inhibits Porphyromonas gingivalis-induced inflammation: identification of active compounds through bioassay-guided isolation, Molecules, 21 (2016) 454.

[107] M. Kobori, H. Nakayama, K. Fukushima, M. Ohnishi-Kameyama, H. Ono, T. Fukushima, Y. Akimoto, S. Masumoto, C. Yukizaki, Y. Hoshi, Bitter gourd suppresses lipopolysaccharide-induced inflammatory responses, J. Agric. Food Chem., 56 (2008) 4004-4011.

[108] H. Shanmugam, P. Acharya, G.K. Jayaprakasha, B.S. Patil, Nanoformulation and characterization of nomilin with different poly (lactic-co-glycolic acid) resomers and surfactants for the enhanced inhibition of α-amylase and angiotensin-converting-enzyme, J Funct Foods, 37 (2017) 564-573.

[109] G. Fu, W. Li, X. Huang, R. Zhang, K. Tian, S. Hou, Y. Li, Antioxidant and alpha-glucosidase inhibitory activities of isoflavonoids from the rhizomes of *Ficus tikoua* bur, Nat. Prod. Res., 32 (2018) 399-405.

[110] M.O. Fatope, Y. Takeda, H. Yamashita, H. Okabe, T. Yamauchi, New cucurbitane triterpenoids from Momordica charantia, J. Nat. Prod., 53 (1990) 1491-1497.

[111] B.G. Panlilio, A.P.G. Macabeo, M. Knorn, P. Kohls, P. Richomme, S.F. Kouam, D. Gehle, K. Krohn, S.G. Franzblau, Q. Zhang, A lanostane aldehyde from Momordica charantia, Phytochem Lett, 5 (2012) 682-684.

[112] L. Peng, L. Jian-Feng, K. Li-Ping, Y. He-Shui, L.-J. ZHANG, S. Xin-Bo, M. Bai-Ping, A new C30 sterol glycoside from the fresh fruits of Momordica charantia, Chinese journal of natural medicines, 2 (2012) 88-91.

[113] G.-T. Zhao, J.-Q. Liu, Y.-Y. Deng, H.-Z. Li, J.-C. Chen, Z.-R. Zhang, L. Zhou, M.-H. Qiu, Cucurbitane-type triterpenoids from the stems and leaves of Momordica charantia, Fitoterapia, 95 (2014) 75-82.

[114] L. Harinantenaina, M. Tanaka, S. Takaoka, M. Oda, O. Mogami, M. Uchida, Y. Asakawa, *Momordica charantia* constituents and antidiabetic screening of the isolated major compounds, Chem. Pharm. Bull., 54 (2006) 1017-1021.

[115] M. Taha, S. Imran, F. Rahim, A. Wadood, K.M. Khan, Oxindole based oxadiazole hybrid analogs: Novel α-glucosidase inhibitors, Bioorg. Chem., 76 (2018) 273-280.

[116] G.D. Brayer, Y. Luo, S.G. Withers, The structure of human pancreatic α-amylase at 1.8 Å resolution and comparisons with related enzymes, Protein Sci., 4 (1995) 1730-1742.

[117] M. Qian, R. Haser, G. Buisson, E. Duee, F. Payan, The Active Center of a Mammalian. alpha.-Amylase. Structure of the Complex of a Pancreatic. alpha.-

Amylase with a Carbohydrate Inhibitor Refined to 2.2-. ANG. Resolution, Biochemistry, 33 (1994) 6284-6294.

[118] X. Sui, Y. Zhang, W. Zhou, In vitro and in silico studies of the inhibition activity of anthocyanins against porcine pancreatic α-amylase, J Funct Foods, 21 (2016) 50-57.

[119] H. Sun, D. Wang, X. Song, Y. Zhang, W. Ding, X. Peng, X. Zhang, Y. Li, Y. Ma, R. Wang, Natural prenylchalconaringenins and prenylnaringenins as antidiabetic agents: α-glucosidase and α-amylase inhibition and in vivo antihyperglycemic and antihyperlipidemic effects,

J. Agric. Food Chem., 65 (2017) 1574-1581.

[120] A.A. Alghasham, Cucurbitacins–a promising target for cancer therapy, Int. J. Health Sci., 7 (2013) 77.

[121] H. Sun, W.-S. Fang, W.-Z. Wang, C. Hu, Structure-activity relationships of oleanane-and ursane-type triterpenoids, Bot. Stud., 47 (2006) 339-368.

[122] T. Moses, K.K. Papadopoulou, A. Osbourn, Metabolic and functional diversity of saponins, biosynthetic intermediates and semi-synthetic derivatives, Crit. Rev. Biochem. Mol. Biol., 49 (2014) 439-462.

[123] L.-W. Qi, C.-Z. Wang, C.-S. Yuan, American ginseng: potential structure–function relationship in cancer chemoprevention, Biochem. Pharmacol., 80 (2010) 947-954.

[124] J.L. Perez, G.K. Jayaprakasha, K. Crosby, B.S. Patil, Evaluation of bitter melon (*Momordica charantia*) cultivars grown in Texas and levels of various phytonutrients, J. Sci. Food Agric., (2018).

[125] J.L. Perez, G.K. Jayaprakasha, B.S. Patil, Separation and identification of cucurbitane-type triterpenoids from bitter melon, ACS Symp. Ser., 1185 (2014) 51-78.

[126] N.X. Nhiem, P. Van Kiem, C. Van Minh, N.K. Ban, N.X. Cuong, N.H. Tung, M.H. Le, T.H. Do, B.H. Tai, T.H. Quang, α-Glucosidase inhibition properties of cucurbitane-type triterpene glycosides from the fruits of *Momordica charantia*, Chem. Pharm. Bull., 58 (2010) 720-724.

[127] M.-J. Tan, J.-M. Ye, N. Turner, C. Hohnen-Behrens, C.-Q. Ke, C.-P. Tang, T. Chen, H.-C. Weiss, E.-R. Gesing, A. Rowland, Antidiabetic activities of triterpenoids isolated from bitter melon associated with activation of the AMPK pathway, Chem. Biol. (Oxford, U. K.), 15 (2008) 263-273.

[128] K.-W. Lin, S.-C. Yang, C.-N. Lin, Antioxidant constituents from the stems and fruits of *Momordica charantia*, Food Chem., 127 (2011) 609-614.

[129] J.-R. Weng, L.-Y. Bai, C.-F. Chiu, J.-L. Hu, S.-J. Chiu, C.-Y. Wu, Cucurbitane triterpenoid from *Momordica charantia* induces apoptosis and autophagy in breast cancer cells, in part, through peroxisome proliferator-activated receptor γ activation, Evid Based Complement Alternat Med, 2013 (2013).

[130] J. Zhang, Y. Huang, T. Kikuchi, H. Tokuda, N. Suzuki, K.i. Inafuku, M. Miura, S. Motohashi, T. Suzuki, T. Akihisa, Cucurbitane triterpenoids from the leaves of

Momordica charantia, and their cancer chemopreventive effects and cytotoxicities, Chem. Biodiversity, 9 (2012) 428-440.

[131] S. Hasani-Ranjbar, N. Nayebi, B. Larijani, M. Abdollahi, A systematic review of the efficacy and safety of herbal medicines used in the treatment of obesity, World J. Gastroenterol., 15 (2009) 3073.

[132] P.-C. Hsiao, C.-C. Liaw, S.-Y. Hwang, H.-L. Cheng, L.-J. Zhang, C.-C. Shen, F.-L. Hsu, Y.-H. Kuo, Antiproliferative and hypoglycemic cucurbitane-type glycosides from the fruits of *Momordica charantia*, J. Agric. Food Chem., 61 (2013) 2979-2986.

[133] E. Lontchi-Yimagou, E. Sobngwi, T.E. Matsha, A.P. Kengne, Diabetes mellitus and inflammation, Curr. Diabetes Rep., 13 (2013) 435-444.

[134] U.P.D.S. Group, Overview of 6 years' therapy of type II diabetes: a progressive disease. UK Prospective Diabetes Study 16, Diabetes, 44 (1995) 1249-1258.

[135] M. Garcia, M. Saenz, M. Gomez, M. Fernandez, Topical antiinflammatory activity of phytosterols isolated from *Eryngium foetidum* on chronic and acute inflammation models, Phytotherapy Research: An International Journal Devoted to Pharmacological and Toxicological Evaluation of Natural Product Derivatives, 13 (1999) 78-80.

[136] S. Reuter, S.C. Gupta, M.M. Chaturvedi, B.B. Aggarwal, Oxidative stress, inflammation, and cancer: how are they linked?, Free Radical Biol. Med., 49 (2010) 1603-1616.

[137] C. Porta, E. Riboldi, A. Sica, Mechanisms linking pathogens-associated inflammation and cancer, Cancer Lett. , 305 (2011) 250-262.

[138] P. Dandona, A. Aljada, A. Bandyopadhyay, Inflammation: the link between insulin resistance, obesity and diabetes, Trends Immunol., 25 (2004) 4-7.

[139] H. Shanmugam, P. Acharya, G.K. Jayaprakasha, B.S. Patil, Nanoformulation and characterization of nomilin with different poly (lactic-co-glycolic acid) resomers and surfactants for the enhanced inhibition of α-amylase and angiotensin-converting-enzyme, J. Funct. Foods, 37 (2017) 564-573.

[140] H. Okabe, Y. Miyahara, T. Yamauchi, Structures of momordicosides F1, F2, G, I, K and L, novel cucurbitacins in the fruits of *Momordica charantia* L, Tetrahedron Lett., 23 (1982) 77-80.

[141] H. Matsuda, S. Nakamura, T. Murakami, Structures of new cucurbitane-type triterpenes and glycosides, Karavilagenins D and E, and Karavilosides VI, VII, VII, IX, X, and XI, from the fruit of *Momordica charantia*, Heterocycles, 71 (2007) 331-341.

[142] T. Tanaka, T. Nakashima, T. Ueda, K. Tomii, I. Kouno, Facile discrimination of aldose enantiomers by reversed-phase HPLC, Chem. Pharm. Bull., 55 (2007) 899-901.

[143] J. Schaefer, E. Stejskal, R. McKay, W.T. Dixon, Phenylalanine ring dynamics by solid-state 13C NMR, J. Magn. Reson. (1969-1992), 57 (1984) 85-92.

[144] E.K. Lim, D.A. Ashford, B. Hou, R.G. Jackson, D.J. Bowles, Arabidopsis glycosyltransferases as biocatalysts in fermentation for regioselective synthesis of diverse quercetin glucosides, Biotechnol. Bioeng., 87 (2004) 623-631.

[145] H. Matsuura, C. Asakawa, M. Kurimoto, J. Mizutani, α-Glucosidase inhibitor from the seeds of balsam pear (*Momordica charantia*) and the fruit bodies of *Grifola frondosa*, Biosci., Biotechnol., Biochem., 66 (2002) 1576-1578.

[146] T. Uebanso, H. Arai, Y. Taketani, M. Fukaya, H. Yamamoto, A. Mizuno, K. Uryu, T. Hada, E. Takeda, Extracts of *Momordica charantia* suppress postprandial hyperglycemia in rats, J. Nutr. Sci. Vitaminol., 53 (2007) 482-488.

[147] J. Yue, J. Xu, J. Cao, X. Zhang, Y. Zhao, Cucurbitane triterpenoids from *Momordica charantia* L. and their inhibitory activity against α-glucosidase, α-amylase and protein tyrosine phosphatase 1B (PTP1B), J. Funct. Foods, 37 (2017) 624-631.

[148] M. Liu, B. Hu, H. Zhang, Y. Zhang, L. Wang, H. Qian, X. Qi, Inhibition study of red rice polyphenols on pancreatic α-amylase activity by kinetic analysis and molecular docking, J. Cereal Sci., 76 (2017) 186-192.

[149] J. Yang, D. Gu, M. Wang, D. Kou, H. Guo, J. Tian, Y. Yang, *In silico*-assisted identification of α-amylase inhibitor from the needle oil of *Pinus tabulaeformis* Carr, Ind. Crops Prod., 111 (2018) 360-363.

[150] X. Sui, Y. Zhang, W. Zhou, *In vitro* and *in silico* studies of the inhibition activity of anthocyanins against porcine pancreatic α-amylase, J. Funct. Foods, 21 (2016) 50-57.

[151] E. Lo Piparo, H. Scheib, N. Frei, G. Williamson, M. Grigorov, C.J. Chou, Flavonoids for controlling starch digestion: structural requirements for inhibiting human α-amylase, J. Med. Chem., 51 (2008) 3555-3561.

[152] H. Sun, D. Wang, X. Song, Y. Zhang, W. Ding, X. Peng, X. Zhang, Y. Li, Y. Ma, R. Wang, Natural prenylchalconaringenins and prenylnaringenins as antidiabetic agents: α-glucosidase and α-amylase inhibition and *in vivo* antihyperglycemic and antihyperlipidemic effects, J. Agric. Food Chem., 65 (2017) 1574-1581.

[153] J. Rios, M. Recio, S. Maáñez, R. Giner, Natural triterpenoids as anti-inflammatory agents, Stud. Nat. Prod. Chem., Elsevier2000, pp. 93-143.

[154] H.-L. Cheng, C.-Y. Kuo, Y.-W. Liao, C.-C. Lin, EMCD, a hypoglycemic triterpene isolated from *Momordica charantia* wild variant, attenuates TNF-α-induced inflammation in FL83B cells in an AMP-activated protein kinase-independent manner, Eur. J. Pharmacol., 689 (2012) 241-248.

[155] M. Gasparrini, T.Y. Forbes-Hernandez, F. Giampieri, S. Afrin, J.M. Alvarez-Suarez, L. Mazzoni, B. Mezzetti, J.L. Quiles, M. Battino, Anti-inflammatory effect of strawberry extract against LPS-induced stress in RAW 264.7 macrophages, Food Chem. Toxicol., 102 (2017) 1-10.

APPENDIX

Table A1 ^{1}H and ^{13}C NMR data for purified compound **3** from the EtOAc extract of *Momordica charantia*

Position	**Compound 3 MeOH-d_4**	
	δ_H (ppm)	**δ_C (ppm)**
1	1.65; 1.70 m	22.7
2	1.87; 2.00 m	27.0
3	4.82 m	81.1
4	-	41.2
5	-	146.5
6	5.93 dd, 1H (*J*= 5.6; 1.6 Hz)	124.2
7	4.03 d, 1H (*J*= 5.4 Hz)	66.9
8	1.94 br s, 1 H	51.3
9	-	51.2
10	2.65 dd, 1H (*J* = 13.2, 4.3 Hz)	37.3
11	1.48; 2.39 m	23.3
12	1.42; 1.98 m	28.7
13	-	46.8
14	-	48.8
15	1.40; 1.40 m	35.7
16	1.68; 1.68 m	30.2
17	1.56 m	51.4
18	0.92 s, 3H	15.5
19	9.84 s, 1H	209.4
20	1.55 m	37.7
21	0.92 d, 3H	19.3
22	1.78; 2.16 m	40.4
23	5.58 m, 2H	125.9
24	5.58 m, 2H	141.0
25	-	71.3
26	1.25 s, 6H	30.3
27	1.25 s, 6H	30.2
28	1.17 s, 3H	27.5
29	1.21 s, 3H	25.6
30	0.82 s, 3H	18.8
3-COOH	-	168.3

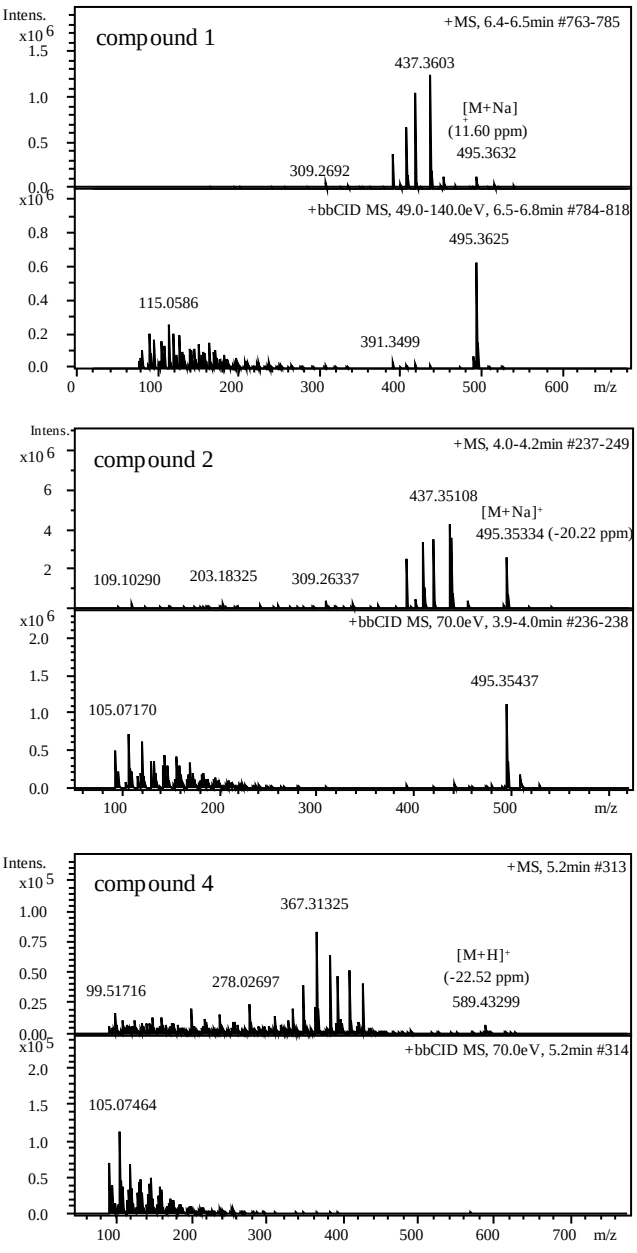

Figure A1 High-resolution mass spectra by electrospray chemical ionization of purified compounds (**1, 2 and 4**) from the EtOAc extract of *Momordica charantia.*

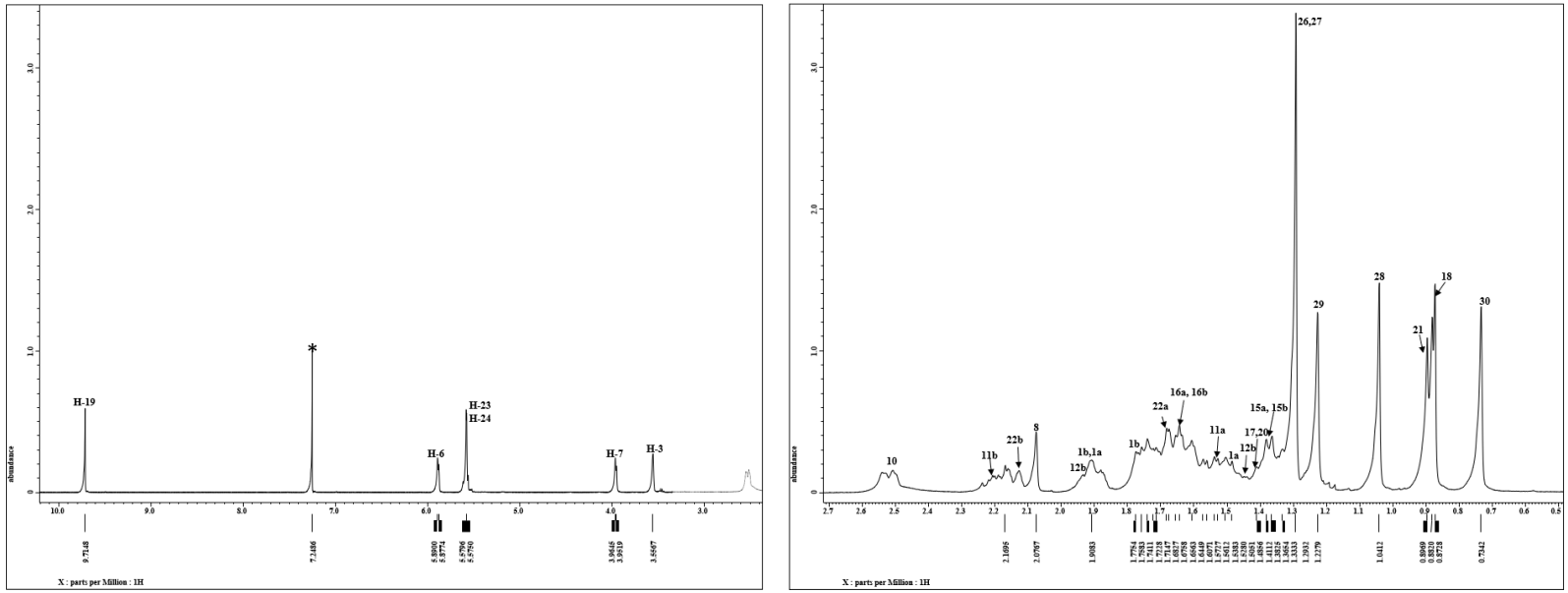

Figure A2 Complete assignments of ^{1}HNMR spectrum of compound **1 (**$CDCl_3$), recorded on a JEOL ECS NMR spectrometer at 400 MHz, solvent signal is marked with an asterisk (*).

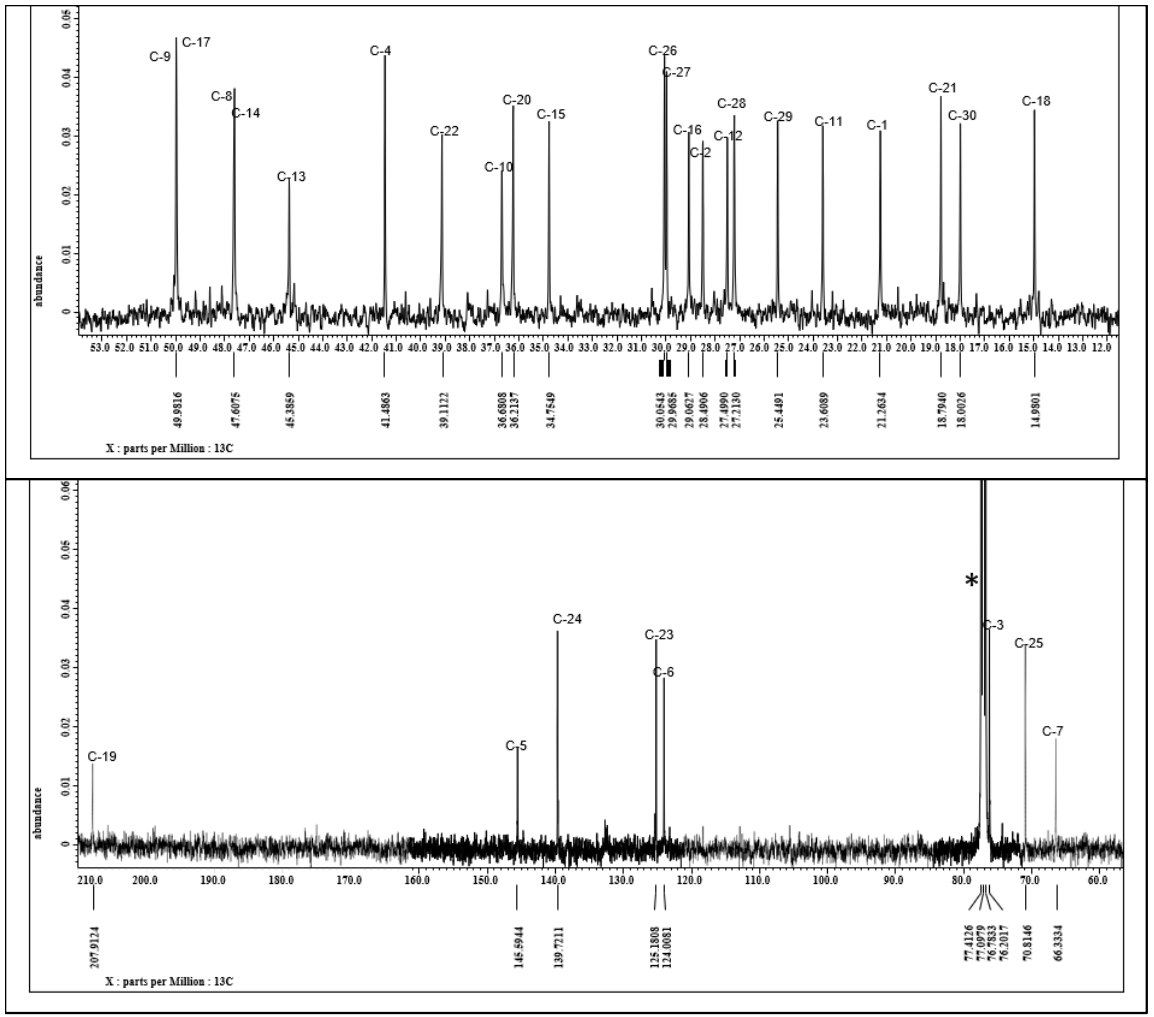

Figure A3 Complete assignments of ^{13}CNMR spectrum of compound **1**. Spectra was recorded in $CDCl_3$ at 100 MHz, solvent signal is marked with an asterisk (*).

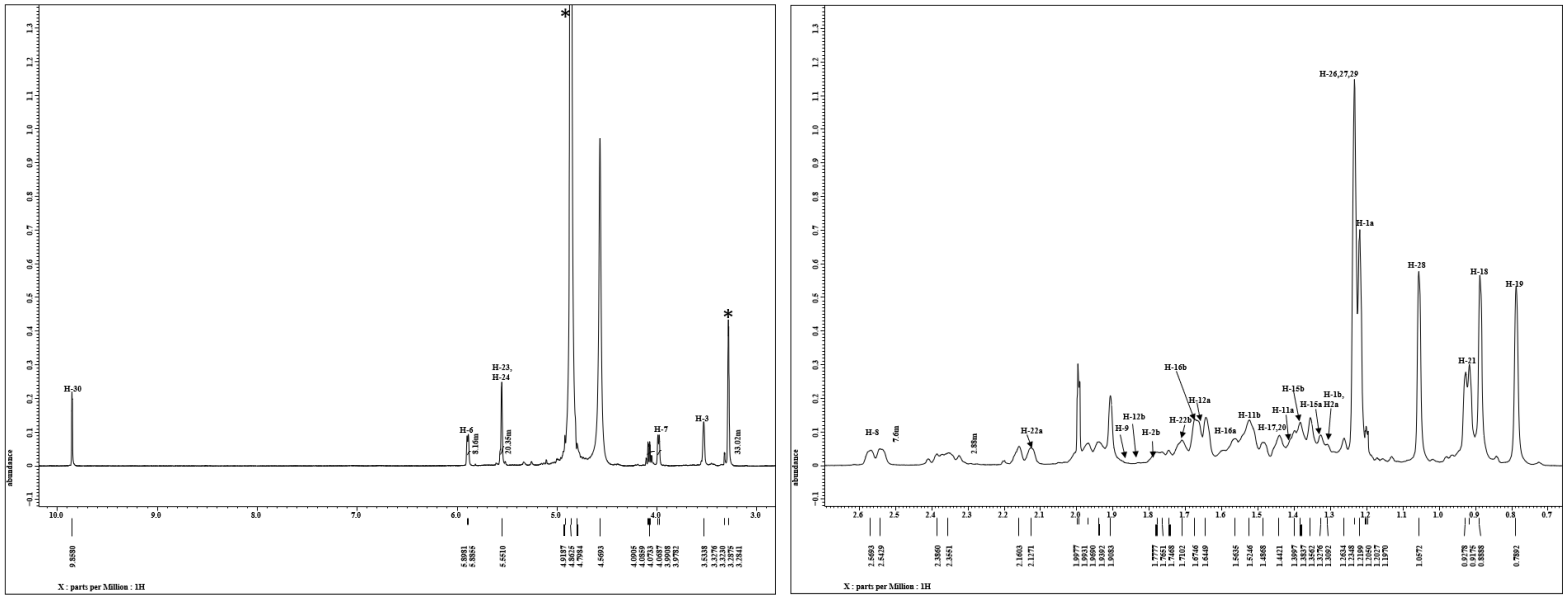

Figure A4 Complete assignments of ^{1}HNMR spectrum of compound **2** ($CDCl_3$), recorded on a JEOL ECS NMR spectrometer at 400 MHz, solvent signal is marked with an asterisk (*).

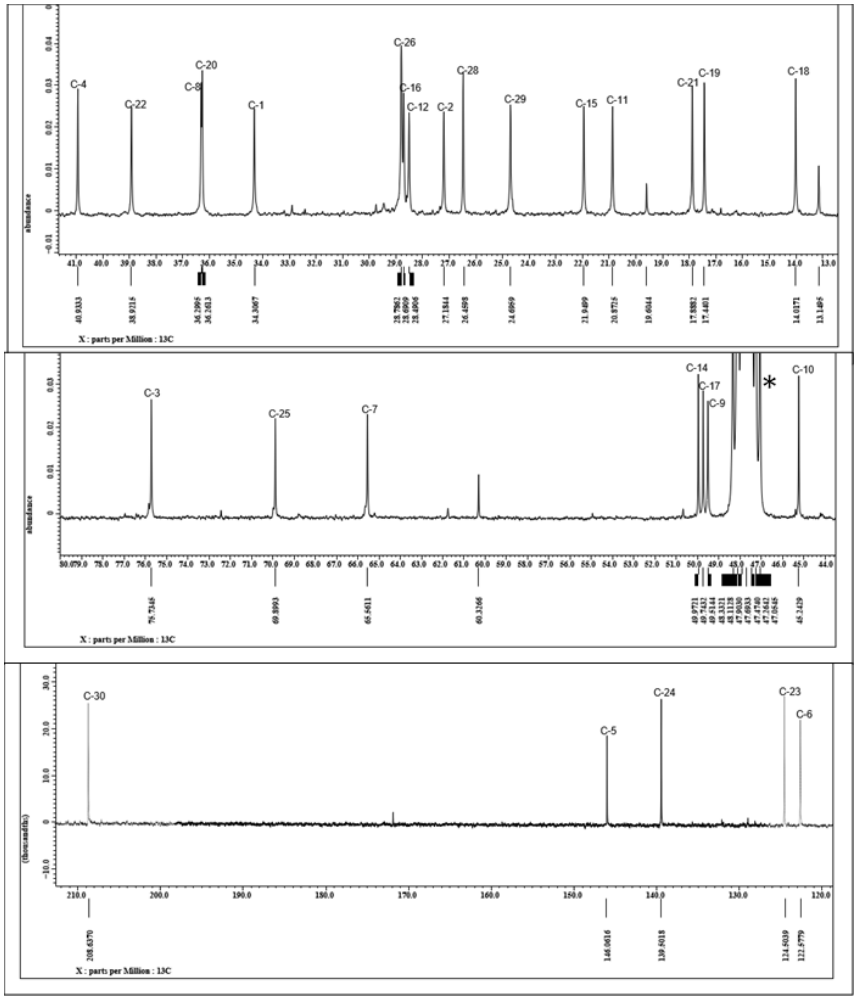

Figure A5 Complete assignments of ^{13}CNMR spectrum of compound **2**. Spectra was recorded in $CDCl_3$ at 100 MHz, solvent signal is marked with an asterisk (*).

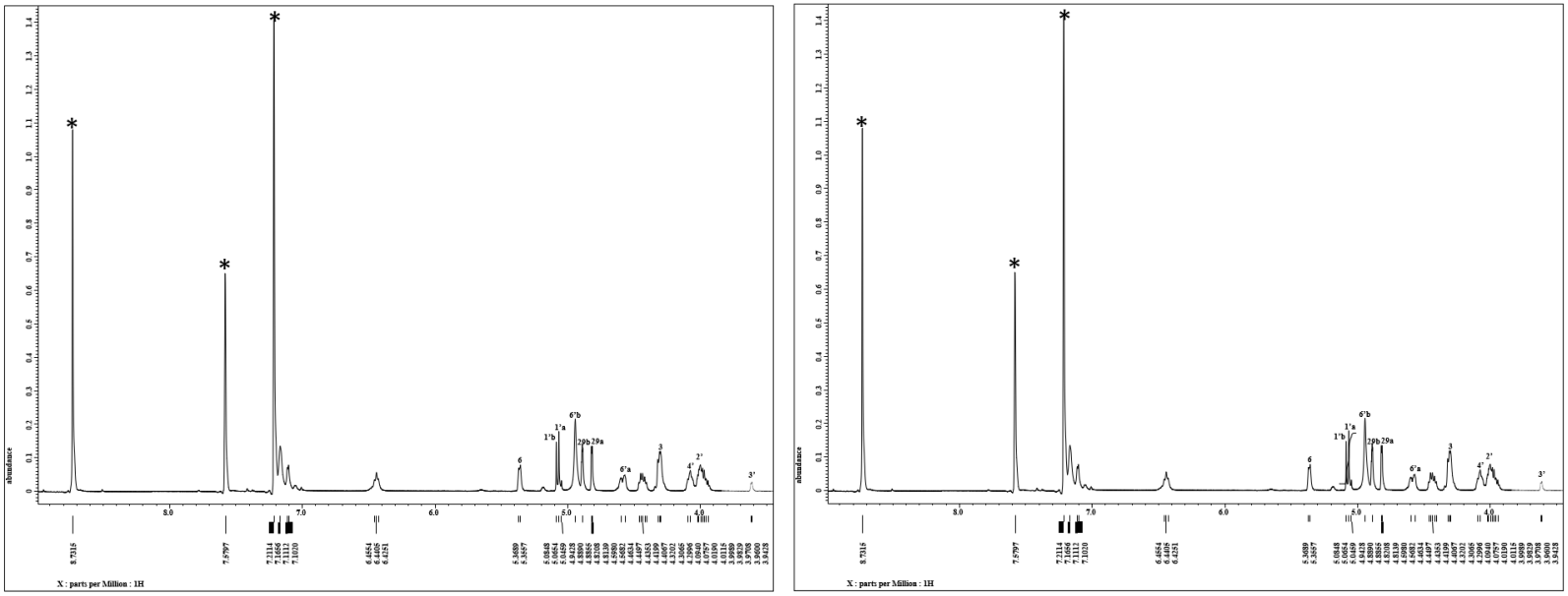

Figure A6 Complete assignments of ^{1}HNMR spectrum of compound **4** (C_5D_5N), recorded on a JEOL ECS NMR spectrometer at 400 MHz, solvent signal is denoted with an asterisk (*).

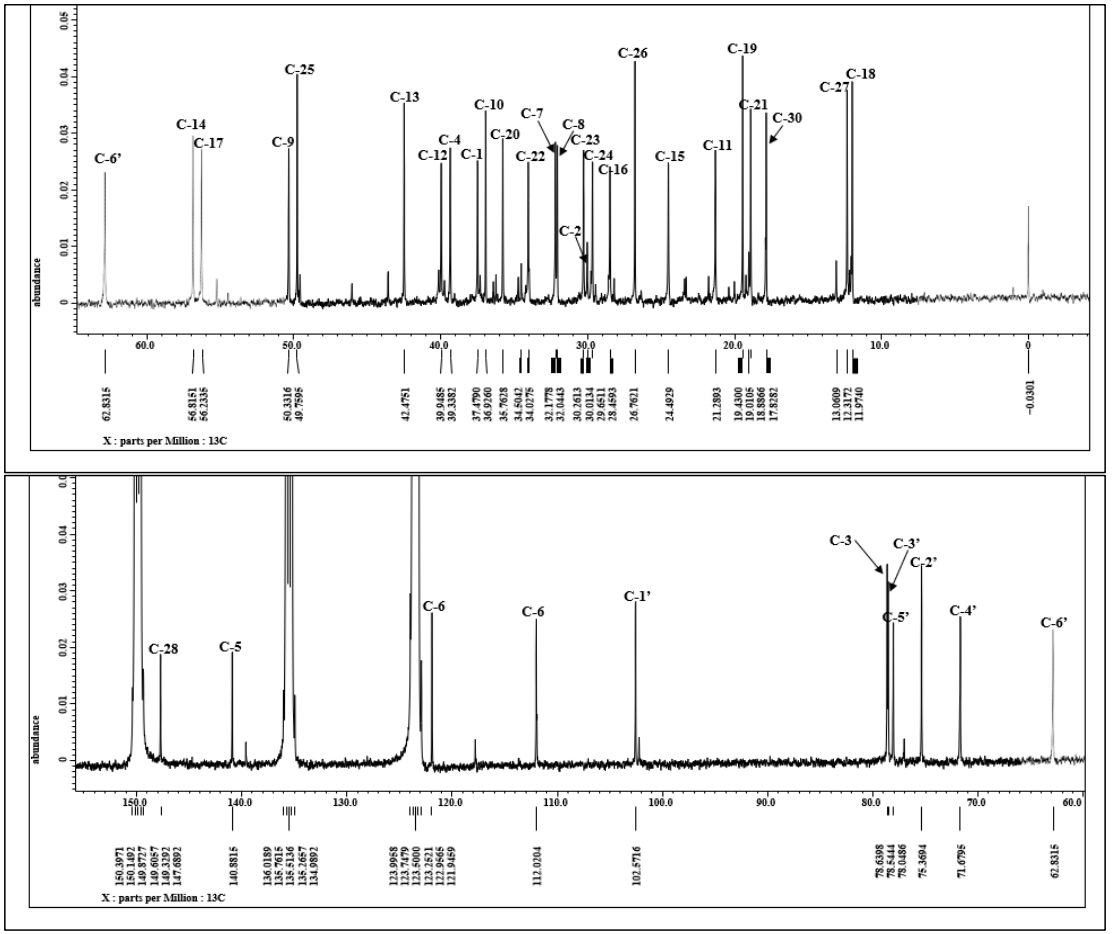

Figure A7 Complete assignments of ^{13}CNMR spectrum of compound **4**. Spectra was recorded in C_5D_5N at 100 MHz, solvent signal is demoted with an asterisk (*).

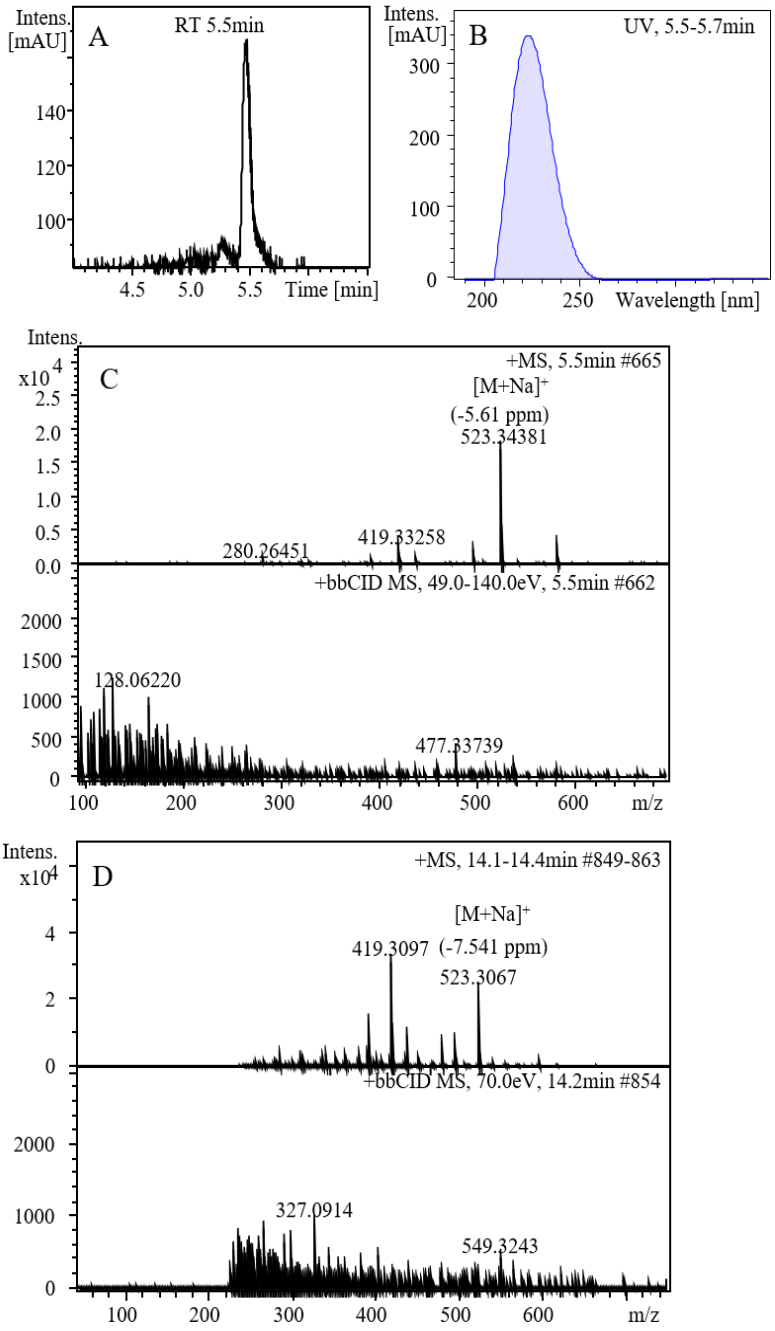

Figure A8 Identification of compound 3 by UV spectra and mass spectral analysis. (A). HPLC chromatogram of compound 3, (B). UV spectra, high resolution mass spectra obtained from (C). Electrospray ionization by positive mode and (D). Atmospheric pressure chemical ionization. Both the techniques confirm the molecular weight of compound **3**.

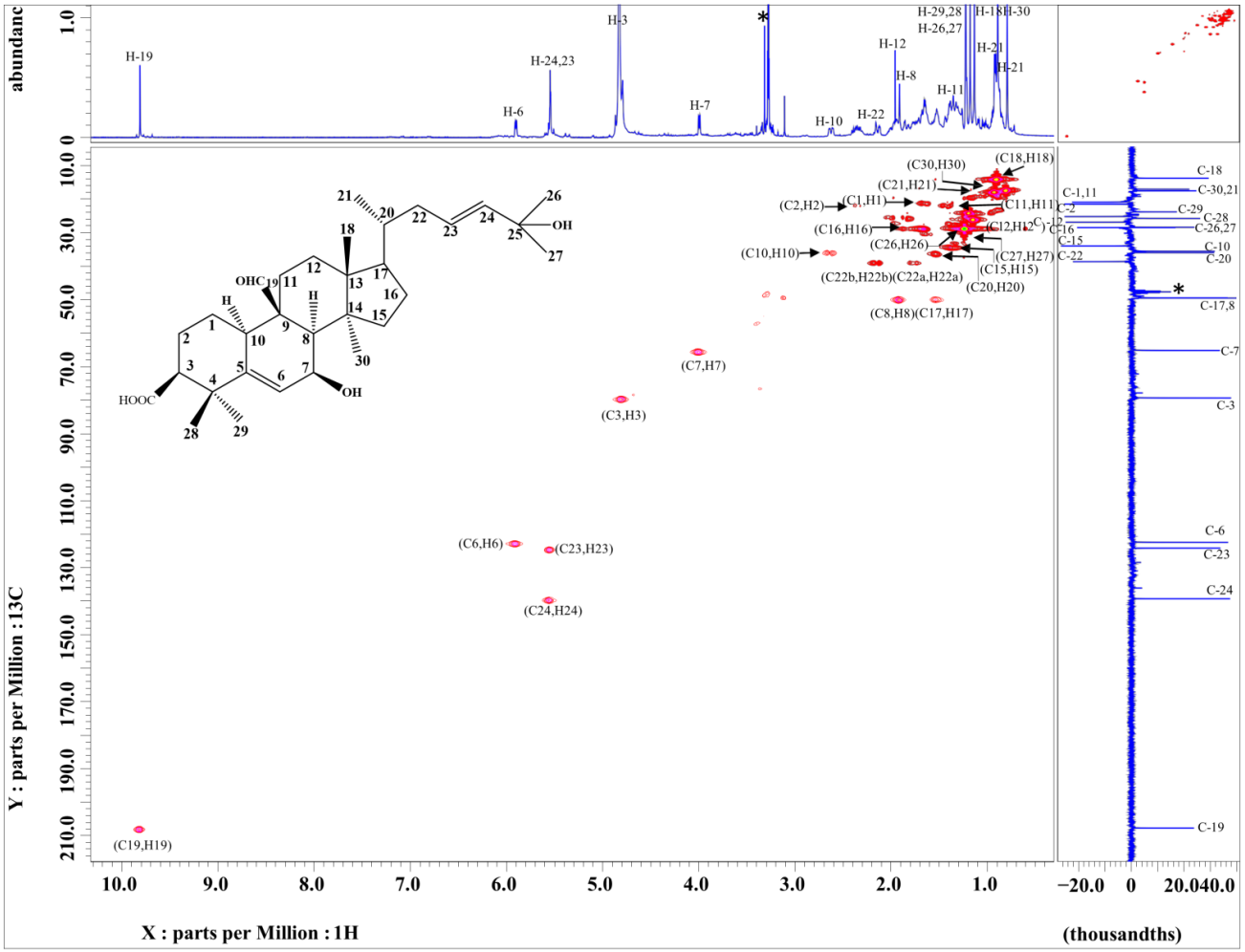

Figure A9 Complete assignment of HMQC spectra of compound (**3**) (charantoside XI). Spectrum was recorded in CD_3OD. ^{1}H-NMR spectrum on X-axis and DEPT-135 is on Y-axis of the spectrum. The solvent signal is marked with an asterisk

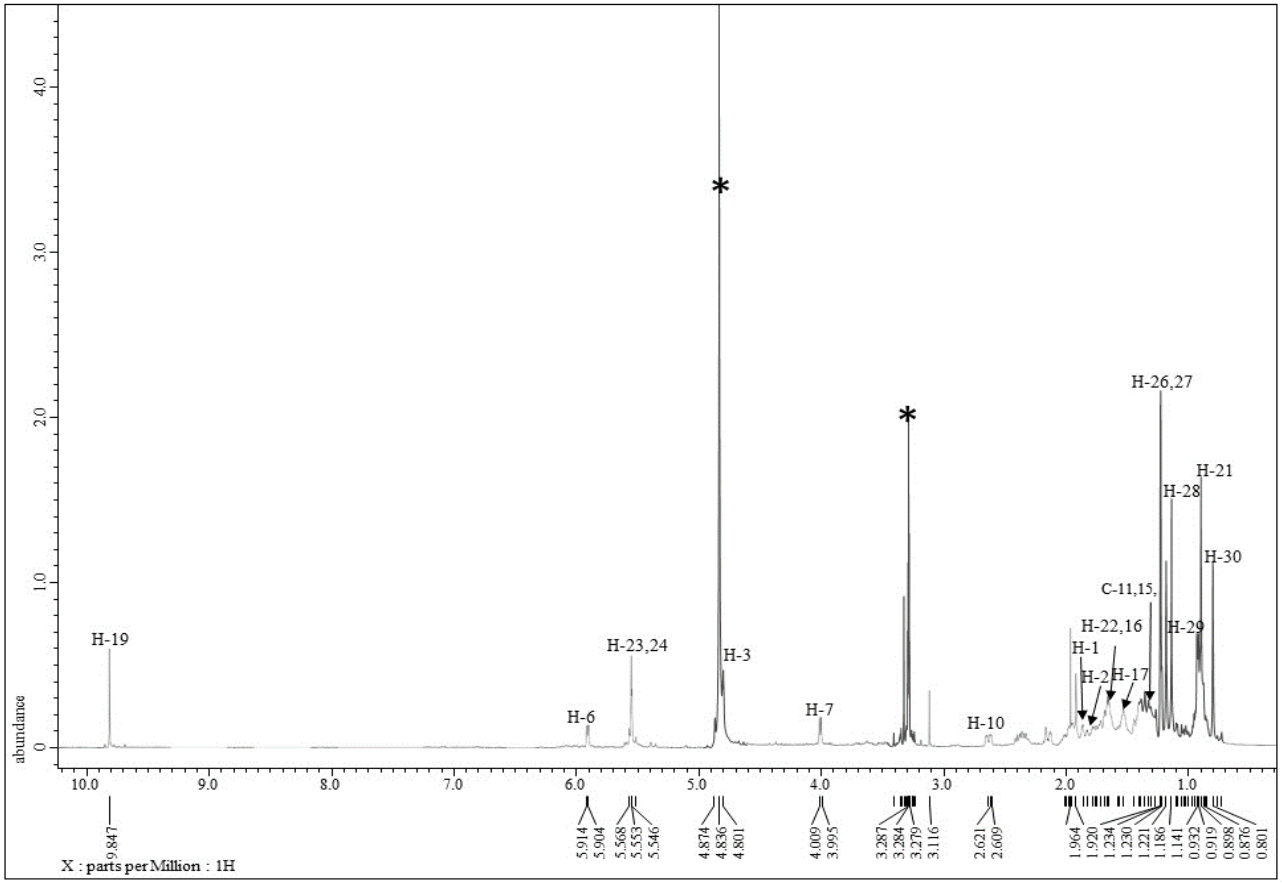

Figure A10 Complete assignments of ^{1}HNMR spectrum of compound **3 (**CD_3OD), recorded on a JEOL ECS NMR spectrometer at 400 MHz, solvent signal is marked with an asterisk (*).

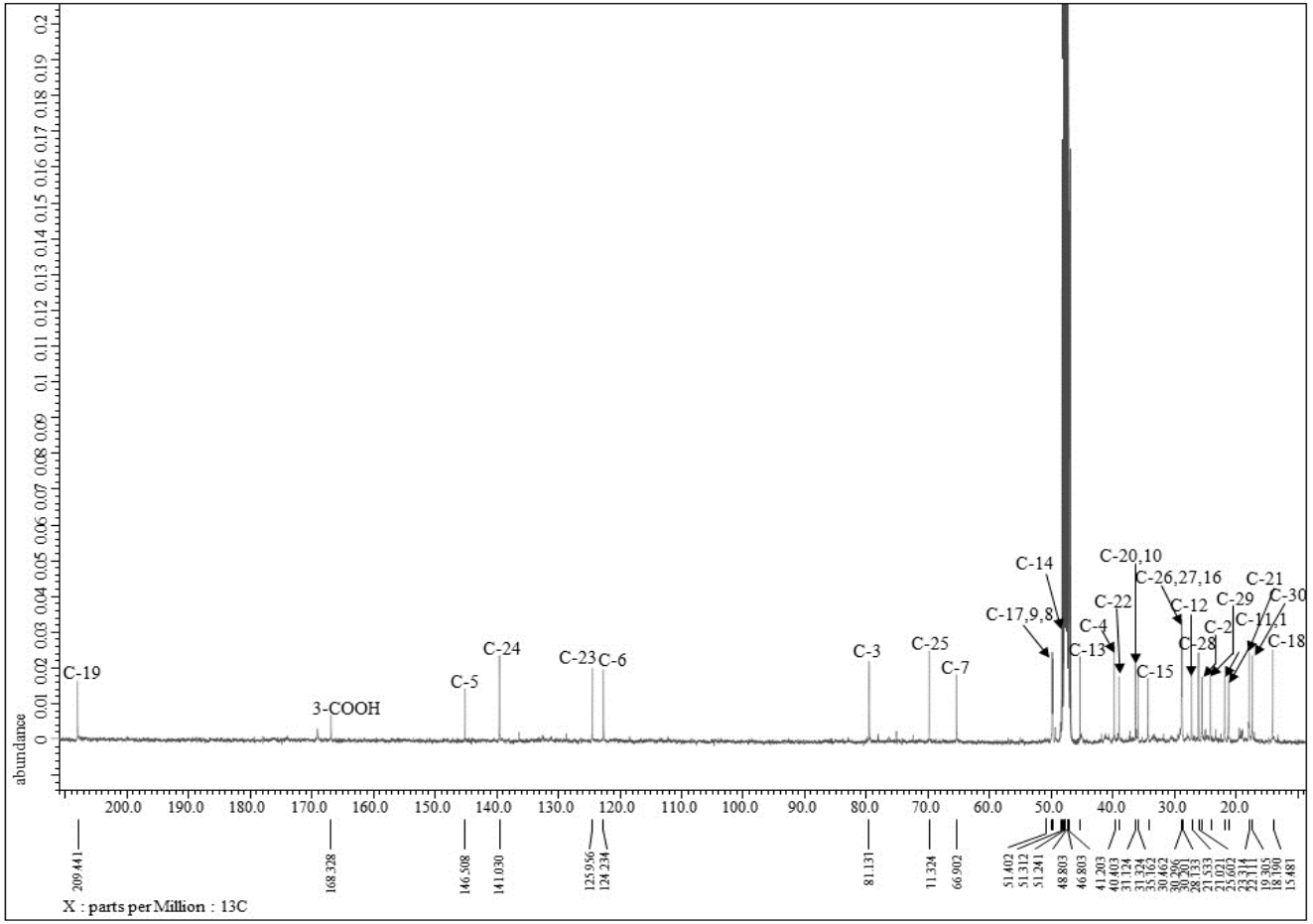

Figure A11 Complete assignments of ^{13}CNMR spectrum of compound **3**. Spectrum was recorded in CD_3OD at 100 MHz.

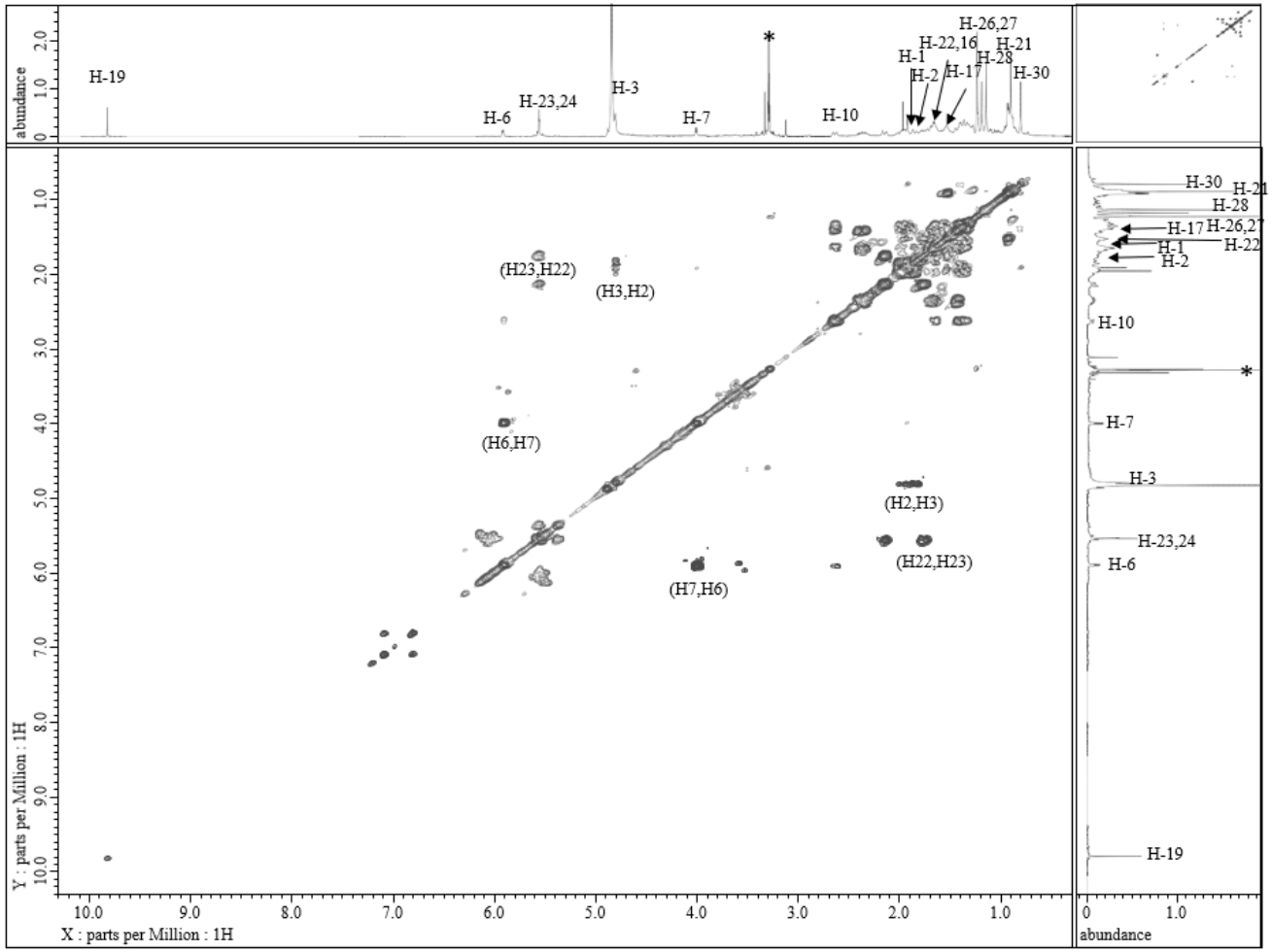

Figure A12 The key DQF-COSY correlations of compound **3.** Spectrum was recorded in CD_3OD at 100 MHz.

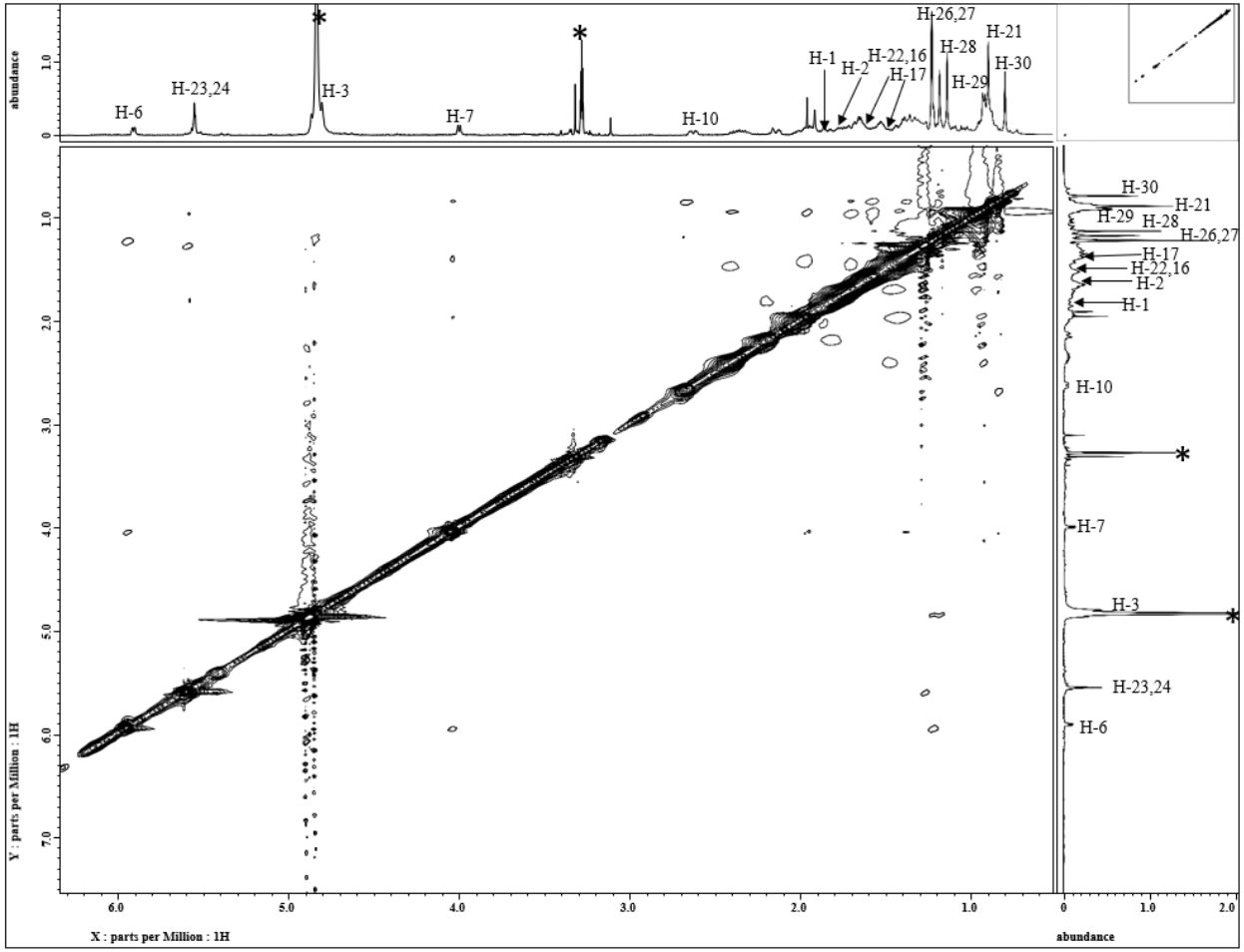

Figure A13 NOESY spectrum of compound **3**

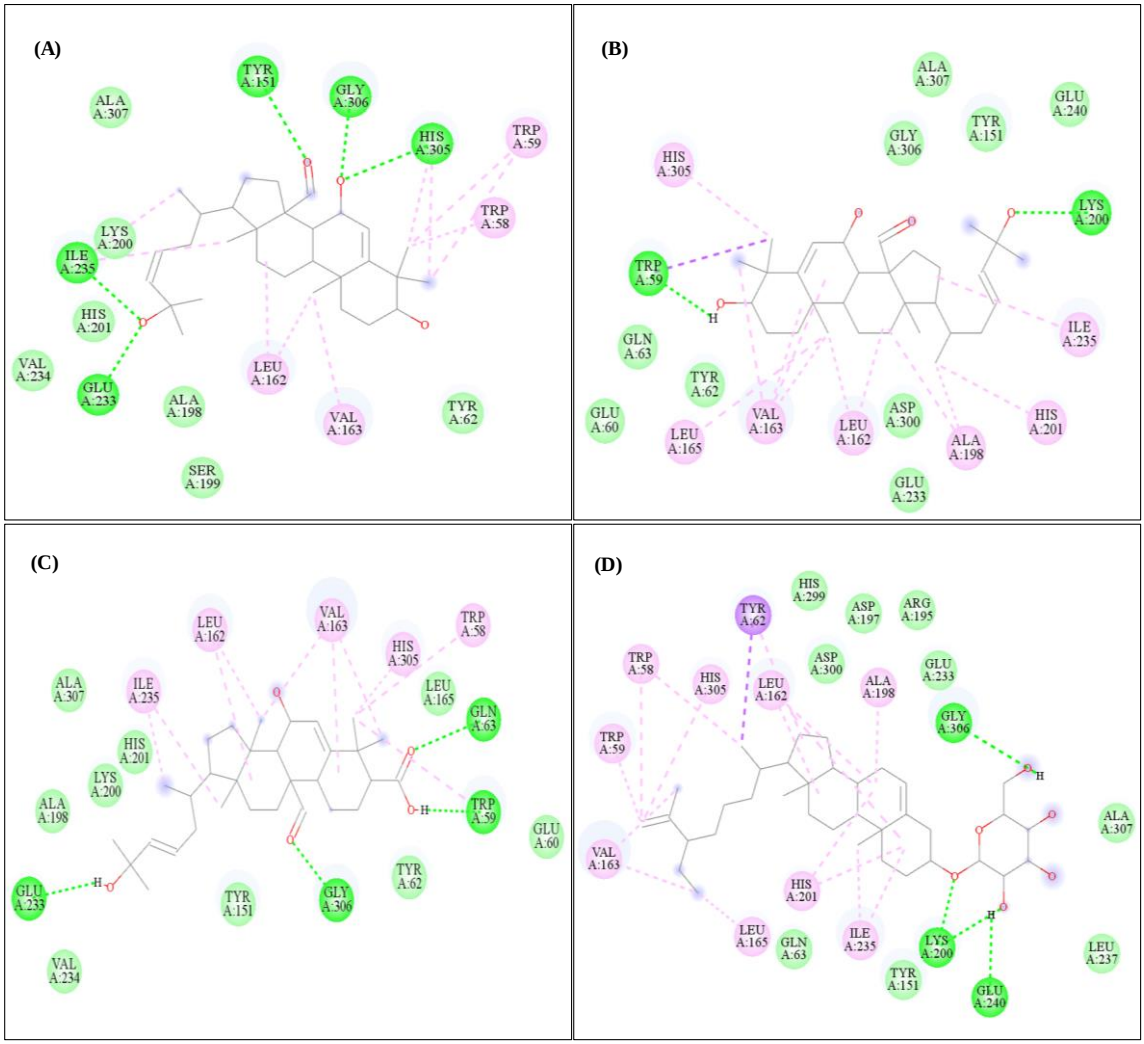

Figure A14 The 2D ligand-protein interactions of purified compounds (**A**). 3β,7β,25-trihydroxycucurbita-5,23(E)-dien-19-al, (**B**). charantal, (**C**), charantoside XI and (**D**). 25ξ-isopropenylchole-5, 6-ene-3-O-D-glucopyranoside with α-amylase enzyme. Legends below the figure shows the different types of bonding between compounds and the enzymatic pocket of α-amylase.

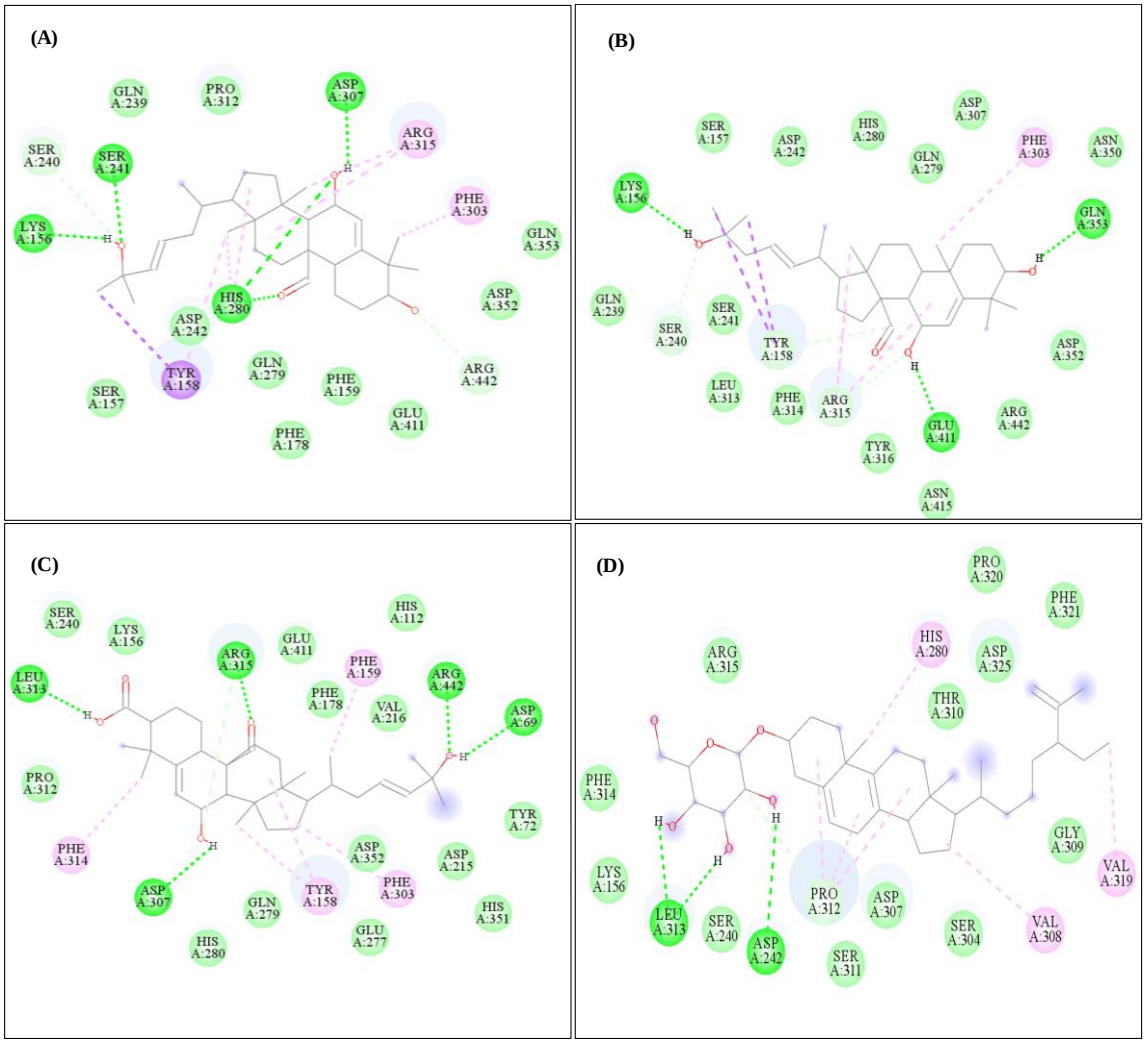

Figure A15 2D ligand-protein interactions of purified compounds (**A**). 3β,7β,25-trihydroxycucurbita-5,23(E)-dien-19-al, (**B**). charantal, (**C**), charantoside XI and (**D**). 25ξ-isopropenylchole-5, 6-ene-3-O-D-glucopyranoside with α-glucosidase enzyme. Legends below the figure shows the different types of bonding between compounds and the enzymatic pocket of α-glucosidase

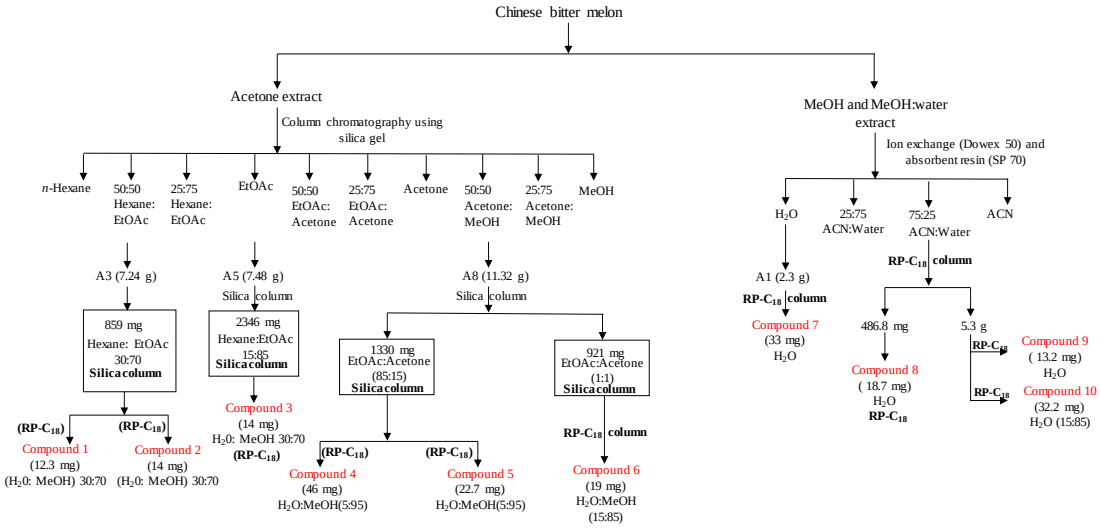

Figure A16 Isolation scheme for compounds **1-10** from Chinese bitter melon.

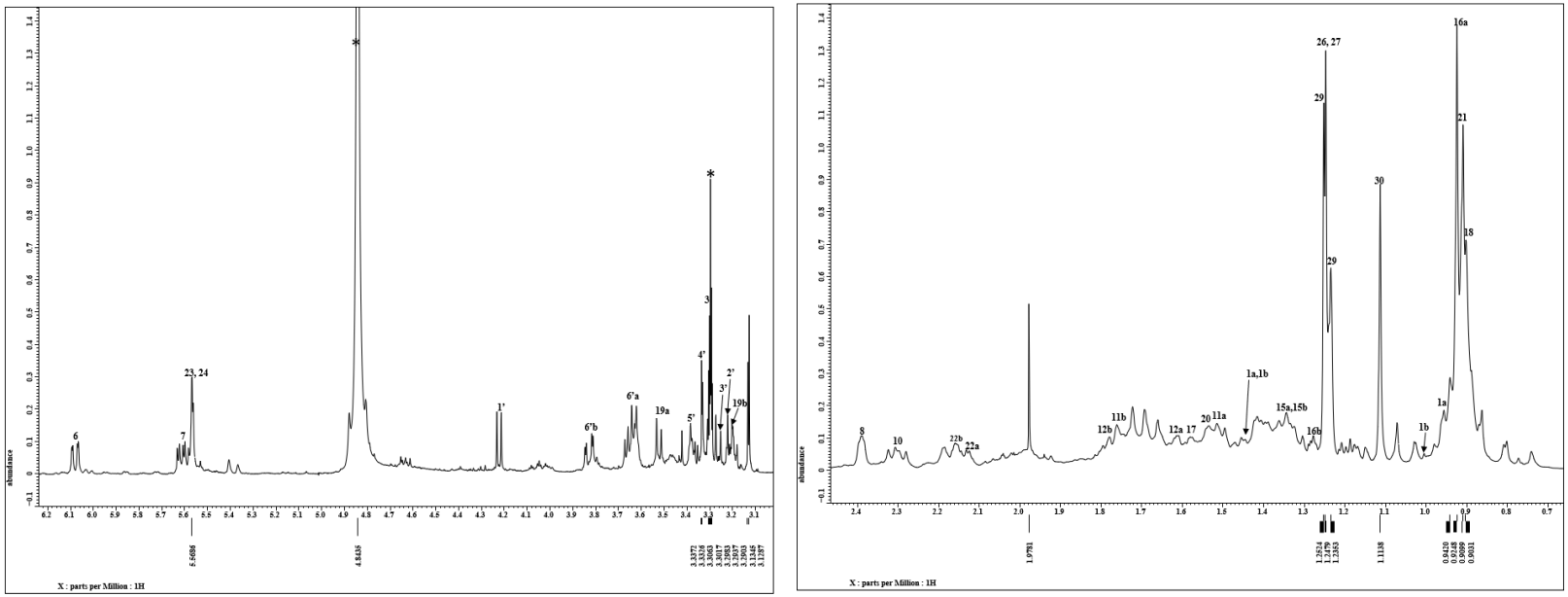

Figure A17 Complete assignments of ^{1}H-NMR spectra of compound **1** in MeOD, recorded at 400 MHz. using standard JEOL pulse programs. The solvent signal was marked as (*) asterisk.

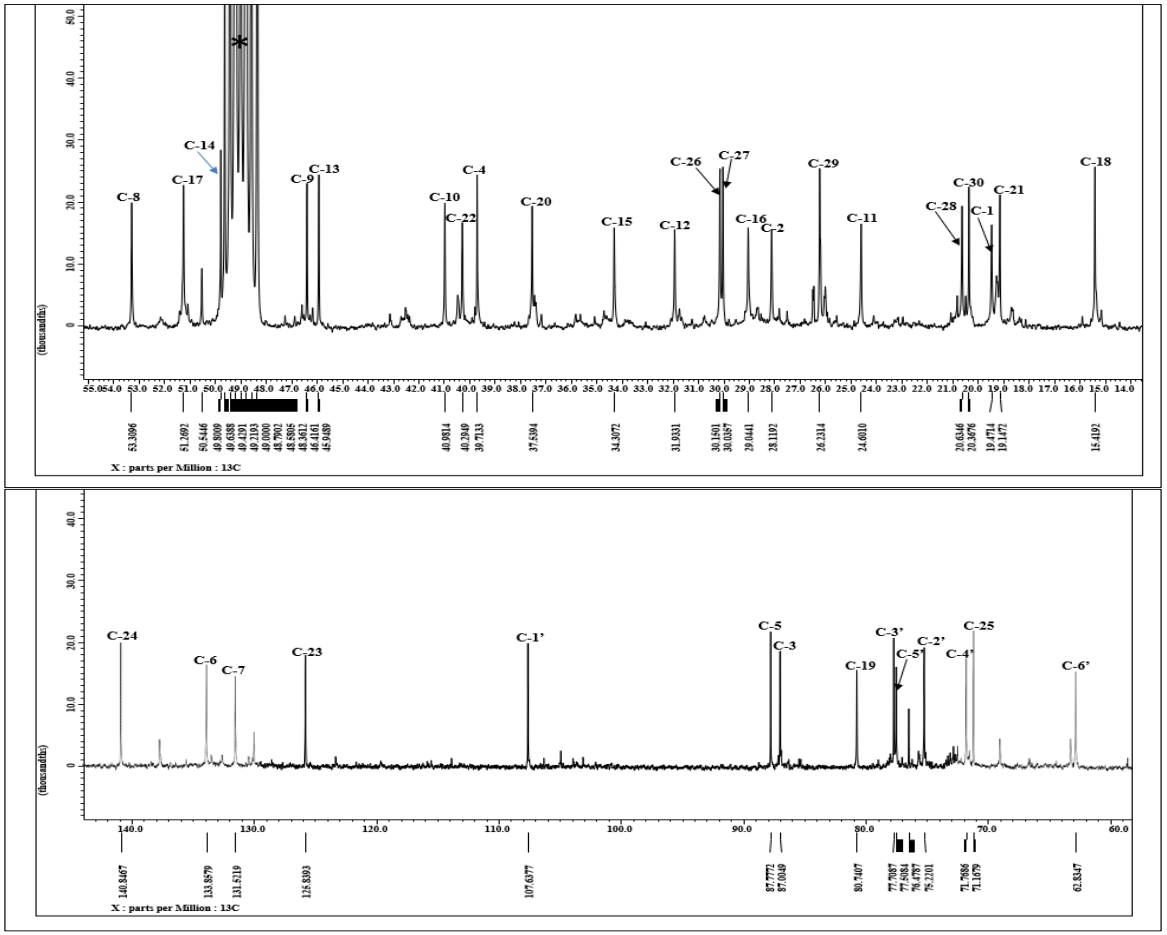

Figure A18 Complete assignments of ^{13}CNMR spectra of compound **1** in MeOD, recorded at 100 MHz using standard JEOL pulse programs. The solvent signal was marked as (*) asterisk.

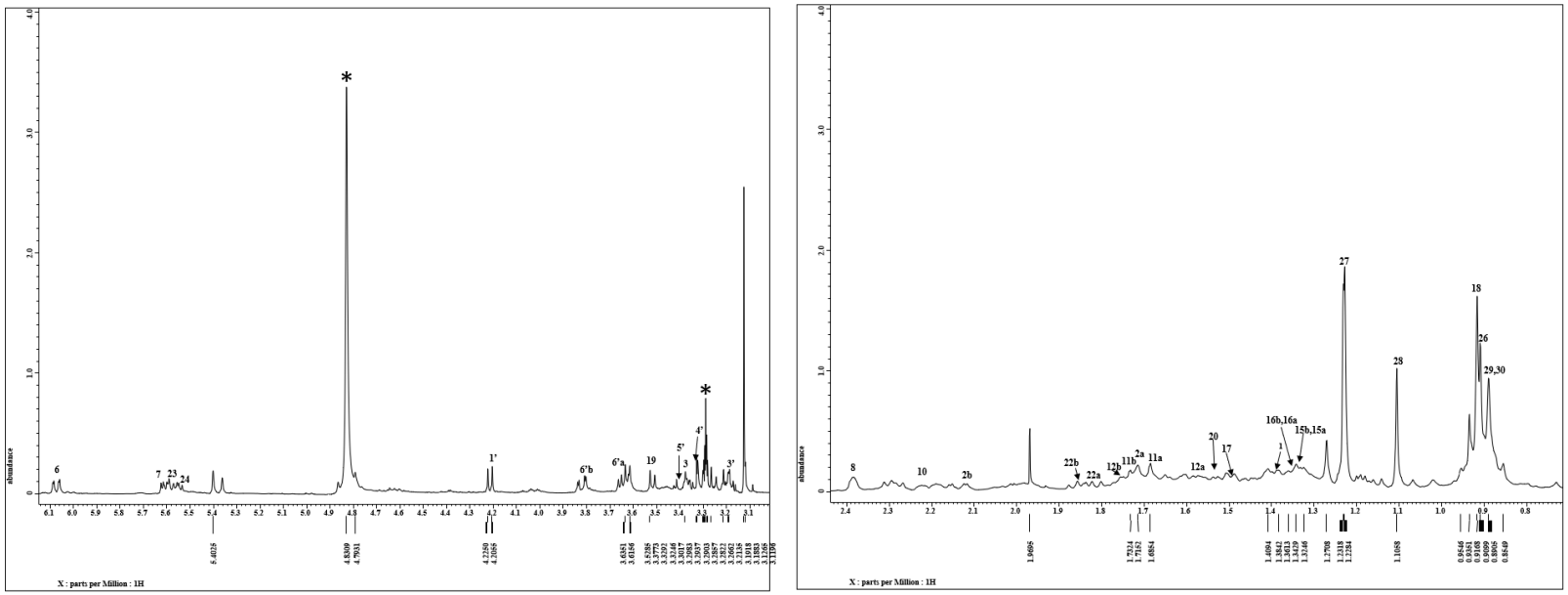

Figure A19 Complete assignment of ^{1}HNMR spectra of compound **2** in MeOD, recorded at 400 MHz (^{1}H). The solvent signal was marked as (*) asterisk.

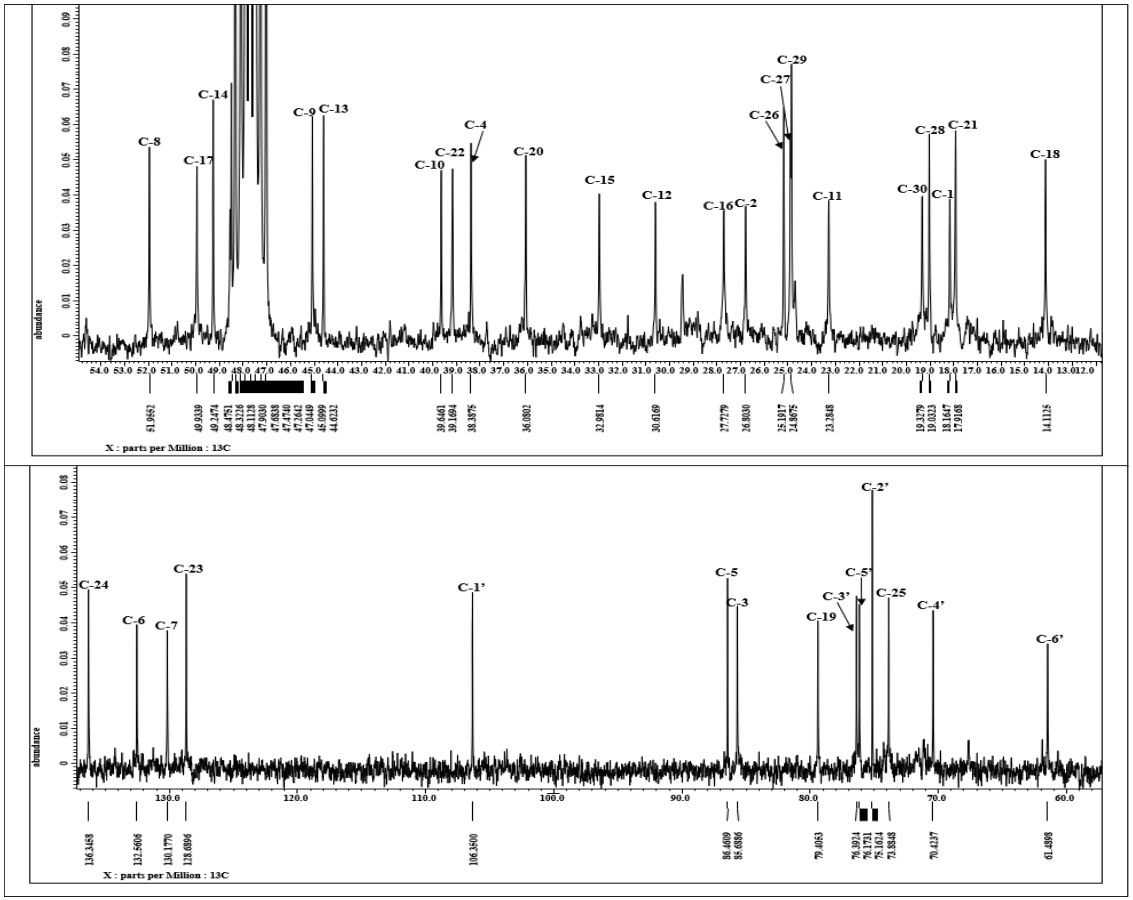

Figure A20 Complete assignments of ^{13}CNMR spectra of compound **2** in MeOD, recorded at 100 MHz. The solvent signal was marked as (*) asterisk.

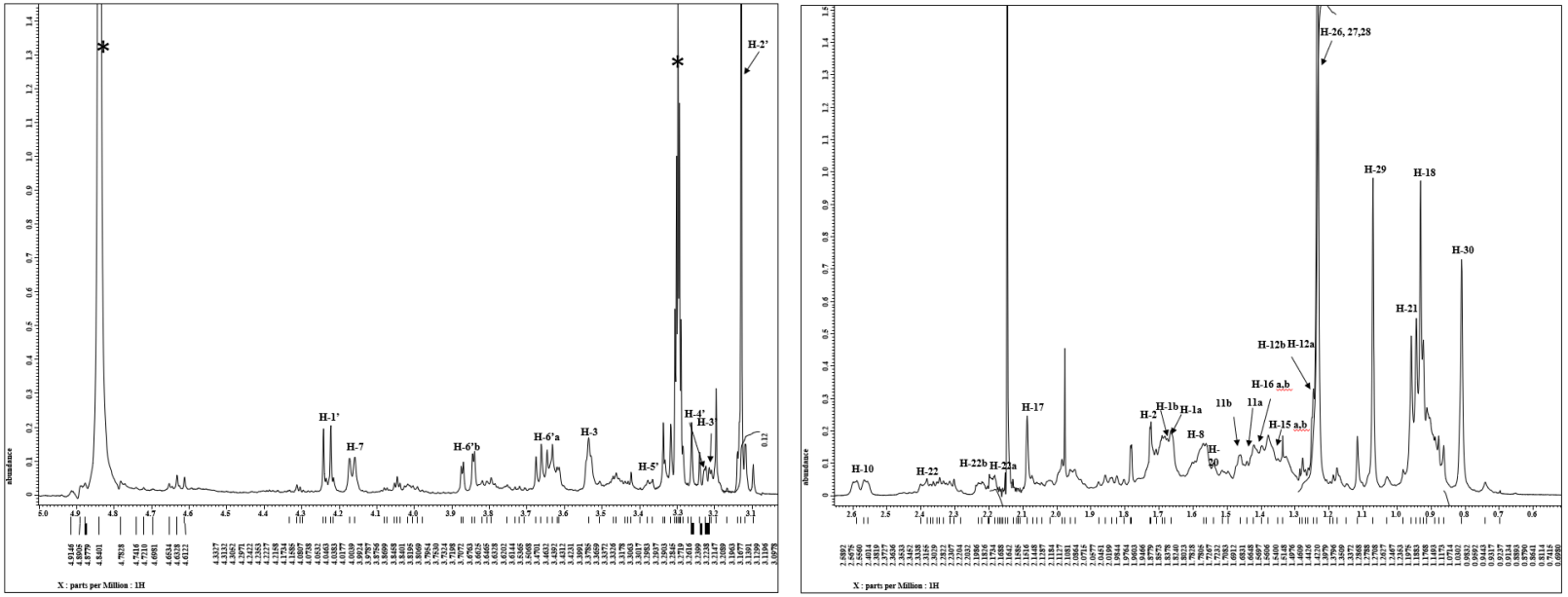

Figure A21 Complete assignments of [1]HNMR spectra of compound **3** in MeOD, recorded at 400 MHz . The solvent signal was marked as (*) asterisk.

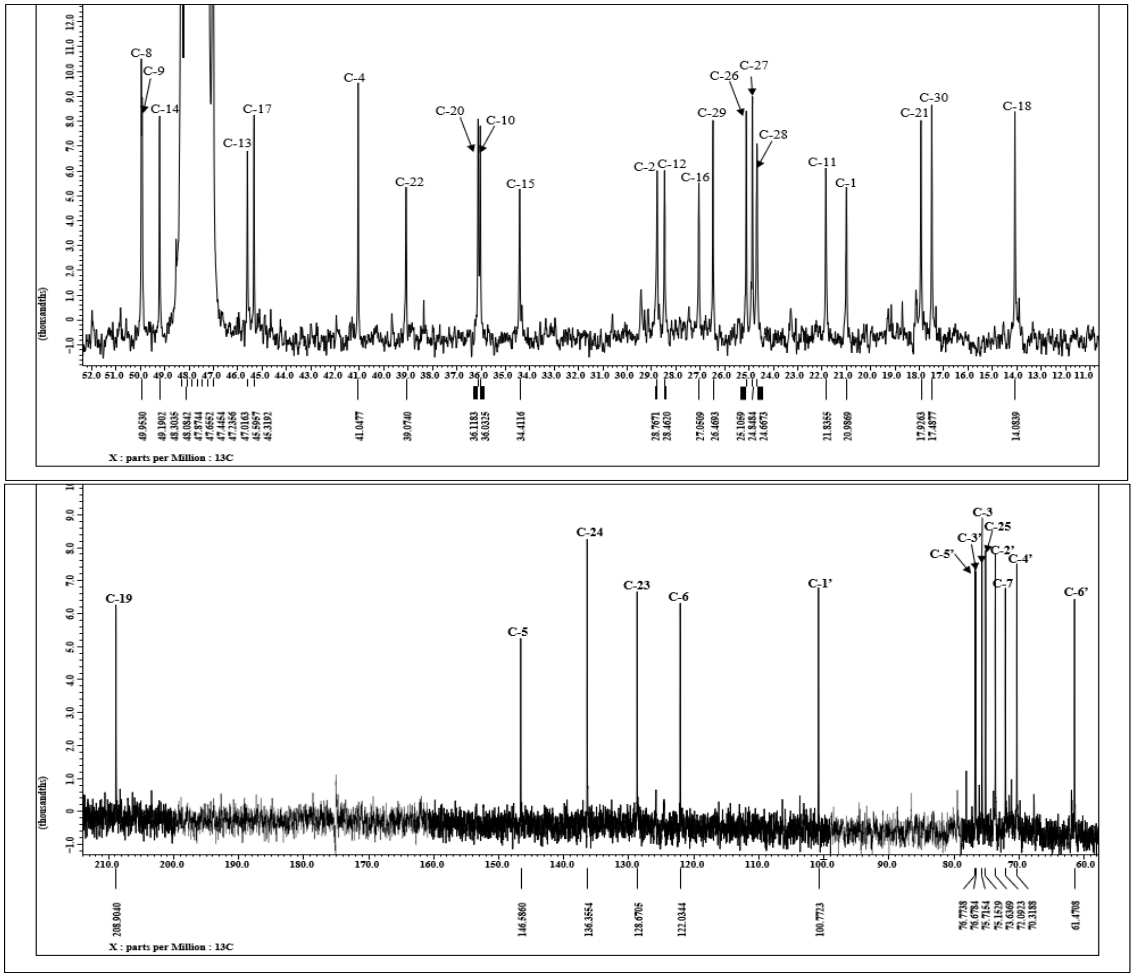

Figure A22 Complete assignments of ^{13}CNMR spectra of compound **3** in MeOD**,** recorded at 100 MHz. The solvent signal is marked as (*) asterisk.

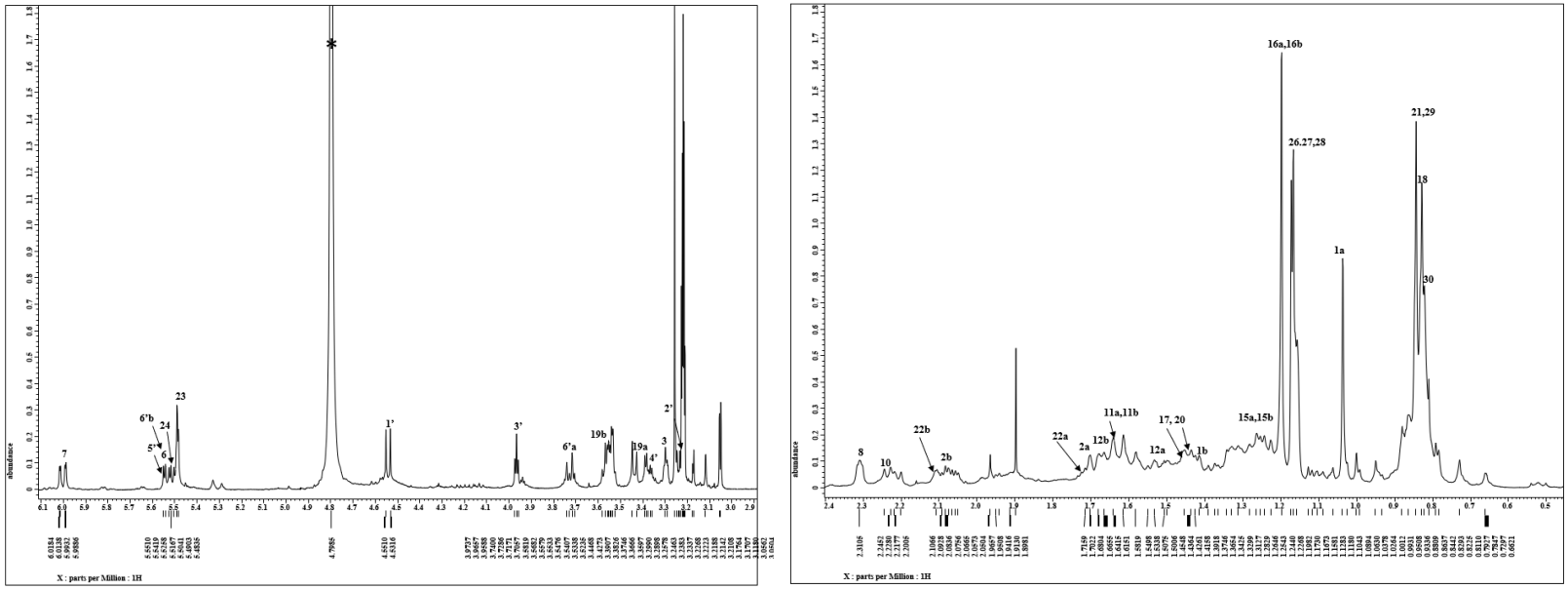

Figure A23 Complete assignments of ^{1}HNMR spectra of compound **4** in MeOD, recorded using 400 MHz. The solvent signal is marked as (*) asterisk.

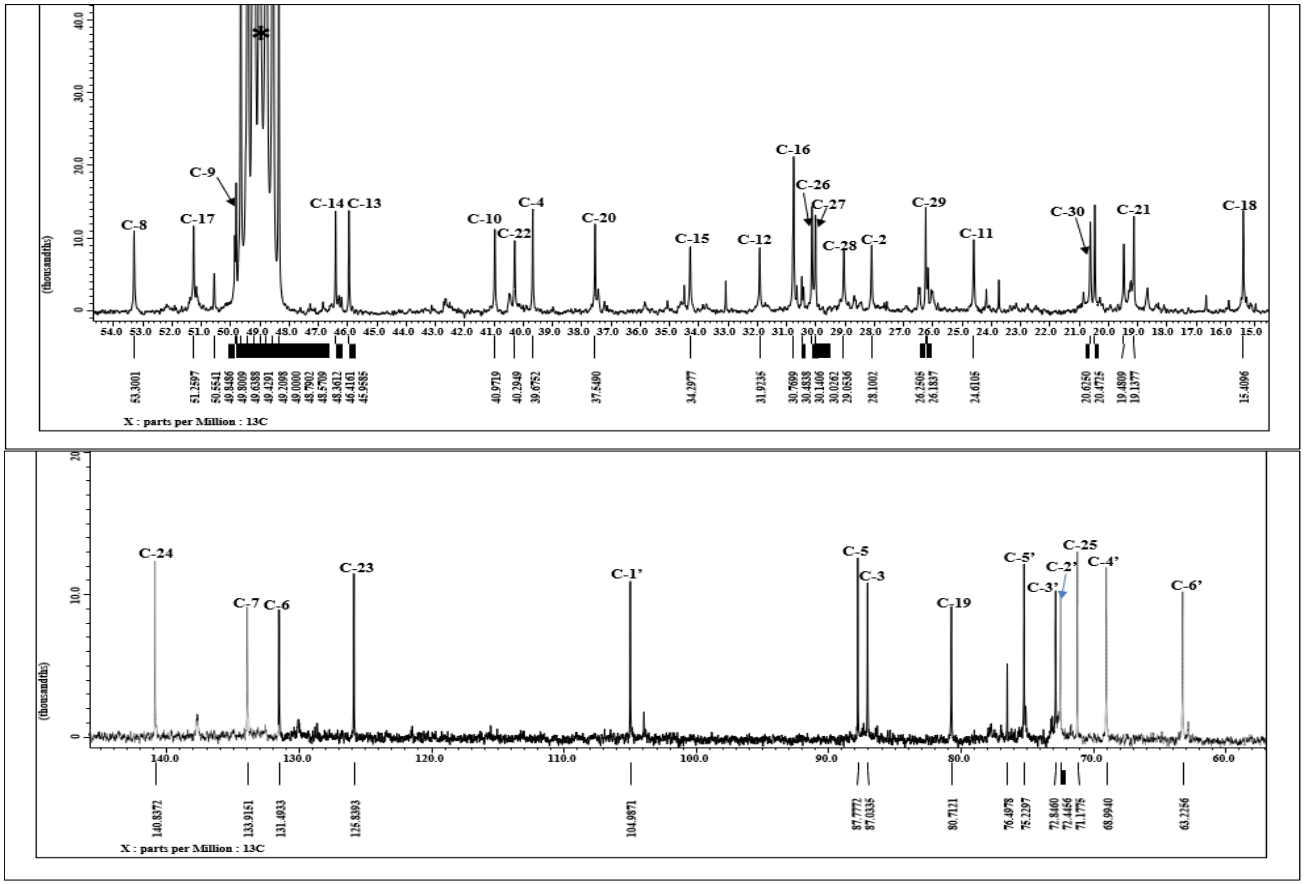

Figure A24 Complete assignments of ^{13}CNMR spectra of compound **4** in MeOD, recorded at 100 MHz. The solvent signal is marked as (*) asterisk.

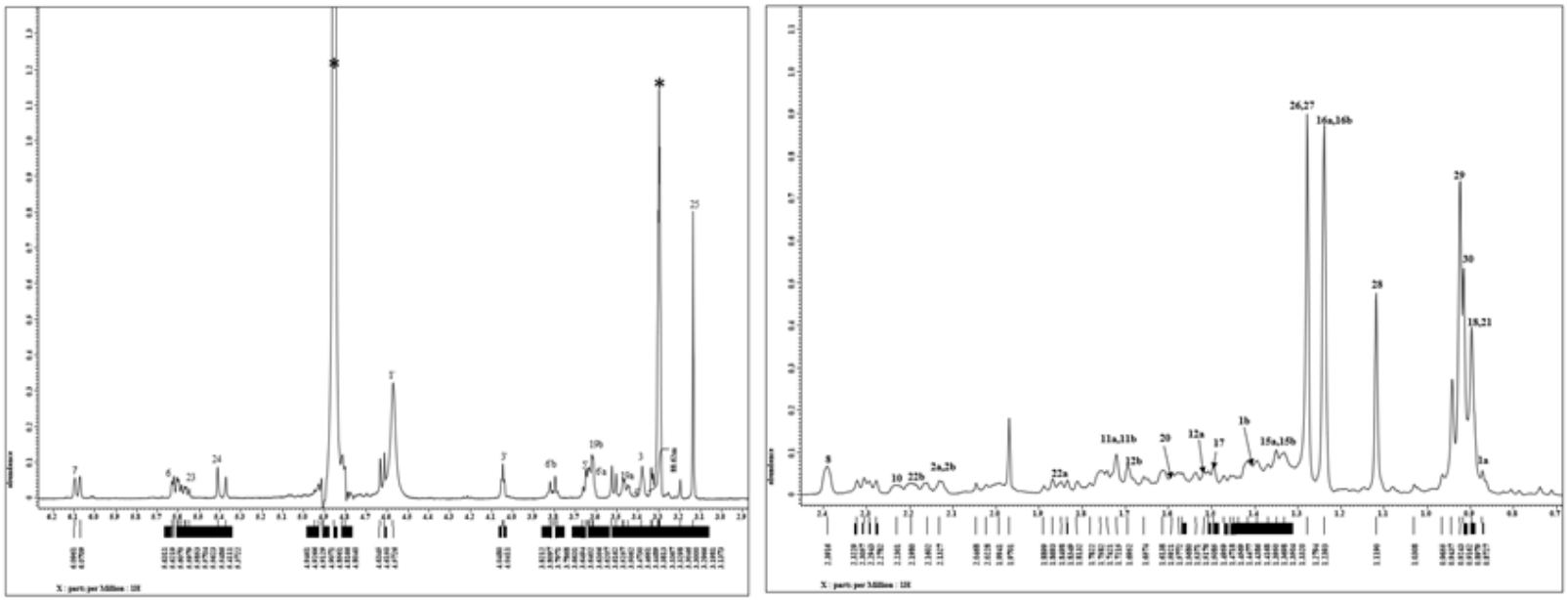

Figure A25 Complete assignments of ^{1}HNMR spectra of compound **5** in MeOD, recorded at 400 MHz. The solvent signals are marked as (*) asterisk.

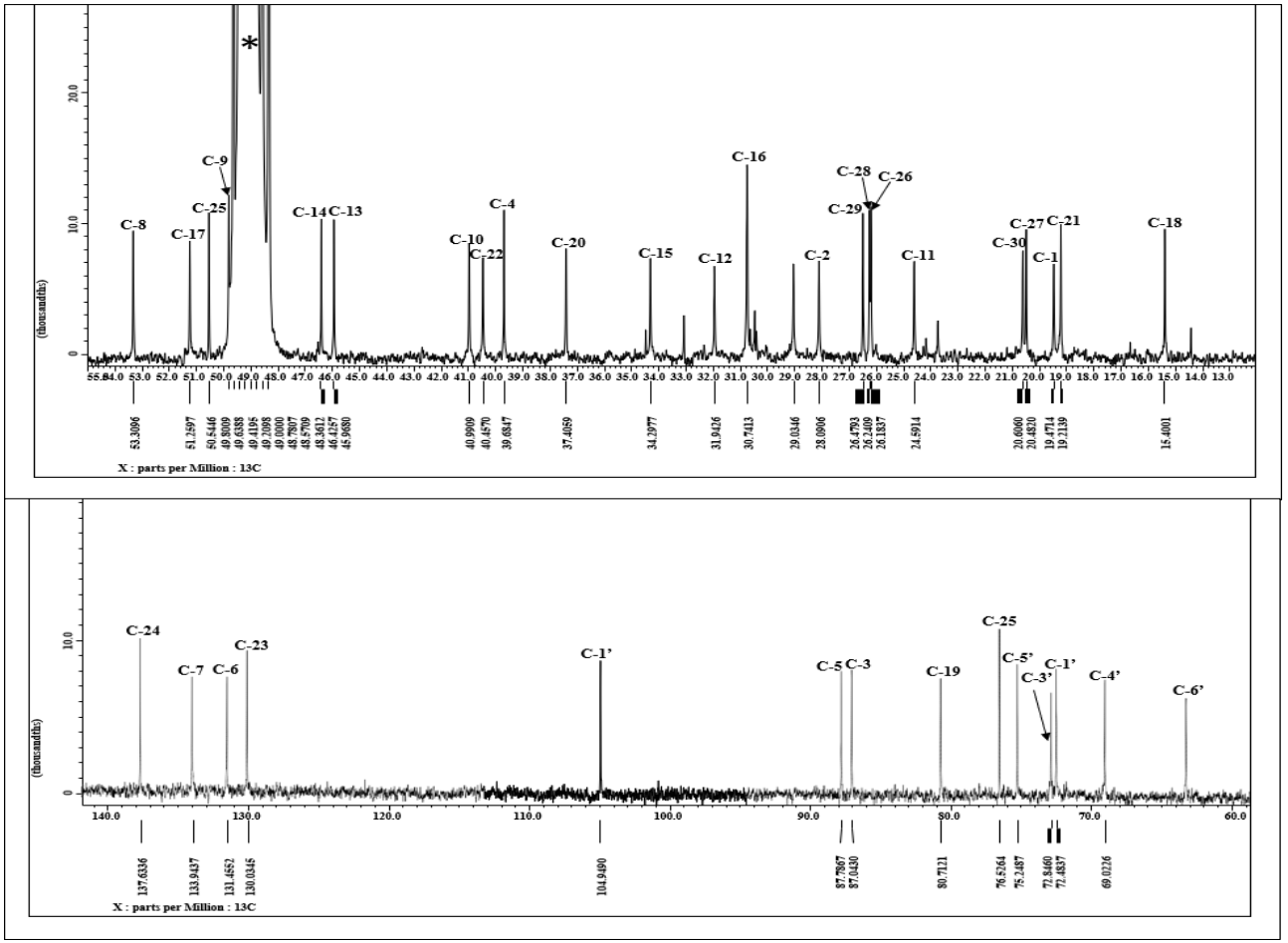

Figure A26 Complete assignments of ^{13}CNMR spectra of compound **5** in MeOD, recorded at 100 MHz. The solvent signal is marked as (*) asterisk.

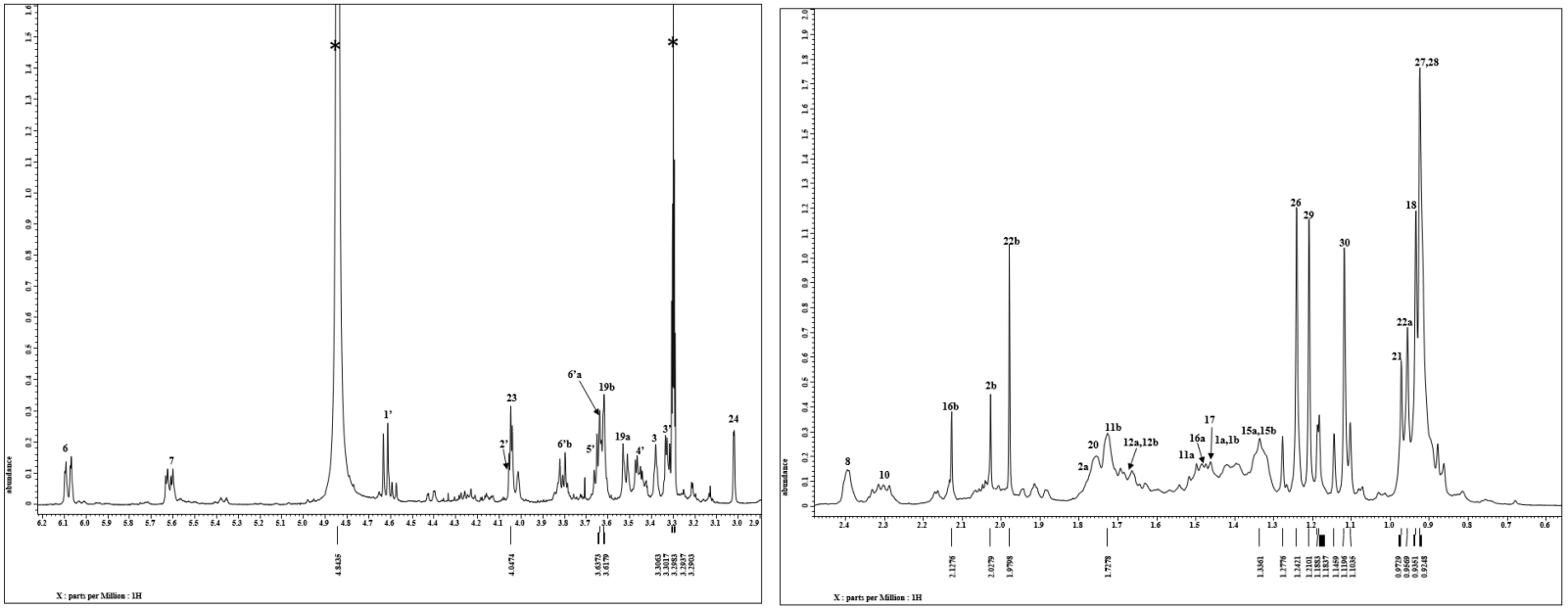

Figure A27 Complete assignments of ^{1}HNMR spectra of compound **6** in MeOH, recorded at 400 MHz . The solvent signal was marked as (*) asterisk.

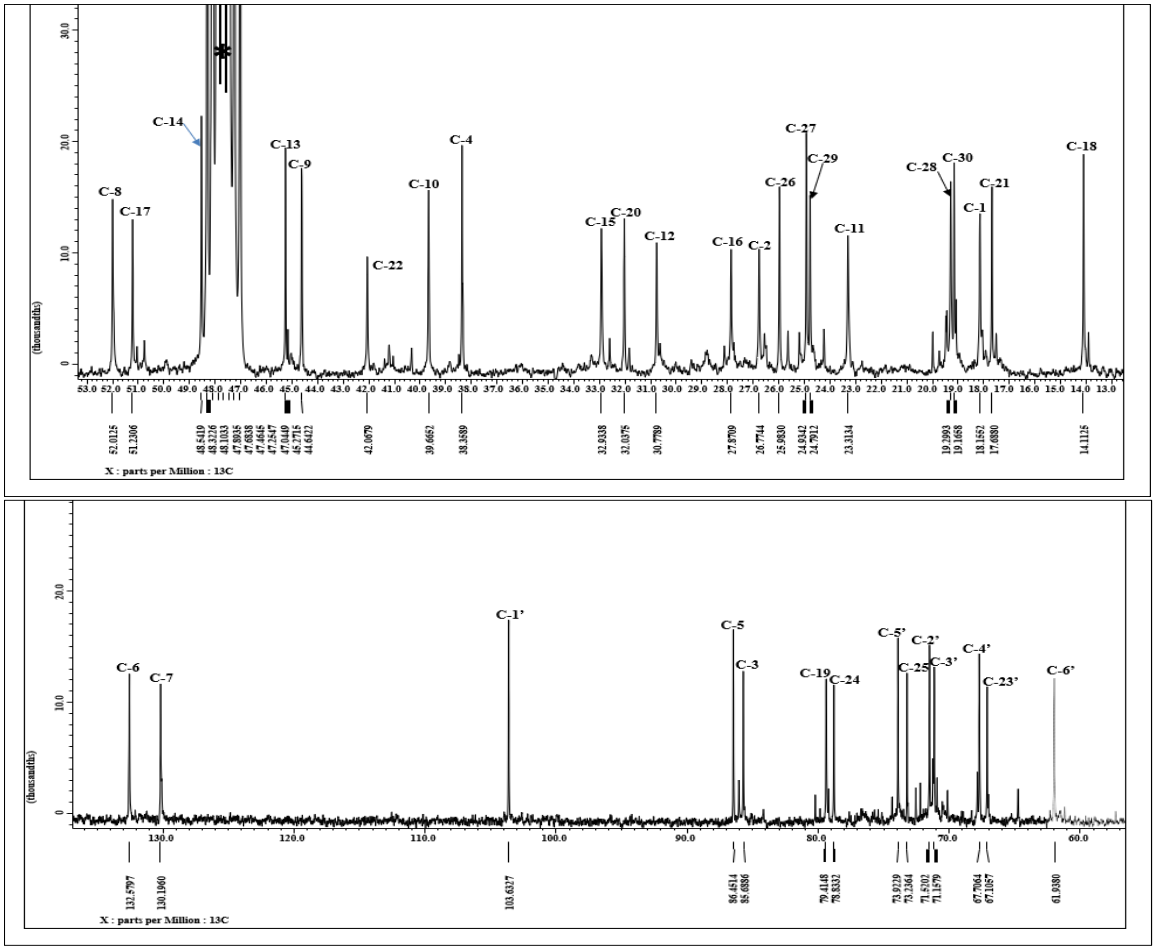

Figure A28 Complete assignments of ^{13}CNMR spectra of compound **6** in MeOD, recorded at 100 MHz. The solvent signal is marked as (*) asterisk.

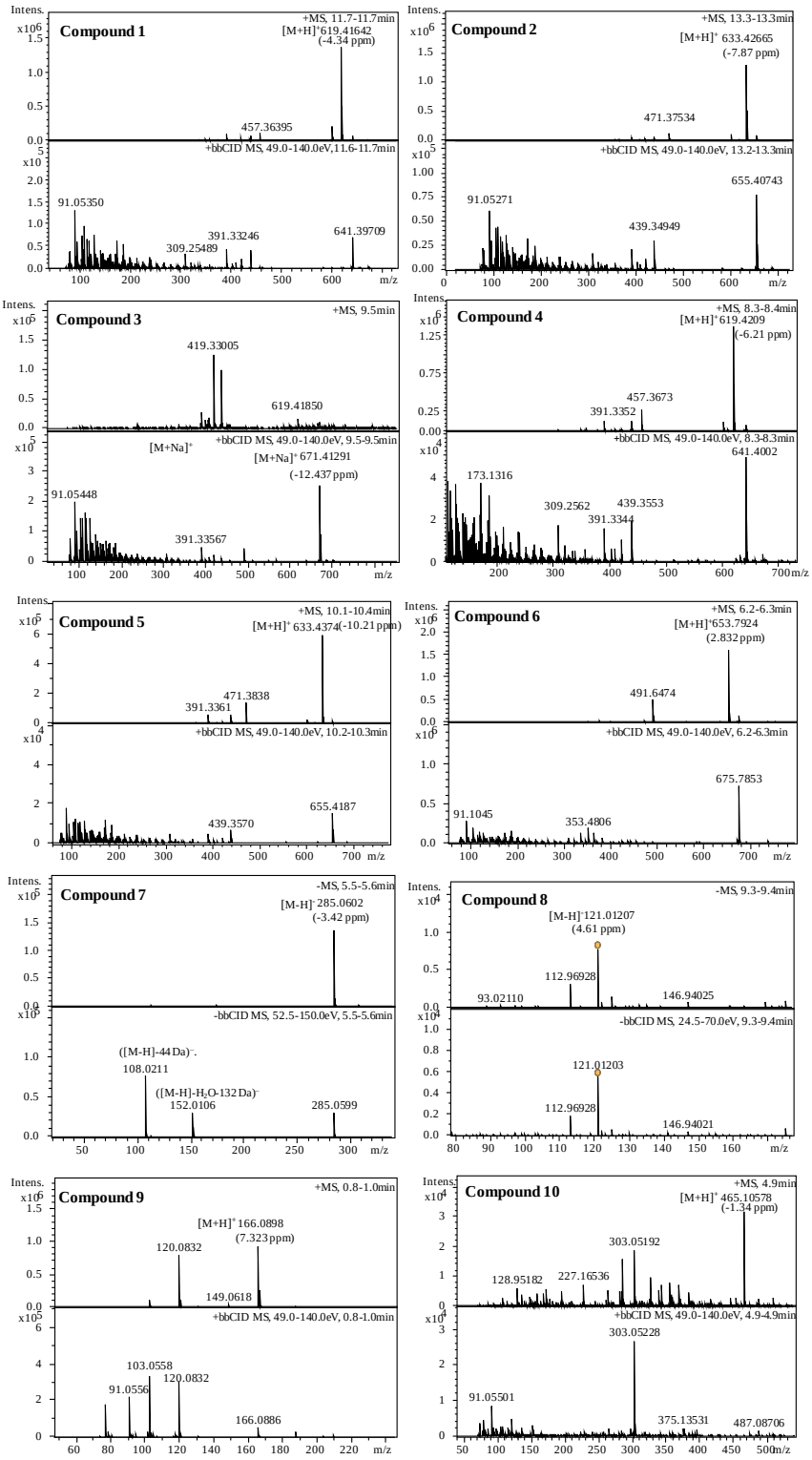

Figure A29 High-resolution mass spectra of purified compounds (**1-7**) from the acetone and methanol extract of *Momordica charantia*.

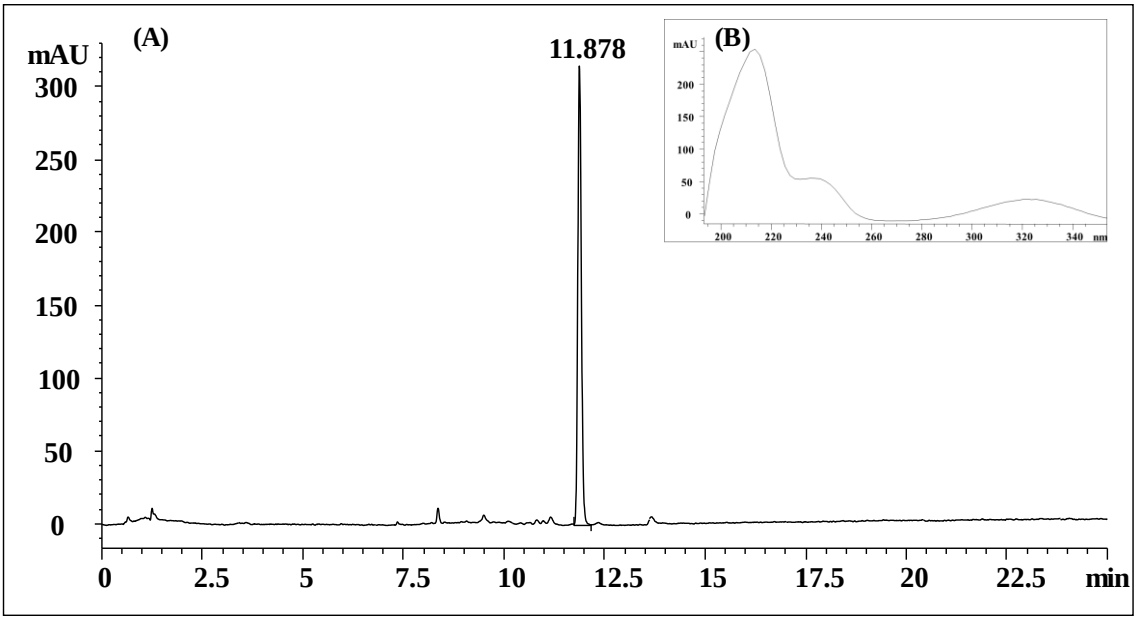

Figure A30 (**A**) HPLC Chromatogram of compound **7**and (**B)**. UV spectrum of compound

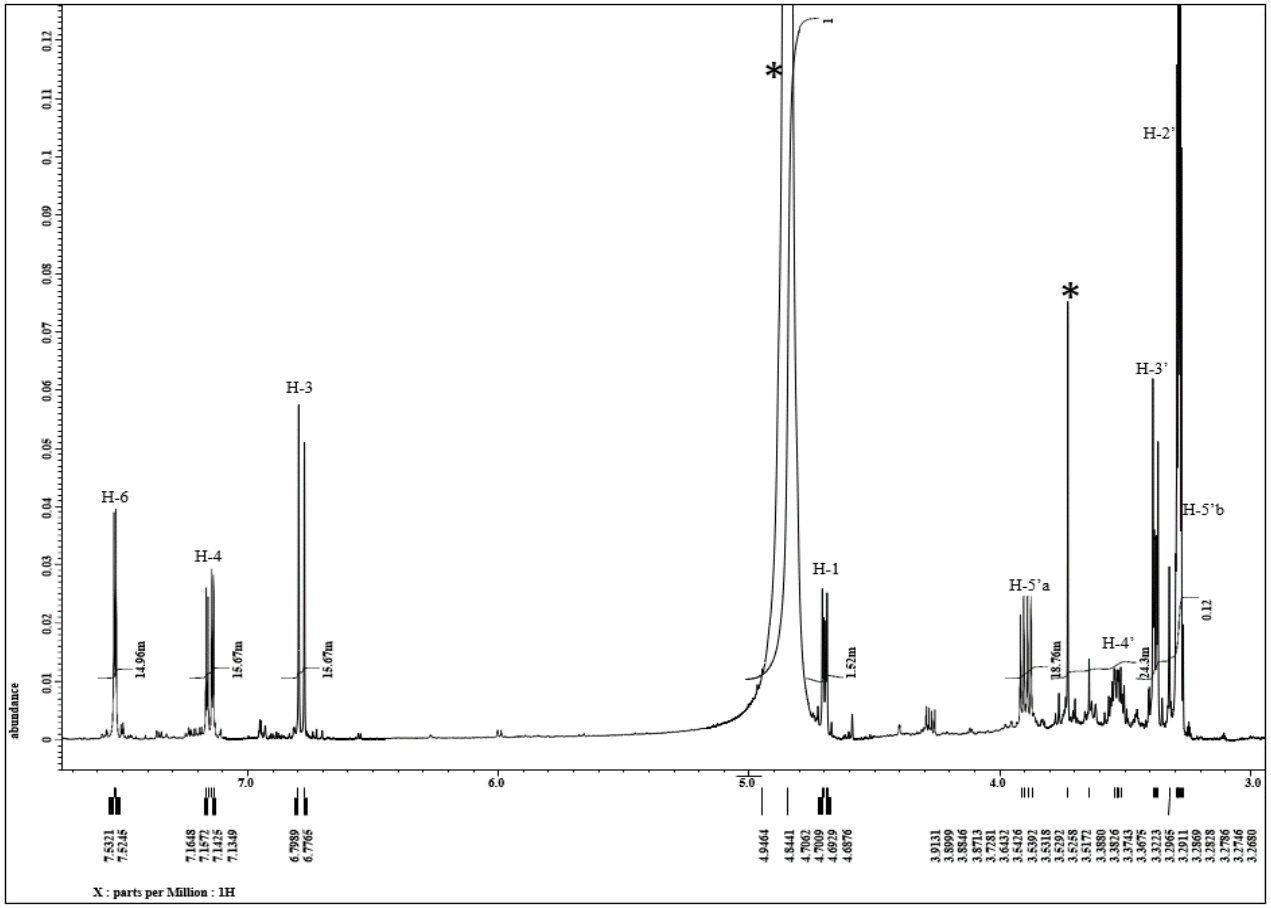

Figure A31 Complete assignments of [1]HNMR spectra of compound **7** in MeOH, recorded at 400 MHz using standard JEOL pulse programs. The solvent signal was marked as (*) asterisk.

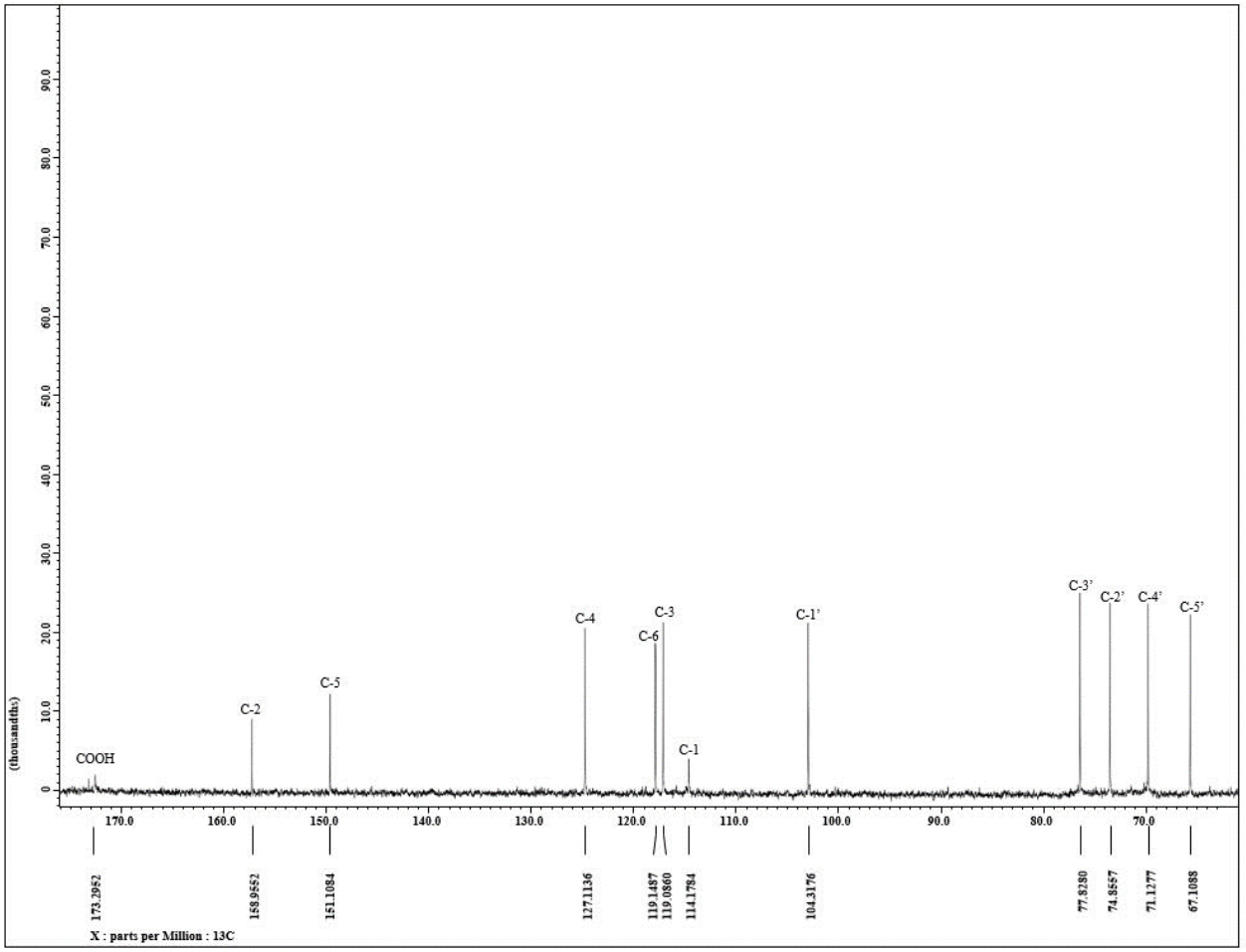

Figure A32 Complete assignments of ^{13}CNMR spectra of compound **7** in MeOD, recorded at 100 MHz using standard JEOL pulse programs.

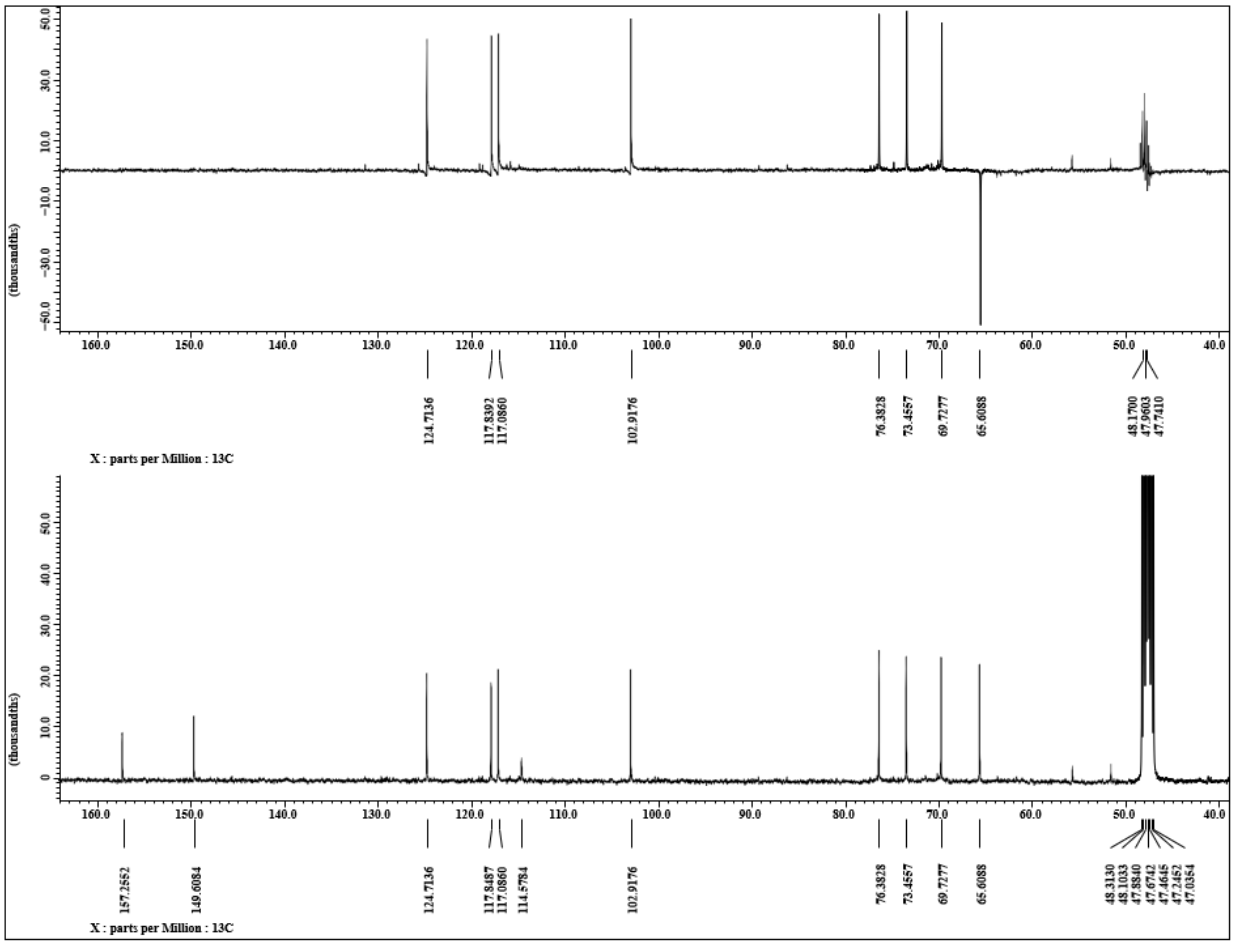

Figure A33 DEPT-135 spectra of compound **7** in MeOD, recorded at 100 MHz using standard JEOL pulse programs.

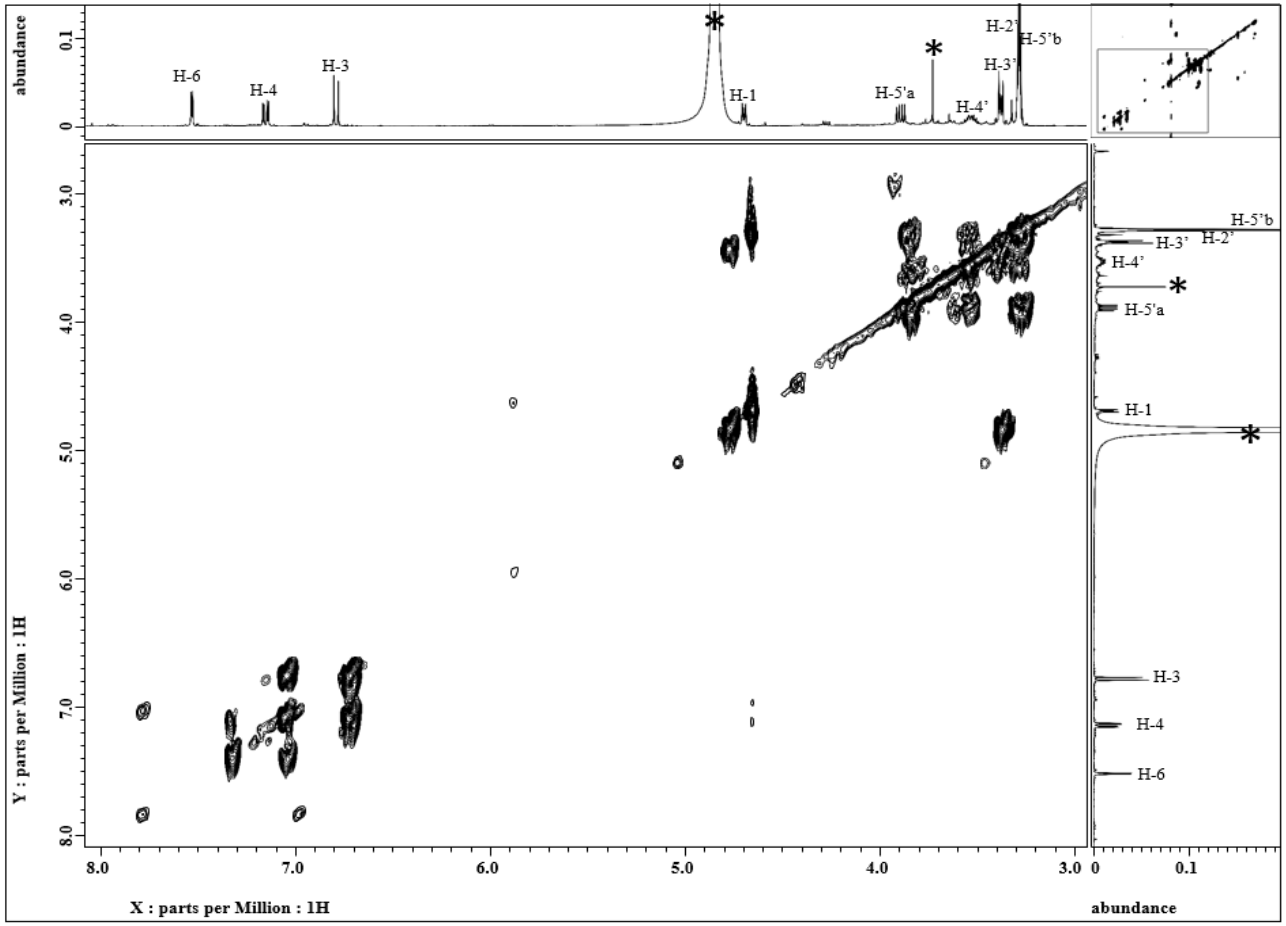

Figure A34 DQF-COSY spectra of compound **7** in MeOD.

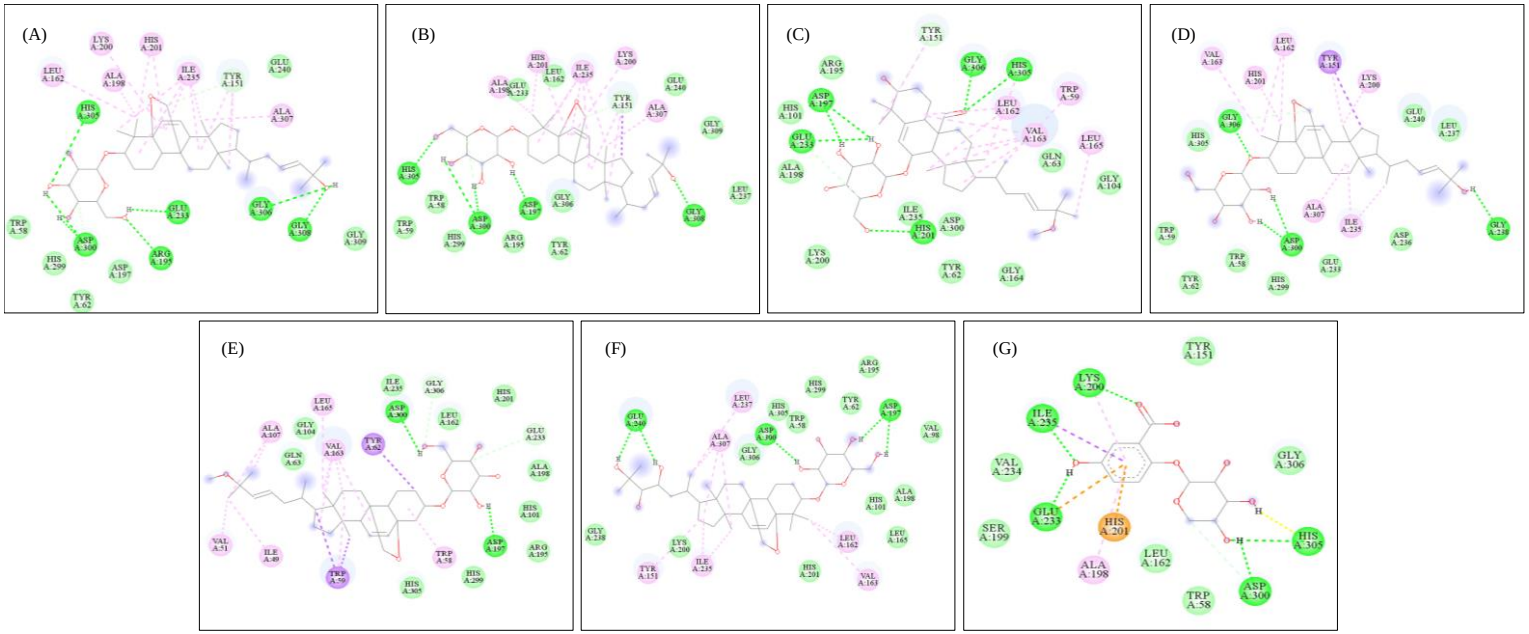

Figure A35 The 2D ligand-protein interactions for (**A**). momordicoside I, (**B**). momordicoside F_1, (**C**). momordicoside K, (**D**). momordicoside F_2, (**E**). momordicoside G, (**F**). karaviloside XI and (**G**). 2-hydroxy-5-*O*-β-D-xylopyranosyl benzoic acid in the binding pocket of α-amylase. Legends below each figure are showing types of bonding between a compound and the enzymatic pocket of α-amyalse.

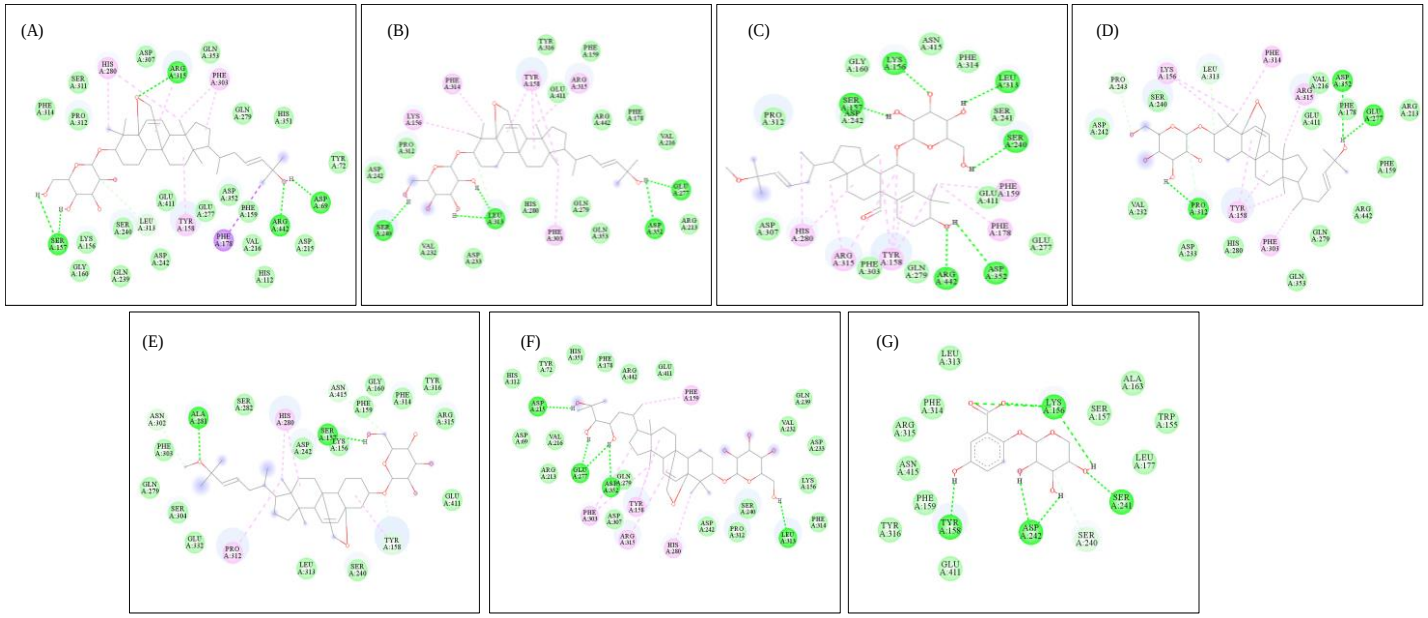

Figure A36 The 2D ligand-protein interactions for (**A**). momordicoside I, (**B**). momordicoside F_1, (**C**). momordicoside K, (**D**). momordicoside F_2, (**E**). momordicoside G, (**F**). karaviloside XI and (**G**). 2-hydroxy-5-*O*-β-D-xylopyranosyl benzoic acid in the binding pocket of α-amylase. Legends below each figure are showing types of bonding between a compound and the enzymatic pocket of isomaltase.